Winter 1996

Investigation of pd(A)(20)pd(T)(20) in the analytical electrophoresis apparatus

John Oliver Wooll
University of New Hampshire, Durham

INFORMATION TO USERS

This manuscript has been reproduced from the microfilm master. UMI films the text directly from the original or copy submitted. Thus, some thesis and dissertation copies are in typewriter face, while others may be from any type of computer printer.

The quality of this reproduction is dependent upon the quality of the copy submitted. Broken or indistinct print, colored or poor quality illustrations and photographs, print bleedthrough, substandard margins, and improper alignment can adversely affect reproduction.

In the unlikely event that the author did not send UMI a complete manuscript and there are missing pages, these will be noted. Also, if unauthorized copyright material had to be removed, a note will indicate the deletion.

Oversize materials (e.g., maps, drawings, charts) are reproduced by sectioning the original, beginning at the upper left-hand corner and continuing from left to right in equal sections with small overlaps. Each original is also photographed in one exposure and is included in reduced form at the back of the book.

Photographs included in the original manuscript have been reproduced xerographically in this copy. Higher quality 6" x 9" black and white photographic prints are available for any photographs or illustrations appearing in this copy for an additional charge. Contact UMI directly to order.

UMI

A Bell & Howell Information Company
300 North Zeeb Road, Ann Arbor MI 48106-1346 USA
313/761-4700 800/521-0600

INVESTIGATION OF $pd(A)_{20} \cdot pd(T)_{20}$ IN THE ANALYTICAL ELECTROPHORESIS APPARATUS

BY

JOHN WOOLL
B.S., University of California at Santa Barbara, 1992

DISSERTATION

Submitted to the University of New Hampshire
in Partial Fulfillment of
the Requirements for the Degree of

Doctor of Philosophy

in

Biochemistry

December 1996

This dissertation has been examined and approved.

Dissertation Director, Thomas L. Laue
Professor of Biochemistry

Andrew P. Laudano
Associate Professor of Biochemistry

John Collins
Associate Professor of Biochemistry

Harvey K. Shepard
Professor of Physics

Howard R. Mayne
Professor of Chemistry

Date

ACKNOWLEDGMENTS

Like all journeys, a Ph.D. thesis is accomplished with numerous small and large contributions from others. My friends, my family, my lab mates, myself (a faux pas?) and my *buffer boy* have all been invaluable in this campaign.

Why the acknowledgments, which are written last (dead last in my case-), are put in the front of the thesis is to me incongruent. They or it should rightly find a spot nestled in the appendix. But like many of life's responsibilities I am forced to "conform"and "acknowledge" the people that have helped and supported me. unfortunately I'm not the mood (I said it was dead last) to specify individuals. You know who you are and you know how important you have been. I'm deeply gradiated (past and continuing tense of gratified) for your efforts

TABLE OF CONTENTS

LIST OF TABLES

LIST OF FIGURES

TABLE OF SYMBOLS

Symbols	Units	Description
AEA		Analytical electrophoresis apparatus
SSE		Steady-state electrophoresis
E	volts/cm	Electric field (E field)
e	1.6029×10^{-19} Coulombs	The charge on an electron (cgs)
Z	units of e	Formal charge
κ	cm^{-1}	Inverse Debye length
Q_{app}	units of e	The apparent charge as measured in the SSE
σ	cm^{-1}	A parameter in an exponential fit
μ	cm^2/volt·sec	The electrophoretic mobility
μ_{ave}	cm^2/volt·sec	A μ averaged from several E fields
v	cm/sec	Velocity in an E field
v_o	cm/sec	Velocity at zero E field
F	10^{-7} cm^2/sec	Fick, diffusion coefficient unit
D_o	F	Diffusion coefficient at E = 0
f_o	g·cm/sec^2	Frictional coefficient at E = 0
D_e	F	Diffusion coefficient at E ≠ 0
f_e	g·cm/sec^2	Frictional coefficient at E ≠ 0
ϵ	(dimensionless)	Dielectric constant
I	amps	Current
A	cm^2	Cross sectional area of an AEA cuvette
κ	seimans/cm^2	Specific conductivity
N_a	6.0221×10^{23} particles/mol	Avogadro's number
k_b	1.38×10^{-16} erg/K	Boltzmann's constant
T	°K	Temperature
L	nm	Length of the DNA
d	nm	Diameter of the DNA
ρ	poise	Density
ν	ml/g	Partial specific volume
Re	(dimensionless)	Reynolds number

ABSTRACT

INVESTIGATION OF $pd(A)_{20} \cdot pd(T)_{20}$ IN THE ANALYTICAL ELECTROPHORESIS APPARATUS

by

JOHN WOOLL

University of New Hampshire, December, 1996

The analytical electrophoresis apparatus (AEA) is capable of generating and monitoring the electrophoretic migration of macroions. The oligonucleotide $pd(A)_{20} \cdot pd(T)_{20}$ was use as a model to compound to evaluate the range and validity of AEA measurements under a variety of electric fields and solvent conditions. A broad range of electric fields yield consistent, reproducible values. The charge determination from different procedures, steady state electrophoresis (SSE) and electrophoretic mobility, have not been consolidated into a consistent theory but advancements in the scope and understanding of the AEA's potential have been made. The apparent charge from the AEA measured electrophoretic mobility, μ, of $pd(A)_{20} \cdot pd(T)_{20}$ shows more sensitivity to solution conditions (different chloride salts or ionic strength in a buffer of 20 mM Tris, pH 8.0, at 20 °C) than the SSE determined Q_{app}. The electrophoretic mobility of $pd(A)_{20} \cdot pd(T)_{20}$ increases with decreasing ionic strength (100 mM KCl to 20 mM KCl salt conditions) and show a direct relationship (possibly coupled flow) to the mobility (and the cation affinity to DNA) of the different chloride salt [Li^+, Na^+, K^+, and $(CH_3)_4N^+$]. The combined SSE data (global nonlinear fit of all fields, one solution condition) suggest a single value for the apparent charge of around 5 e (electron units)

INTRODUCTION

Developments in Electrophoretic Analysis

The phenomenon of electrical attraction and repulsion was first measured quantitatively by Charles Augustin de Coulomb in 1785. The terms positive and negative charge were coined by Benjamin Franklin to describe the *kind* of electricity that appeared on particular substances. In modern biochemistry, it is known that the interplay between charged groups on macromolecules significantly influences their stability and association. Progress has been made on the theoretical aspects of these relations. However, charge is difficult to measure in solution. Electrophoresis is the most direct means of ascertaining a macromolecule's charge. The development of electrophoretic techniques has been an essential component in characterizing the role of charge

Early theoretical work on electrophoretic migration was done by such luminaries as Helmholtz (26, 32) and Smoluchowski (18, 32). Practical applications, such as isoelectric focusing, were being investigated in the early twentieth century by Hardy (5, 22) and Michaelis (5, 43), among others. Significant advances on these works were to come later from Hückel, Henry, Overbeek and Booth (5, 32, 55). Experimental investigation of the evolving theory, however, was hampered not only by the inherent difficulties in trying to measure the charge, but also by the limitations of the experimental apparatus. The development of devices capable of analytical electrophoresis has been essential in expanding

the understanding of the charge-related properties of macromolecules.

The Hittorf method (circa 1868) was the first regularly-employed procedure for measuring the electrophoretic velocity of a material. A current was sent through a homogeneous colloidal solution and the amount of colloid that accumulated at the electrode after a specific time was considered proportional to the velocity of the material.

Building on this technique was the moving boundary method. The observation that an electric field (E field) displaced the boundary between solutions containing dispersed ions and one free of those particles inspired the development of U-shaped tubes capable of monitoring such boundaries. An apparatus used by Burton (circa 1904) and Michaelis had the lower portion of the tube filled with the solution and the top filled with solvent. A current was applied through electrodes at opposite openings of the tubes and the movement of the boundaries (ascending and descending limbs) was proportional to the velocity of the ionic species. However, such a large number of experimental conditions needed to be met that only a limited set of substances were investigated successfully with this method. Improvements to the technique were required.

Applying the same fundamental principles and design as found with the moving boundary method, the Tiselius apparatus (developed in the 1930's) incorporated several advances which permitted significantly broader applications (5, 32). Techniques based on this apparatus dominated electrophoretic velocity determination for the next 50 years. This apparatus provided a cleaner boundary between pure solvent and the macromolecular solution by sliding two parts of the U-tube across each other. Furthermore, optical detection of the moving boundary was made easier by making the U-shaped tube rectangular instead of

circular. Separate chambers were added for the electrodes to reduce contamination from electrolysis products. Schlieren and interference optics were added as those technologies developed. The Tiselius apparatus allowed many of the theoretical developments in electrophoresis and electrostatics to be investigated experimentally.

The Tiselius apparatus is not without its limitations. Analysis requires significant quantities of material and skilled operators. The Analytical Electrophoresis Apparatus (AEA), presently under development, offers the same sorts of measurements as the Tiselius device but requires substantially less material and allows several measurements to be made on a single sample (51). In addition to the traditional electrophoresis and diffusion measurements, the AEA provides the unique capacity of generating and measuring steady-state gradients.

Macroion charge characteristics can be investigated in the AEA using four complementary measurements: 1) the steady-state electrophoresis (SSE) concentration distribution, 2) the electrophoretic mobility (μ), 3) the diffusion coefficient in the absence of an electric field (D_o), and 4) the diffusion coefficient in the presence of an electric field (D_e). One purpose of this work is to explore this range of measurements using a model compound to further the development of the AEA as a biophysical tool.

Using $pd(A)_{20} \cdot pd(T)_{20}$ as a Model Compound

A model compound was selected to explore the range and validity of measurements in the AEA. A 20 base pair piece of DNA, $pd(A)_{20} \cdot pd(T)_{20}$, was chosen for these reasons: 1) DNA is an important biological molecule, 2) a 20 base pair oligonucleotide is a stable

molecule that is easily detectable and 3) 20 base pair DNA has been characterized extensively by other techniques and has been used in a number of theoretical calculations (12, 44, 45, 50, 62).

Structure and Solution Behavior of $pd(A)_{20} \cdot pd(T)_{20}$

NMR and x-ray diffraction studies of polyA·polyT oligonucleotides show them to have conformations in the B-DNA family (1). The minor groove is distinctly narrow and the base pair per turn is approximately 10.1. The length of a similar 20 base pair oligonucleotide was measured at 6.88 nm (12) by light scattering. Investigation into the hydration pattern of oligonucleotides showed there to be two classes of associated water. The first class directly contacts the DNA at a density of 10-12 waters per nucleotide and is partially manifested as a "spine of hydration" in the minor groove (30). The second class, 8-9 waters per nucleotide, is H-bonded to site bound class 1 molecules. Hydration of the bases and phosphate backbone adds an additional 0.6 to 0.8 nm to the 2.0 nm diameter of the oligonucleotide (62).

The solution behavior of oligonucleotides influences electrophoretic migration. Oligonucleotides of identical composition but different sequences have been shown to have different electrophoretic mobilities in agarose gels (63). Bending in the DNA, base pair openings, and end fraying can have significant effects on migration and hamper the modeling of a 20 base pair DNA as a rigid rod. The duplex helices of polyA·polyT oligonucleotides show considerable curvature at lengths exceeding 60 base pairs, but can be considered linear at 20 (1, 4). NMR investigation into the bonding of internal tracts of AT base pairs show the bonding across the axis to have lifetimes of between 3 and 6 milliseconds, with lifetimes being independent of neighboring sequences (30, 34, 48). The external two A·T base pairs at each

end of the oligonucleotide are known to fray (29). Lifetimes of these base pairs are less than one millisecond. The effect that base-pair opening and end-pair fraying have on electrophoretic mobilities is hard to predict. The millisecond time scales suggest that their contribution will appear as a homogeneous average value in the measured properties.

The rotational (D_r) and translational (D_o) diffusion coefficients of a 20 base pair oligonucleotide have been obtained from light scattering experiments (12). The oligonucleotide was shown have a D_r of 10.3 x 10^6 s^{-1}. The energy randomizing the rotational position of the DNA far exceeds the electrical potentials available in the AEA to align the DNA with the electric field (59). The D_o of the 20 base pair DNA (extrapolated to zero DNA concentration in 50 mM phosphate, 100 mM NaCl, 2 mM EDTA at pH 7.0 and corrected to 20 °C) was measured at 11 Fick (F or 10^{-7} cm^2/s)and can be compared to the AEA derived diffusion coefficient of $pd(A)_{20}$•$pd(T)_{20}$ and to theoretical predictions.

Theoretical Estimates of the Hydrodynamic Properties of $pd(A)_{20}$•$pd(T)_{20}$

The hydrodynamic frictional coefficient, f_o, of $pd(A)_{20}$•$pd(T)_{20}$ can be estimated by modeling the DNA as either a prolate ellipsoid or a string of touching beads.

To a good approximation (13), an oligonucleotide of length L_d and diameter d can be approximated as a prolate ellipsoid of major axis $a = L_d/2$. For the ellipsoid to have the same volume as a cylinder the size of the DNA, V_d, the axial ratio a/b of the ellipsoid must be

(1) $$\left(\frac{a}{b}\right) = \left(\frac{2}{3}\right)^{\frac{1}{2}} \frac{L_d}{d}$$

The frictional coefficient of an ellipsoid of revolution was calculated by Perrin in 1936. In terms of the ellipsoid axes, he solved for the ratio of f_o over f (7, 60)

(2)
$$\frac{f_o}{f} = \frac{\left(\frac{a}{b}\right)^{\frac{2}{3}}\left(1-\frac{b^2}{a^2}\right)^{\frac{1}{2}}}{\ln\left(\frac{1+\left(1-\frac{b^2}{a^2}\right)}{\frac{b}{a}}\right)}$$

where f is the calculated frictional coefficient of a sphere of volume equal to V_d

(3)
$$f = 6\pi\eta R$$

with

(4)
$$R = \left(\frac{3}{16} L_d d^2\right)^{\frac{1}{3}}$$

where R is the Stokes radius and η is the viscosity of the solution.

The second method for determining the frictional coefficient uses the Kirkwood and Riseman model (13) of "touching beads". Here the DNA, of length L_d, is modeled as a string of M numbered touching beads, each of diameter δ. The length of the string, L_b, is $M \cdot \delta$. If the total volume of the beads, V_b equals V_d then the frictional coefficient is calculated as

(5) $$f = \frac{3\pi M\delta}{\ln M}$$

Equating V_b/L_b with V_d/L_d gives an expression for δ in terms of the length and volume of the DNA

(6) $$\frac{V_d}{L_d} = \frac{\left(\frac{4}{3}\right)\pi\left(\frac{\delta}{2}\right)^3 M}{M\delta}$$

thus

(7) $$\delta = \left(\frac{24V_d}{4\pi L_d}\right)^{\frac{1}{2}}$$

M easily follows from the length of the DNA and equation 5 can be solved for the frictional coefficient of the DNA.

A third method for obtaining a hydrodynamic coefficients for the oligonucleotide takes into account end effects. Tirado and de la Torre (62) carried out numerical evaluation based on rigorous application of the Kirkwood-Riseman theory with extrapolation to the shell model limit. They obtained the diffusion coefficient for oligonucleotides by solving;

(8) $$D_o = \left(\frac{k_b T}{3\pi\eta_o L}\right)\left[\ln\left(\frac{L}{d}\right) + \beta\right]$$

where η_o is the solvent viscosity, k_b is Boltzmann's constant, T is temperature in degrees Kelvin and β is the end effect correction which is solved by a polynomial approximation to

their numerical results

(9) $$\beta = 0.312 + 0.565\left(\frac{d}{L}\right) - 0.100\left(\frac{d}{L}\right)^2$$

Under 100 mM salt conditions, the theoretical D_o of Tirado and de la Torre is 10.9 Fick.

Theoretical Estimates of the Charge on $pd(A)_{20}$•$pd(T)_{20}$

The AEA determined value for the apparent charge of $pd(A)_{20}$•$pd(T)_{20}$, Q_{app}, (see THEORY) can be compared to theoretical prediction in a manner that investigates both the apparatus and the soundness of the predictions. Two approaches to charge prediction of oligonucleotides are the semi-empirical counterion condensation theory with its counterion association parameter Ψ and grand canonical Monte Carlo (GCMC) simulations with its preferential interaction parameter Γ (see THEORY). Both theories predict little or no dependency of the apparent charge on ionic strength, cation type, or base sequence. For a 20 base pair oligonucleotide, the Q_{app} based on values for Ψ (taking end effects into account) is 7.4 e (e is the charge on an electron) while GCMC predicts a significantly higher value of 17 e.

OBJECTIVES

Purpose of the Project

Developing the AEA as a viable biophysical tool is accomplished by investigating the effects that the ionic characteristics of the solution have on the measured charge properties of $pd(A)_{20}$•$pd(T)_{20}$, and by defining the conditions under which the AEA measurements reflect properties of the macroion and not properties of the method or the apparatus. Each of the four types of measurements has been made on $pd(A)_{20}$•$pd(T)_{20}$ and the results analyzed to determine precision and compared to theoretical estimates. These investigations can be summarized in three objectives: 1) determine the contributions to the observed concentration distribution that are a consequence of the *apparatus* or the process of *electrophoresis*, 2) determine the effects of different monovalent cations on the electrophoretic properties of $pd(A)_{20}$•$pd(T)_{20}$, and 3) determine the effects of varying the concentration of KCl on the electrophoretic properties of $pd(A)_{20}$•$pd(T)_{20}$.

Determine the Contributions to the Observed Concentration Distribution That are a Consequence of the *Apparatus* or the Process of *Electrophoresis*

Results presented below reveal behavior that is in contrast to simple theory (see THEORY). In particular, the charge properties determined from SSE differ significantly from those determined by mobility experiments. Individually, each procedure appears to be consistent, but they yield apparent charge estimates that differ by two to three fold. An additional inconsistency with theory is the increase in the apparent D_e with increasing E field.

Currently there is no theoretical basis for this behavior. In order to interpret the results from the AEA properly, it is essential to characterize the extent to which these observations are influenced by processes and properties not associated with the macroion. Optical problems and flows other than those due to the E field or diffusion are two main areas of concern.

A fundamental assumption made in the operation of the AEA, and in all theoretical descriptions, is that flow through the cuvette is laminar and not turbulent. Fluid flowing through a channel is subject to viscous shear. Confirming that the flow through the AEA should be laminar is the initial step in addressing influences on the concentration distribution.

In fluid dynamics (16, 41), the Reynolds number, Re, is the ratio of inertia to the viscous forces acting on the fluid and is a good indication of the transition (increasing Re) from laminar to turbulent flow:

(10)

$$Re = \frac{v_m D_h}{\frac{\eta}{\rho}}$$

with

(11)

$$D_h = \frac{4wL}{2(w+1)}$$

where v_m is the mean velocity through the cuvette, ρ is the solvent density, η is the solvent viscosity, and D_h is the hydraulic diameter opening of the cuvette with width w and length L. Using the maximum velocity through the 0.2 cm x 0.2 cm opening of the AEA cuvette for v_m (twice that of the chloride ion at the maximum E field used), the Re is is less than 0 .1. This

is well below the Re of 10 which is generally considered to be the upper range of laminar flow (41).

Even with the flow through the cell being laminar, there are potential problems in accurately detecting the concentration of the migrating macroion in a cross-sectional area of the cuvette (Figure 1). If the mobility of the macroion is different at the walls of the cuvette than at the center, a *non-laminar concentration distribution* will occur. This could affect the absorbance profile and detrimentally influence analysis. A non-uniform E field and electroosmotic flow are processes capable of altering the mobility of the macroion at the cuvette wall.

In the AEA, the applied electric field must go from a finite value inside the cuvette to a value of zero at the cuvette wall (no current is carried at the wall). The expectation is that this transition occurs on atomic dimensions which amounts to significantly less than 0. 1% of the distance across the cuvette. If, however, the transition encompasses a much larger distance then the absorbance profile may be distorted (Figure 1). A potential outcome of a large non-uniform E field would be an apparent increase in the spreading of the electrophoretic boundary, which could lead to an E field dependence for D_e (see THEORY). It is also possible that non-laminar mobility would lead to convection and the disruption of the concentration distribution of the macroion. The extent of the influence of a non-uniform E field on the concentration distribution is difficult to measure and is currently unanswered. Altering the dimensions of the cuvette could indicate the significance of the non-uniform E field since the fractional amount will decrease with increasing optical pathlength.

Electrophoretic migration of charged molecules past stationary charged surfaces, or

Figure 1. Potential concentration profile of a moving boundary if the environment at the cuvette wall promotes either acceleration (—▫—)or retardation (—△—) of a particle's migration compared to that in the bulk solution

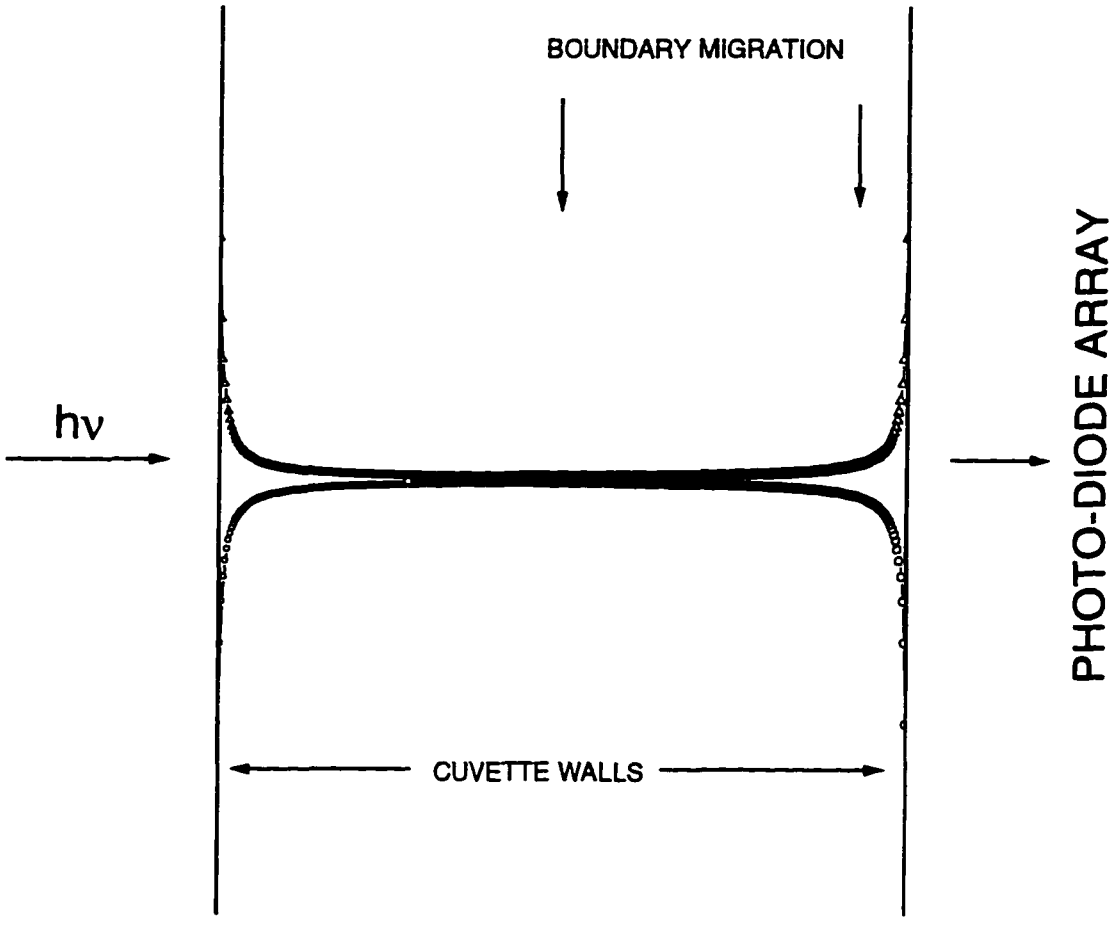

electroosmosis, can result in non-laminar flow and, consequently, the distortion of the macroion concentration distribution in the AEA. The quartz cuvette and the dialysis membranes employed in the AEA contain slight negative charges which will result in an unequal distribution of charge in the adjacent fluid. Electroosmosis has the property of being field dependent. Measurements that exhibit an unexpected field dependence may reflect the consequences to electroosmosis. Thus, the extent of disruption to laminar flow due of electroosmosis is most likely to be observed in velocity measurements, steady state concentration distributions, and electric field dependence of the diffusion coefficient.

The regenerated cellulose membranes used in the AEA contain slight negative charges. Attraction or repulsion of elements of the solution can potentially alter the normal flow through the cuvette. By varying the pore size, and therefore, the amount of membrane (See MATERIALS and METHODS), the extent of membrane perturbation can be investigated.

Flow from sources other than electrophoresis or diffusion can disrupt laminar flow and can introduce an additional velocity term unaccounted for in theory. Extraneous flows, or bulk fluid flow, can be either electric field dependent or independent. Electric field dependent bulk fluid flows can come from the electrophoretic migration of hydrated ions or from the osmotic pressure differences at the two membranes. A zero-field bulk fluid flow can come from hydrostatic pressure differences across the cuvette.

A difference in the number of water molecules in the hydration spheres of the cation and anion of the solvent can lead to bulk fluid flow. If the sum of the flows of the current carrying hydrated ions is not zero (i.e. one ion type carries more water with it), then there will be a net flow of material. Similar to the investigation into electroosmosis, the influence of this

bulk fluid flow on the AEA-determined charge properties is most likely to be observed in the electric field dependency of macroion mobility, SSE gradients and diffusion profiles. Direct comparison of these measurements in two different salt conditions which should have alternate directions of bulk fluid flow should indicate the severity and electric field dependency of this phenomena. Using chloride salts of either larger [Li^+] or smaller [$(CH_3)_4N^+$] cation hydration spheres (compared to chloride's) should produce bulk fluid flows in opposite directions.

The asymmetric distribution of macroions in the AEA raises the concern of an induced *osmotic flow* capable of altering the concentration distribution of the macroion in ways unaccounted for by present theory. If osmotic flow is a significant concern, then situations leading to a build-up of macroions at the bottom of the cuvette membranes and a depletion at the top might lead to a flow which impedes electrophoretic migration. This would result in a slowing down of the boundary during an electrophoretic mobility experiment. The concentration gradients established in SSE and diffusion experiments might also be sensitive to osmotic flow.

The AEA is designed to match the flow of buffer through the top and bottom buffer chambers so as to balance the hydrostatic pressure. Exact matches are not always possible. Simulated data suggest that flows as little as a 75 nanoliter per hour can influence SSE gradients (Thomas Moody, Thomas Laue personal communication). The potential influence of hydrostatic pressure differences are investigated by comparing experimental data taken under a variety of mismatched flow rates.

Determine the Effects of Different Monovalent Cations on the Electrophoretic Properties of $pd(A)_{20}$•$pd(T)_{20}$

Different monovalent cations have different affinities for DNA, different size hydration spheres, and different electrophoretic mobilities. Varying the monovalent cation of an XCl salt, while holding the ionic strength constant, allows the investigation of the effects of these ion properties on the electrophoresis of DNA. Accordingly, the four measurements available with the AEA have been made on the $pd(A)_{20}$•$pd(T)_{20}$ in four different chloride salts, Li^+, Na^+, K^+, and $(CH_3)_4N^+$ at 100 mM. The data can be compared to theoretical predictions and previous studies.

The Poisson-Boltzmann description of the ionic atmosphere around a charged macroion has a slight cation size dependency (see THEORY). The ability of the counterion to shield the macroion from experiencing an electric field in a solution containing either Na^+, K^+ or Li^+ (which have similar radii compared to the macroion's), would be similar. The expectation from the Manning counterion condensation theory (see THEORY) is for μ to be nearly independent of the type of cation. Modifications and improvements on these theories generally predict electrophoretic migration to have little cation size dependency.

Ross and Scruggs performed a series of mobility experiments on longer DNA in the early 1960's (52, 53). They found reduction of the DNA's mobility to be consistent with the order of interaction for univalent alkali metal ions to phosphate groups, $Li^+ > Na^+ > K^+, > (CH_3)_4N^+$ (53). They also found ionic strength dependencies for mobilities that were unique for each cation investigated. It was clear from these studies that theoretical prediction could not completely account for experimental observation.

The effects of cation type on the measured diffusion coefficient are expected to arise from a change in the hydrodynamic properties of the DNA. Changes can result from differences in the total volume of the DNA (and the element of solution it carries) due to differences in radius, hydration number and affinities of the cations for DNA. Alternatively, cation induced conformational changes in the DNA, especially if they promote bending or base pair dissociation, can affect the intrinsic frictional coefficient of the species. The volume changes in the DNA predicted with different cations are not expected to lead to substantial differences in D_0 but cation-induced conformational changes have the potential to alter D_0 significantly.

Determine the Effects of Varying the Concentration of KCl on the Electrophoretic Properties of $pd(A)_{20} \cdot pd(T)_{20}$

Theory predicts (8, 10, 27, 19, 20,) that the salt concentration directly affects the number density, and therefore, the shielding capacity of counter-ions around the $pd(A)_{20} \cdot pd(T)_{20}$. AEA investigation of $pd(A)_{20} \cdot pd(T)_{20}$ in 20 mM Tris buffers of varying KCl concentrations (20, 60, 80 and 100 mM) provides data on the relationship between salt concentration and counter-ion shielding.

The distribution of counterions around DNA is a function of the high electrostatic potential of the DNA and the bulk solvent concentration of the counterions. The Debye-Hückel approximate solution to the Poisson-Boltzmann equation predicts that the shielding of the charge on a macroion will follow a square root dependence with ionic strength (see THEORY). To the degree that this shielding is a valid representation of the

solution behavior of DNA, the measured apparent charge and the electrophoretic mobility might be expected to increase with decreasing ionic strength in a square root dependence. Manning's counterion condensation (MCC) theory predicts a 76% drop in the electrostatic potential of the DNA due to condensation (see THEORY). The remaining 24% presumably can participate in Debye-Hückel shielding. Minor increases in Q_{app} and μ with decreasing ionic strength are predicted with MCC.

The change in the diffusion coefficient of $pd(A)_{20} \cdot pd(T)_{20}$ with decreasing ionic strength should not be significant. No structural or hydrodynamic changes to the DNA are expected in the range of salt concentrations used in these experiments. However, the charge-dependent thermodynamic nonideality will increase roughly as the inverse of the salt molality (3, 31) leading to a predicted increase in D with decreasing salt concentration.

THEORY

Reduction of Charge

When considering the electrophoretic properties of macroions, factors such as the formal charge, ion shielding, ion binding, and the hydrodynamic properties of the macroion must be taken into account. The starting point in electrostatic analysis is the formal charge. Simply put, the formal charge is the excess or deficiency of electrons as compared to the number of protons in a molecule. In biochemistry this is most often accomplished by the gain or loss of hydrogen ions. The formal charge can be estimated from the composition of the macroion along with the known acid-base titration behavior of the components of the molecule (under the pH and ionic strength conditions of the solution). Above pH 5, a phosphate group in the backbone of nucleic acids readily gives up a hydrogen ion and adopts a negative charge. For double stranded DNA in millimolar salt at pH 8 the formal charge is estimated to be equal to the total number of phosphates.

The electrostatic potential produced by a highly charged macroion such as DNA results in the attraction of counter-ions and the repulsion of co-ions. "The free energy of interaction between a central ion and its surrounding counterions or *ion atmosphere* is responsible for the deviation from ideality of the dilute solutions of electrolyte."[1] Fundamental work by Gouy (19, 20) and Chapman (8) led to the development of the concept

---

[1]Eisenberg, D., Crothers, D., (1979) Physical Chemistry with Applications to the Life Sciences, page 354

of a double layer based on the Poisson-Boltzmann (PB) equation. These theories address the relationship between a charged species and an electrolyte solution. The resultant decrease of the electrostatic potential (screened Coulomb potential) of the DNA due to the presence of counterions is an important consideration in the interpretation of electrophoretic migration.

Ionic Shielding

The Debye-Hückel theory (10, 13) is a linear approximation of the PB equation in which the distribution of counterions depends upon the macroion's potential and the solution's ionic strength. One parameter that characterizes the distribution of counterions around a macroion is the Debye length, κ^{-1}, which is the most probable distance from the macroion to find a counterion, or equivalently, it is the radius of a sphere, centered on the macroion, in which the greatest density of counterion charge exists. The inverse of the Debye length is:

(12)
$$\kappa = \left(\frac{8\pi N_a e^2}{1000 \epsilon k_b T} \right)^{1/2} I^{1/2}$$

where ϵ is the dielectric constant of the bulk solution, N_a is Avogadro's number, and I is the ionic strength of the solution (mol/L).

The Debye length can be used to describe the distance dependence (r) of the electrostatic potential, ϕ_r, of the macroion in an ion atmosphere:

(13)
$$\phi_r = \phi_{ion} \frac{\exp^{-\kappa(r-a)}}{1+\kappa a}$$

with

$$\phi_{ion} = \frac{Ze}{\epsilon r} \quad (14)$$

where ϕ_{ion} is the potential of the isolated macroion, Z is its formal charge, and a is the center to center distance of closest approach between the macroion and the counterion, and $\exp^{-\kappa r}$ is the *screening factor.*

An effective charge, Q_{eff}, can be predicted due to the lower electrostatic potential,

$$Q_{eff} = Z - Z\left(\frac{\kappa a}{1 + \kappa a}\right) \quad (15)$$

This charge can be pictured as residing at the center of a non-conducting sphere of radius a. If the electrical double layer were to fall at this same radius, then the electrostatic driving force would be proportional to Q_{eff}.

The greater the ionic strength of the solution, the larger κ becomes, and the greater the shielding of the macroion potential. The importance of the counterion distribution in AEA measurements lies in the ability of the counter-ions to *shield* the macroion from experiencing an applied electric field, and the degree to which the ion cloud can be considered as a *part* of the migrating macroion.

Counterion-Condensation

The high electrostatic potential of DNA is theorized to generate counterion binding, or condensation, as a means of reducing the energetically unfavorable high potential (37, 50, 58). A counterion condensed on the DNA neutralizes an amount of negative charge equal

to its valence. The formal charge of the DNA will be reduced as follows;

(16) $$Z_M + nZ_i = Z_{net}$$

where Z_M is the formal charge of the DNA, n is the number of counterions of valence Z_i bound, and Z_{net} is the net or effective valence of the DNA.

The Manning counterion condensation theory (MCC) is an interpretation of the PB equation in which the high electrostatic potential of a linear polyion dictates the local behavior of counterions (35-38). In particular, Manning contends that counterions condense on the surface of a linear polyion (thereby neutralizing charge) to a degree that is dependent on the distance separating the individual charges of the macroion, but in a fashion that is independent of the solvent ionic strength (except at very low salt concentrations). It should be noted that for the monovalent cations such as Na^+ and K^+ condensation refers to the cations as being "localized" to the surface of the DNA. That is, these cations do not behave like site bound ions, but are *territorially bound* and capable of migrating along the surface of the DNA.

MCC describes the fraction (*f*) of the macromolecular charge *compensated* by ion condensation as

(17) $$f = 1 - \left(\frac{e^2}{\varepsilon k_b T b} \right)$$

where b is the distance between charges on the polyion. For $pd(A)_{20}\bullet pd(T)_{20}$, where b is 0.17 nm, *f* is equal to 0.76. Therefore, only 24% of the formal charge of 40 e is unneutralized. It is theorized that the remaining charge participates in the development of a Debye-Hückel

counter-ion cloud. The MCC predicts that the apparent charge and hence the electrophoretic mobility will be lower than those predicted by the Debye-Hückel theory alone.

As with the DH counterion cloud, the effect of condensed ions on electrophoretic behavior is complicated. It is reasonable to expect the effect on the charge of the macroion from territorially bound counterions to be straight forward and identical to site bound counterions. However, the very high counterion concentration makes it difficult to predict the true extent of the electric field in the immediate vicinity of the macroion.

Theoretical Predictions of the Apparent Charge of 20 Base Pair DNA

Building on advances in the interpretation of the Poisson-Boltzmann equation and counterion condensation theory, estimates of the charge of an oligonucleotide in solution have been made. Record and Lohman (49) combine the polyelectrolyte theories of MCC and DH to generate an empirical counterion association parameter, Ψ, which can be used to find a predicted charge (Q_{pred}) ;

(18) $$Q_{pred} = N[1 - \Psi]$$

where N is the total number of phosphates (nucleotides). For double stranded DNA (N>100) in a helical conformation ,$\Psi^{helix} = 0.88$. This means that long double stranded DNA will expose only 12% of its formal charge. This is consistent with a 1.2 M concentration of condensed counterions around the DNA (37). However, for N <100, the electrostatic potential near the end of DNA is less than that found in the central portion of the DNA and must be taken into account (44). Consequently, counterion condensation and Debye-Hückel shielding are reduced. Addressing this concern, Record and Lohman propose that for helical

oligonucleotides (N<100) Ψ^{helix} is reduced by an empirical factor:

(19) $$\Psi_N^{helix} = 0.88 - \frac{2.53}{N}$$

For N = 40, Ψ^{helix} is equal to 0.82 which yields a $Q_{pred,\Psi}$ of 7.4 e.

Grand canonical Monte Carlo simulations have been carried out to demonstrate the importance of end effects and to refine predictions of the apparent charge (45). Simulations sought to predict the preferential interaction parameter Γ which encompasses all effects that cause the electrolyte concentration in a compartment containing the oligonucleotide to differ from a compartment absent of the macroion. The value of the preferential interaction coefficient for an oligonucleotide of N phosphates, Γ_N, is simulated by reducing the preferential interaction coefficient predicted for an infinite length oligonucleotide, Γ_∞;

(20) $$-\Gamma_N = -\Gamma_\infty + \frac{G}{N}$$

where G is an empirical adjustment parameter dependent on N. A Q_{pred} can be obtained from Γ_N and equation 18 using the following relationship with Ψ;

(21) $$\Psi_{\Gamma_N} = 1 + 2\Gamma_N$$

For N = 40, $-\Gamma_N$ is equal to 0.300 which yields a $Q_{pred,\Gamma}$ of 17.0 e. At this time there is no explanation for the discrepancy between these two ways of calculating Q_{pred}.

Theoretical Description of the AEA Measurements

Electrophoretic Mobility

Presented here is a simplified theory of electrophoresis. A more detailed analysis is in Appendix 1.

Charged particles migrate under the force (F_1) of an electric field (E),

(22) $$F_1 = Q_{app} E$$

with Q_{app} being the charge of a particle capable of experiencing the electric field. The migrating particle experiences a retarding force or frictional force (F_2) which is proportional to the velocity, v, of the particle

(23) $$F_2 = -v f_e$$

where f_e is the frictional coefficient in an electric field. The f_e encompasses the translational frictional coefficient and other retardation effects (Appendix 1).

In an electrophoretic mobility study, the forces on the migrating macroion are balanced so that a constant-velocity boundary is observed

(24) $$F_1 + F_2 = 0$$

therefore

(25) $$Q_{app} E = v f_e$$

The velocity of the macroion divided by the applied electric field is defined as the electrophoretic mobility, thus

(26) $$\mu = \frac{v}{E} = \frac{Q_{app}}{f_e}$$

It is important to note that both μ and Q_{app} encompass the uncertainties outlined above for the DH and MCC.

A Description of Steady-State Electrophoresis

SSE is a unique capacity of the AEA in which the charge properties of the macroion are extracted from the steady-state concentration gradient created when all fluxes (e.g. those due to electrophoresis, diffusion and bulk flow) are balanced. Simple theory (17, 33, 47) claims that steady-state occurs when the flux of the macroion due to electrophoresis, J_e is equal to the flux due to diffusion J_D;

(27) $$J_e = J_D$$

or

(28) $$c\,v = D_e \frac{dc}{dx}$$

where c is the concentration of the macroion, x is the position along the cuvette, and D_e is the diffusion coefficient in the presence of an electric field.

Using equation 25, the balance of fluxes yields,

(29)
$$\frac{cQ_{app}E}{f_e} = D_e\frac{dc}{dx}$$

The resultant relationship can be expressed as an exponential;

(30)
$$c(x) = c_o \exp^{\sigma(x-x_o)}$$

with

(31)
$$\sigma = \frac{Q_{app}E}{f_e D_e}$$

where c_o is the concentration at reference position x_0 and σ describes the steepness of the exponential. In practice, both σ and c_o are determined as fitted parameters in equation 30. The SSE data can be viewed as the ratio of experimentally determined values.

(32)
$$\frac{\sigma}{E} = \frac{Q_{app}}{D_e f_e}$$

The apparent charge, Q_{app}, can be determined from equation 32 using the measured experimental parameters, known constants, and assuming the Einstein-Stokes relationship for the diffusion coefficient ($D_e f_e = k_b T$) holds (14) in an electric field in the presence of salt ions and buffer, and using a definition for the electric field ($E = I/\kappa A$),

(33) $$Q_{app} = \frac{\sigma k_b A T \kappa}{I}$$

where I is the current in amps, κ is the specific conductivity of the solution in seimens/cm^2, and A is the cross sectional area of the cuvette in cm^2.

A predicted mobility, μ_p, can be obtained from the combination of SSE data and a diffusion constant,

(34) $$\mu_p = \sigma \frac{D_e}{E} = \frac{Q_{app}}{f_e}$$

The effects of a net bulk fluid flow through the cuvette on the velocity of the macroion can be estimated by the addition of a velocity term to the relationship described in equation 26;

(35) $$v = \mu E + v_o$$

where v_o is the zero-field velocity of the macroion due to the bulk fluid flow. Consistent with experimental observation and simulated data, the expected magnitude of v_o is small compared to overall velocity in all but the lowest fields used in SSE. The effects of v_o on the true σ, or σ_t, can be estimated;

(36) $$\sigma_a = \sigma_t + \frac{v_o}{D_e}$$

where σ_a is the expected σ in the presence of a bulk fluid assuming σ_t is field independent. The σ_a/E for a particular v_o can calculated from the following equation and compared to experimentally-determined values using:

(37) $$\frac{\sigma_a}{E} = \frac{\sigma_t}{E} + \left(\frac{\sigma_t}{E}\right)\frac{v_o}{\mu E}$$

Diffusion in the Absence of an Electric Field

Concentration gradients are formed during SSE and electrophoretic mobility experiments. Dissipation of these gradients is dependent on the hydrodynamic properties of the species forming the gradient. The diffusion and, therefore, the friction coefficient can be ascertained by monitoring the collapse of a concentration gradient either in the presence or the absence of an electric field.

Transport theory (64) states that an effective force arising from a concentration gradient can be calculated by differentiating the chemical potential with respect to the distance x (assuming u° does not rely on distance x and the E field = 0)

(38) $$u = u^\circ + RT\ln c$$

with

(39) $$\text{Force} = -\frac{du}{dx} = -RT\frac{d\ln c}{dx}$$

In the AEA, the diffusion coefficient in the absence of an electric field, D_o, of a particle

can be obtained from monitoring the relaxation of a gradient (Figure 27 in RESULTS) and employing a variation of the method described by Harned and French (23) in which the time-dependent difference in concentrations at *conjugate* positions (e.g. x_1L and x_2L in which L is the path length of the cuvette and $x_1 + x_2 = 1$) are measured. It can be shown (56) from a separation of variables and using a Fourier series expansion in x that, for times t such that $\pi^2 D_o t/L^2 > 1$:

(40)
$$\ln(\Delta c) \approx \ln B - Dt\left(\frac{\pi}{L}\right)^2$$

where $\Delta c = c_{x2} - c_{x1}$, and B is a constant relating to the initial conditions (DNA concentration, c_o, and initial σ). Using just this first order term of the expansion, along with the 1/3 and 2/3 conjugate positions, yields good approximate solutions for D_o at sufficiently large times (56).

An independent method for determining the diffusion coefficient D_o employs analytical ultracentrifugation (64). Sedimentation velocity experiments yield the sedimentation coefficient s^*, which can be used to calculate the hydrodynamic frictional coefficient, f_o, from the relationship:

(41)
$$f_o = \frac{M(1-\nu\rho)}{s^* N_a}$$

where M is the molecular weight of the macroion, ν is its partial specific volume, ρ is the solvent density, and N_a is Avogadro's number.

The hydrodynamic diffusion coefficient, D_o, is determined from f_o assuming the

Stokes-Einstein relationship:

(42)
$$D_o = \frac{k_b T}{f_o}$$

Diffusion Coefficient in the Presence of an Electric Field

The mathematical model (56) for determining the diffusion coefficient in the presence of an electric field is based on monitoring the spreading of the boundary during mobility measurements. Similar to the SSE derivation (Equation 27), development of the model begins by considering the fluxes of the macroion in electric field.

(43)
$$J = -D\frac{dc}{dx} + cv$$

Using equations 28 and 29, the flux of the macroion can be written,

(44)
$$J = -D\frac{dc}{dx} + c\frac{Q_{app}E}{f_e} = -D\frac{dc}{dx} + cE\mu$$

The change in the concentration of the macroion with time is the derivative of the flux with respect to time,

(45)
$$\left(\frac{\partial c}{\partial t}\right) = -\left(\frac{\partial J}{\partial t}\right) = D\left(\frac{\partial^2 c}{\partial x^2}\right) - \mu E\left(\frac{\partial c}{\partial x}\right)$$

The solution for equation 45 can be approximated for an infinite cell (56). Under these

conditions, the moving boundary in an electrophoretic mobility experiment is an error function. The peak generated when successive scans are subtracted can be fitted to a modified Gaussian,

$$\frac{\Delta c}{\Delta t} = A(x + \mu E t)\, e^{\frac{-(x-\mu E t)^2}{W^2}} \tag{46}$$

with

$$A = \frac{c^{o}}{(16\pi D_e)^{\frac{1}{2}}}\, t^{-\frac{3}{2}} \tag{47}$$

where W is the width at 1/exp of the peak. The width of the peaks are determined concomitantly with velocity determination in mobility experiments. D_e is experimentally determined by fitting a line to the graph of $W^2/4$ as a function of t. The error in D_e determination due to the assumptions in the approximate solution have been shown using simulated data to be less than 10% (Tim Wilson personal communication). Experimentally however, *any* spreading of the moving boundary will be assimilated into D_e.

Molecular Weight Determination and Charge Estimate from Sedimentation Equilibrium

In a sedimentation equilibrium experiment, the molecular weight of a non-associating species can be determined by fitting to an exponential gradient (24, 28, 42). Under thermodynamically ideal conditions the fitting equation is

(48)

$$c(r) = c_0 e^{\frac{M(1-v\rho)}{2RT}\left(\frac{r^2}{2}-\frac{r_o^2}{2}\right)\omega^2}$$

where c_o is the concentration at r_o, M is the molecular weight, ω is the angular velocity and R is the gas constant.

Solutions of nucleic acids are highly non-ideal due to the large charge-charge repulsion between macroions. Equation 48 can be expanded to include the nonideality of charge-charge interactions by means of the second virial coefficient, B:

(49)

$$c(r) = c_0 e^{\frac{M(1-v\rho)}{2RT}\left(\frac{r^2}{2}-\frac{r_o^2}{2}\right) - BM(c_{(r)}-c_o)\omega^2}$$

An estimated Q can be obtained from B (assuming excluded volume and salt-DNA contributions to B are small compared to the charge-charge repulsion effects) from

(50)

$$Q = \left(\frac{4BM^2 m_3}{10^3 v_1}\right)^{\frac{1}{2}}$$

where M is the anhydrous molecular weight of the DNA, m_3 is the molality of the salt, and v_1 is the solvent specific volume (60).

MATERIALS and METHODS

Physical Description of the Apparatus.

A schematic design of an AEA cell can be found in Appendix 2. Briefly described, the objective of the device is to create and monitor the concentration distribution of a macroion in a sealed analysis chamber. The analysis chamber is a $(0.2\ cm)^3$ fused silica cuvette bounded on the top and bottom by dialysis tubing which is sealed by O-rings over the openings to the buffer chambers. Each chamber is filled from a reservoir and drains into an outer chamber containing the electrode. An electric field is generated by passing a current between the two electrodes. A peristaltic pump continuously flows solvent (20-40 ml/hr) through the buffer chambers and past the membranes to flush out electrolysis products and to minimize ion gradients in the cuvette due to electrodialysis.

The entire cell assembly is inserted into a water-jacket for thermal control. The set-up is aligned in a collimated light beam to project the transmitted light through the cuvette and onto the photo diode array.

The current is supplied by a Keithley 224 programmable current source

Membranes

The dialysis membranes that form the semipermeable barriers at the top and bottom of the cuvette are composed of regenerated cellulose. The membranes are designed to carry no fixed charge, but are thought to harbor a slight negative charge due to the oxidation of hydroxyl groups. The membrane casting procedure is such that the amount of regenerated

cellulose per unit area decreases with increasing membrane pore size. Three different molecular weight cut-off (MWCO) membranes were used these experiments; Spectro/Por 3°, 3500 MWCO, Spectro/Por° 1 6-8K, and Spectro/Por 4°, 10-14K MWCO membranes.

Buffers.

All buffer components used in these experiments were reagent grade and purchased from Sigma. The pH of each buffer was adjusted to 8.00 ± 0.05 with an Orion Research 811 pH meter. The specific conductance of the buffers were determined with a VRW Scientific 1052 conductivity meter. Buffers were made in 2 or 4 liter batches (corresponding to 2-4 or 4-8 days worth of experiments)

$pd(A)_{20}$ •$pd(T)_{20}$

The single strand oligonucleotides used to produce $pd(A)_{20}$ •$pd(T)_{20}$ DNA were synthesized and purified by Research Genetics of Huntsville Alabama; $pd(A)_{20}$ sequence # d5041033 and $pd(T)_{20}$ sequence #d50410034. The complementary single strands were mixed and heated to 65 °C in 200 mM KCl, 20 mM Tris, pH 8.0 and then allowed to anneal upon cooling. The double stranded product was verified (by O.D., melting temperature, and circular dichroism) in the laboratories of Dr. Jonathan B. Chaires at the University of Mississippi Medical Center. Prior to use, the oligonucleotides were stored in BPES in a minus 70 freezer .

Experimental Protocol Summary

Electrophoretic Mobility Determination

Experimentally, the mobility of $pd(A)_{20}$•$pd(T)_{20}$ is obtained from the monitoring of the

constant-velocity boundary formed by passing an electric field through the analysis chamber containing an initially homogenous concentration of DNA. Intensity scans (260 nm) of the oligonucleotide migrating to the bottom of the cell (toward the anode) are taken at precise, regular intervals (Figure 2a). Depending on the strength of the fields, the intervals varied between 10 and 60 seconds.

Subtracting successive timed scans yields $\Delta c/\Delta t$ plots (actually, intensity scans are used) in which the peak position represents the center of the boundary (Figure 2b). The position of the peak is determined by fitting the data to equation 46 (determined concomitant with D_e). The peak positions are graphed as a function of the time and the slope of the best fit line is used to estimate of the velocity of the boundary (Figure 2c). Dividing this velocity by the electric field gives μ.

Examination of the μ's at high and low fields is hindered by limitations imposed by the 2 mm-long cells. At low fields (< 0.3 V/cm) the boundaries are poorly defined due to the low velocities of the DNA compared to the rate of diffusion. At high fields (>6.0 V/cm) the boundary moves fast enough that $\Delta c/\Delta t$ is not a sufficiently accurate approximation of dc/dt in equation 46. Additionally, at high fields the boundary reaches the bottom of the cell so fast that an insufficient number of points are obtained to determine a velocity accurately.

Analytical Ultracentrifugation

Sedimentation coefficients, molecular weights, and second virial coefficients, were obtained using a Beckman XLA analytical ultracentrifuge using absorbance optics and a 4-hole titanium rotor. Sedimentation equilibrium experiments used 6-channel Yphantis cells with 12-mm thick Kel-F centerpieces and sapphire windows. Data were collected at 20 °C,

Figure 1. Procedure for electrophoretic mobility determination in the AEA. A 1.7 V/cm experiment with $pd(A)_{20} \cdot pd(T)_{20}$ in 100 mM KCl, 20 mM Tris, pH 8.0, 20 °C: (a) Transmittance profiles of the migrating boundary taken at ■ 2 min., □ 3.25 min. and ○ 5 min. (b) Subtracted timed scans ($\Delta c/\Delta t$) at ■ 2 min, □ 3.25 min, and ○ 5 min.(c) Peak positions of the $\Delta c/\Delta t$ graphs as a function of the 15 second intervals (time between scans). The slope of the best fit line is an estimation of the velocity of the boundary

a

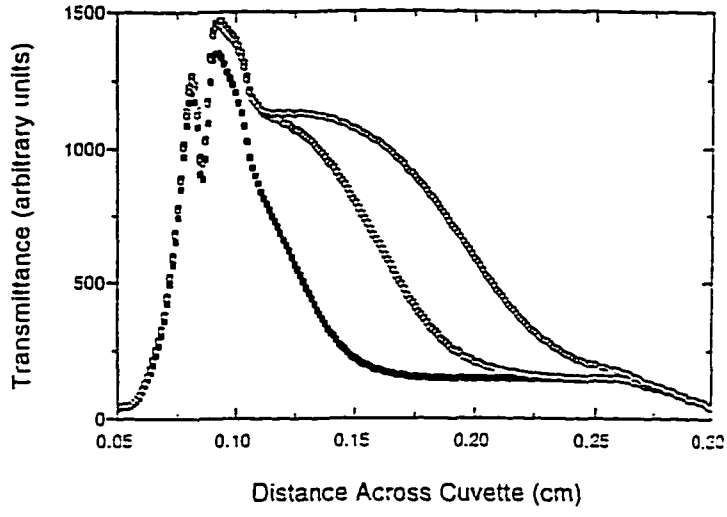

b

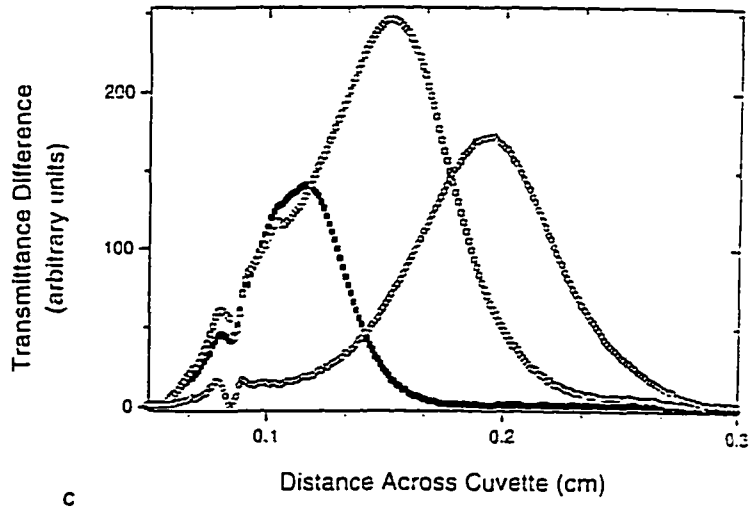

c

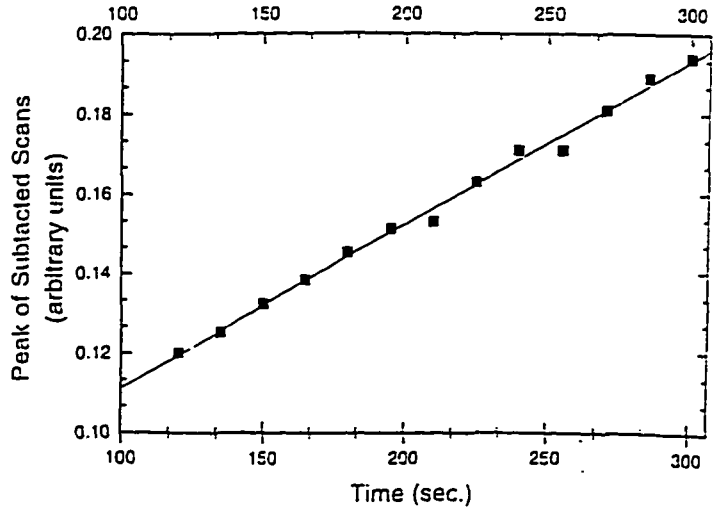

at four or five rotor speeds ranging from 25,000 to 50,000 rpm, at serial dilutions of 1:1, 1:3, and 1:9, and with initial concentrations of approximately 50 μg/ml. Equilibrium was verified by subtracting successive scans (65). The data were edited using REEDIT and analyzed with the nonlinear least square fitting program NONLIN (28). Molecular weights and the second virial coefficient were obtained by fitting multiple channels of sedimentation equilibrium data obtained at different loading concentrations, radial position, and rotor speeds to equation 48. In all data analysis, the partial specific volume used for $pd(A)_{20} \cdot pd(T)_{20}$ was 0.55 (11). A calculated buffer density of 1.0015 g/ml was used.

Sedimentation velocity experiments used double sector cells with charcoal-filled epon centerpieces, quartz windows, and absorbance optics. The apparent sedimentation coefficient s* was calculated according to Stafford (57). Experiments were carried out at 60,000 rpm and 20 °C, with concentrations of 50μg/mL Data were converted to 20 °C in pure water from s* using the method described by (21):

(51)
$$s_{20,w} = s^*_{20,b} \frac{(1-\nu\rho)_{20,w}\,\eta_{20,b}}{(1-\nu\rho)_{20,b}\,\eta_{20,w}}$$

where η is viscosity, and the subscripts refer to the quantity (e.g. solvent density) at the experimental temperature (20 °C) and buffer condition (either water or buffer) respectively.

Capillary Zonal Electrophoresis

The homogeneity of the DNA sample was tested with fractionation by charge in an Hewlett-Packard HP^{3D} CE and by polymeric sieving in a Bio-Rad Bio-Focus 3000.

Verification of duplex 20 base pair DNA was accomplished by comparing the elution times (based on charge) of $pd(A)_{20}$•$pd(T)_{20}$ to a triplex oligomer [$pd(A)_{20}$] $_2$ $pd(T)_{20}$ under conditions that cause one poly A strand to fall off. The $pd(A)_{20}$•$pd(T)_{20}$ elution profile had one prominent peak corresponding to the putative duplex peak (a single strand peak was also seen) from the [$pd(A)_{20}$] $_2$ $pd(T)_{20}$ elution profile. Polymeric sieving of $pd(A)_{20}$•$pd(T)_{20}$ requires conditions unfavorable to duplex DNA (low salt concentration and high temperatures). The elution profile showed three close peaks. It is speculated that if these peaks represent legitimate species that they might represent the fully phosphated $pd(A)_{20}$•$pd(T)_{20}$ along with 20 base pair DNA that have had one or both terminal phosphates removed.

Conversion of Units

The units for Q_{app}, as determined by SSE and μ, are g $cm^2/V\ sec^2$. To convert these units to the charge on an electron the following dimensional analysis is used:

$$\frac{1 g cm^2}{V sec^2} = \left(\frac{erg}{\frac{g cm^2}{sec^2}}\right)\left(\frac{joule}{10^7 erg}\right)\left(\frac{V}{\frac{joule}{coul.}}\right)\left(\frac{e}{1.6\times10^{-19} coul.}\right) = 6.25\times10^{11} e \qquad (52)$$

RESULTS

Electrophoretic studies have been carried out in the AEA on the $pd(A)_{20} \cdot pd(T)_{20}$ over a range of electric fields, in 100 mM chloride salts,at various KCl concentrations, and at different oligonucleotide concentrations. All experiments were conducted at 20 °C in a 20 mM Tris buffer at pH 8.0. These investigations have focused on the extent of counterion shielding as measured in an electric field. Additionally, the results of these inquires have been used to address the concern that disturbances due to either the apparatus or the method may affect the interpretation of the observed concentration distribution of the oligonucleotide.

Electrophoretic Mobility

Electrophoretic Mobilities as a Function of Cation Type

The electrophoretic mobility of $pd(A)_{20} \cdot pd(T)_{20}$ was determined in four different chloride salts (100 mM), LiCl, NaCl, KCl, and $(CH_3)_4NCl$. Each cation type has a different affinity for DNA (53, 37), different size hydration sphere (6, 39), and different electrophoretic mobility (6, 31) (see Table 1). These different cation features are theorized to have different influences on DNA mobility (52, 53).

Figure 3 shows the electrophoretic mobilities of the oligonucleotide in the four salts as a function of electric field. Two main observations can be made. First, there is a cation dependency to the magnitude of the μ's that follows cation affinity for DNA (53). The large cation $(CH_3)_4N^+$, with the lowest DNA affinity, has the highest μ. Similarly, Li^+, with the

TABLE 1

PROPERTIES OF MONOVALENT IONS

Ion	[a] Anhydrous radius (nm)	[b] Hydration number	[b] Molar volume of Hydrated ion ($cm^3\ mol^{-1}$)	[c] Electrophoretic mobilities ($cm^2/V \cdot s$) x 10^4
K^+	0.133	5.1	94.4	7.62
Na^+	0.102	6.5	109.0	5.19
Li^+	0.060	7.4	125.9	4.01
$(CH_3)_4N^+$	0.280	1.8	115.4	4.65
Cl^-	0.181	3.9	93.6	7.91

[a] From Marcus reference (39), crystal ionic radii.
[b] From Marcus reference (39) using Stokes radii
[c] Converted from Burgess reference (6) of limiting ionic conductivities by dividing by 1 Faraday (96,490 coulombs/equiv)

Figure 3. The electrophoretic mobility of $pd(A)_{20}$·$pd(T)_{20}$ (95% confidence intervals) in 100 mM XCl, 20 mM Tris, pH 8.0, 20 °C:-···■···KCl,···□···NaCl,—●—LiCl,- -○- -$(CH_3)_4NCl$

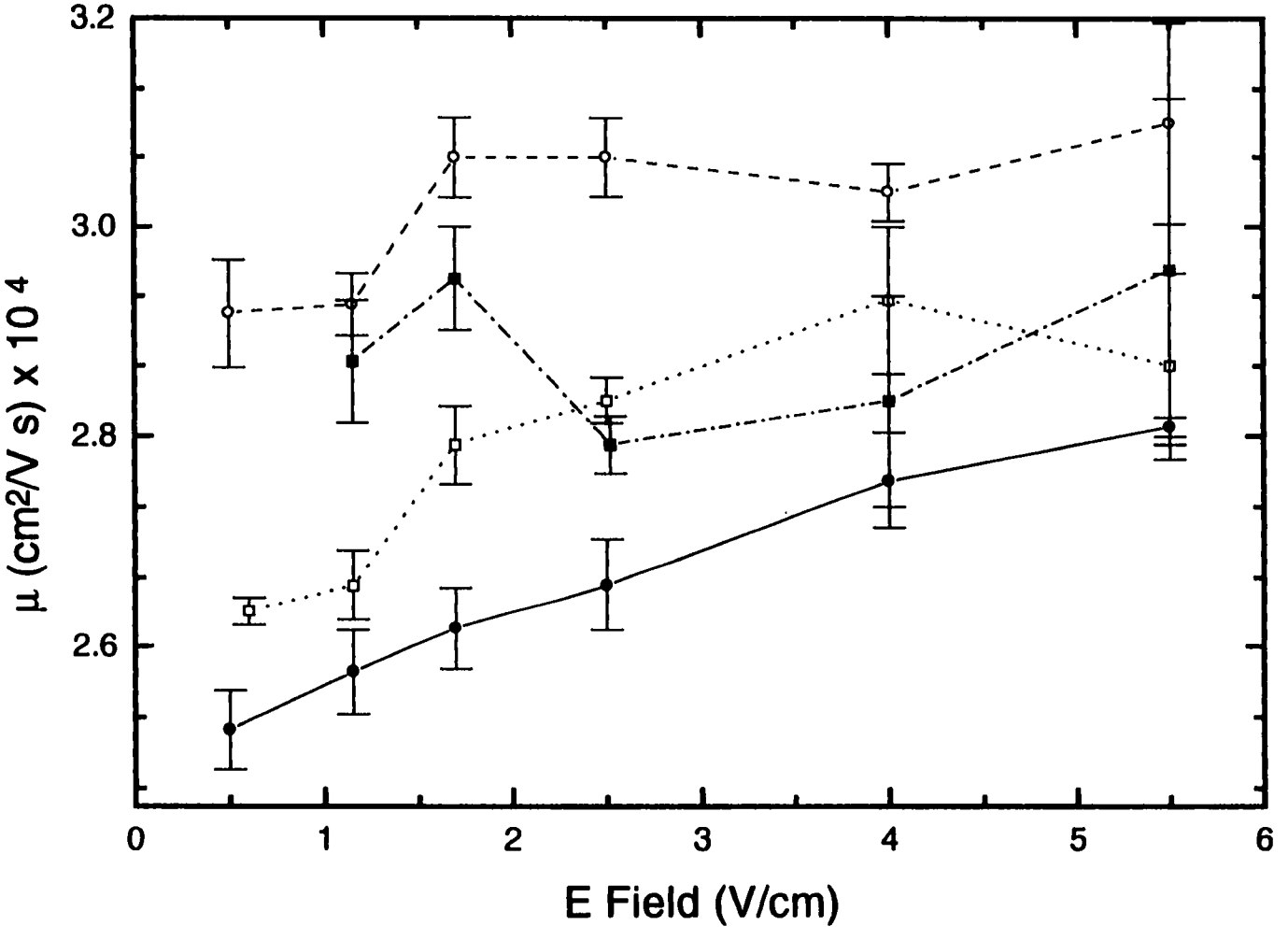

highest DNA affinity, has the lowest μ. Second, in contrast to simple theory and previous experimental observation, the mobilities decrease with decreasing electric fields in a manner apparently independent of cation type.

Examining the DNA's velocity as a function of the electric field can provide insight into the solvent's role at low fields. Figures 4 and 5 show the linear regression fit (95% confidence intervals) for the velocity of the $pd(A)_{20}$•$pd(T)_{20}$ in the four chloride salts as a function of electric filed. It is interesting to note that the zero field intercept of the velocity (v_o) for each condition, with the possible exception of KCl, is slightly negative. This raises the concern that there might be a net solvent flow through the cell that influences the low field velocities. Table 2 lists, for $pd(A)_{20}$•$pd(T)_{20}$ in each of the chloride salt conditions, the v_o and v/E from the slope of velocity verses electric field (Figures 4 and 5), and the mean, μ_{ave}, of the individually determined electrophoretic mobilities (Figure 3). Both the v/E's and the μ_{ave}'s yield similar values and follow the trend of cation affinity for DNA.

Electrophoretic Mobilities of $pd(A)_{20}$•$pd(T)_{20}$ as a Function of Ionic Strength

Reducing the ionic strength of the solution lessens the concentration of counterions near the $pd(A)_{20}$•$pd(T)_{20}$ (10). The expectation from the Debye-Hückel interpretation of the ion distribution is that a decrease in the density of counterion proximal to the DNA will reduce the extent of shielding from the electric field. MCC theory predicts a very small ionic strength dependence with the salt concentrations used in these experiments. Figure 6 compares the μ of $pd(A)_{20}$•$pd(T)_{20}$ in KCl salts of decreasing ionic strength. The increase in μ's seen with decreasing ionic strength is consistent with reduced shielding. As seen earlier, the trend of decreasing mobility with decreasing electric field is observed in these salt concentration

Figure 4. The μ_{ave} of $pd(A)_{20}$·$pd(T)_{20}$ as determined by the slope of velocity versus E field (95% confidence intervals): (a) In 100 mM KCl, 20 mM Tris, pH 8.0, 20°C. (b) in 100 mM NaCl, 20 mM Tris, pH 8.0, 20°C

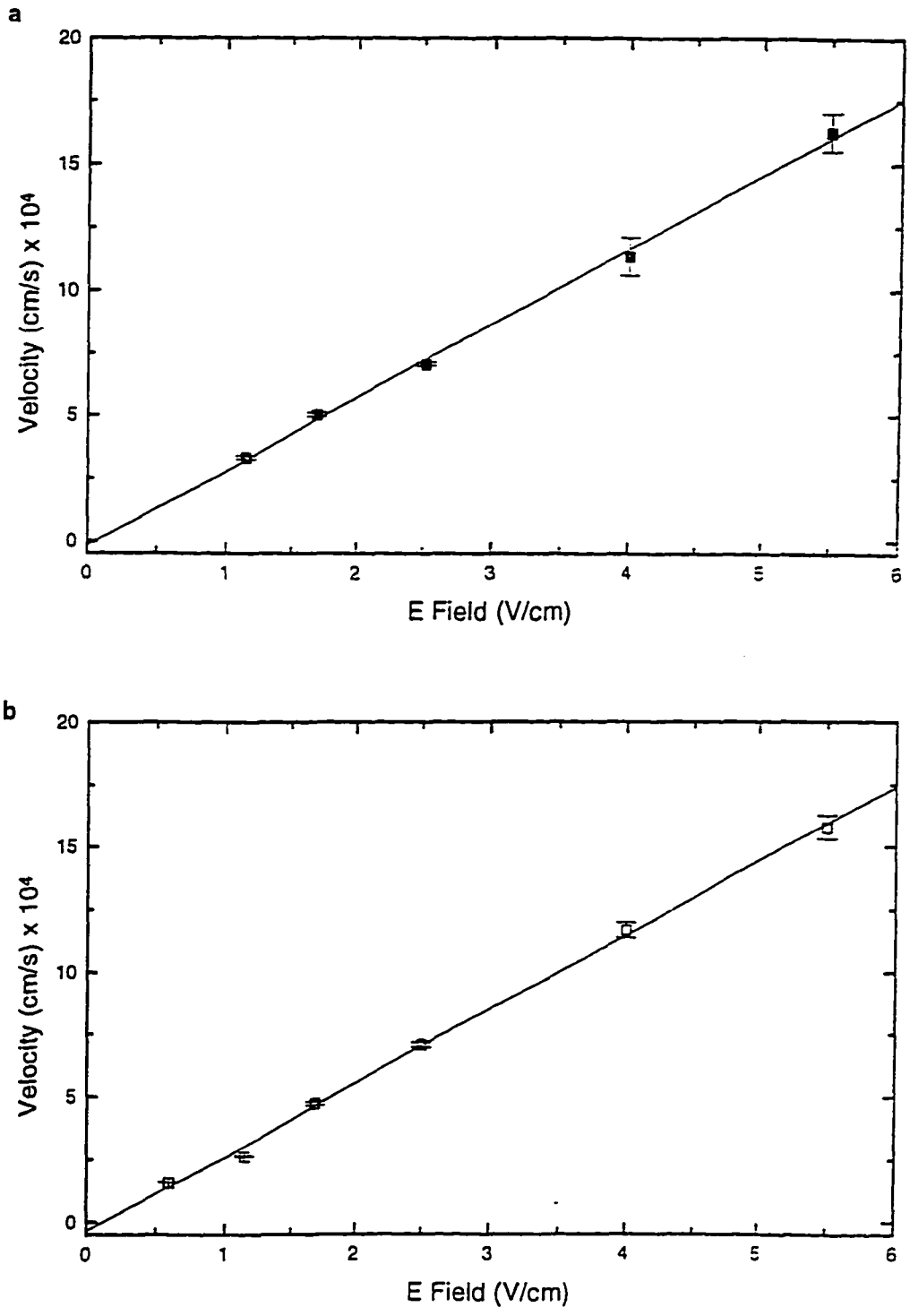

Figure 5. The μ_{ave} of $pd(A)_{20}$·$pd(T)_{20}$ as determined by the slope of velocity versus E field (95% confidence intervals): (a) In 100 mM LiCl, 20 mM Tris, pH 8.0, 20 °C. (b) In 100 mM $(CH_3)NCl$, 20 mM Tris, pH 8.0, 20 °C

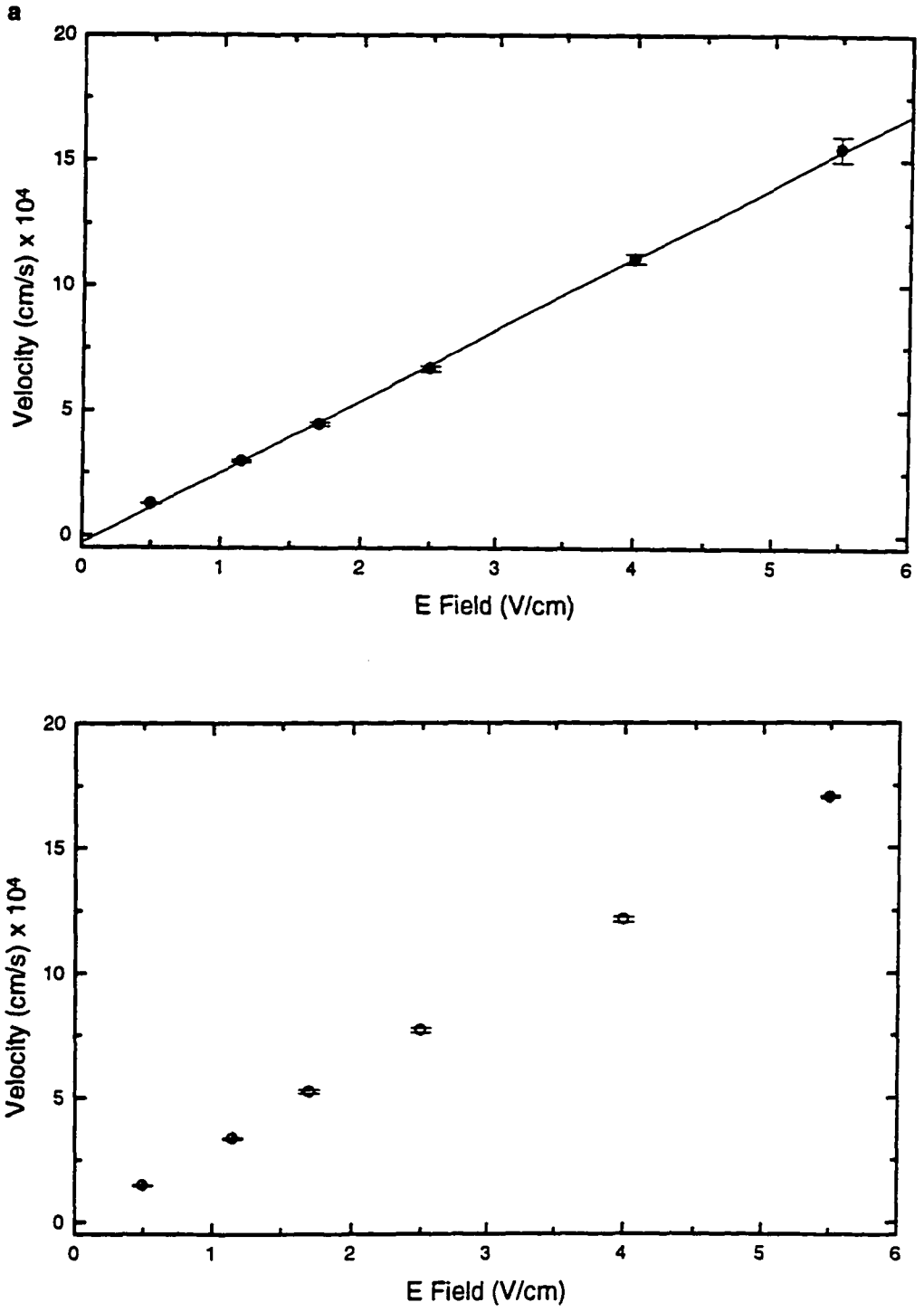

TABLE 2

ELECTROPHORETIC MOBILITY OF $pd(A)_{20} \cdot pd(T)_{20}$
IN DIFFERENT CHLORIDE SALTS

[a] Salt Conditions	[b] v_o (cm/s x 10^{-5})	v/E (cm^2/V s x 10^4)	[c] μ_{ave} (cm^2/V s x 10^4)	[d] Q_{app} (e)
100 mM KCl	-1.93 [e] (-7.28, 7.30)	2.95 (2.80, 3.11)	2.88 (2.74, 3.02)	6.62 (6.30, 6.94)
100 mM NaCl	-3.76 (-7.44, -0.08)	2.96 (2.85, 3.08)	2.79 (2.55, 3.03)	6.41 (5.87, 6.95)
100 mM LiCl	-3.19 (-5.03, -1.35)	2.85 (2.79, 2.91)	2.66 (2.44, 2.88)	6.11 (5.66, 6.66)
100 mM $(CH_3)_4NCl$	-1.29 (-2.86, 0.274)	3.10 (3.05, 3.15)	3.02 (2.86, 3.18)	6.94 (6.58, 7.30)

[a] 20 mM Tris, pH 8.0, 20 °C
[b] Zero field velocity
[c] Mean average of individually determined μ's
[d] Predicted charge from $Q_{app} = (\mu_{ave} \cdot k_b \cdot T/D)$ with D = 11 F
[e] Confidence interval are at 95%

Figure 6. The electrophoretic mobility of $pd(A)_{20}$·$pd(T)_{20}$ (95% confidence intervals) in X mM KCl, 20 mM Tris, pH 8.0, 20°C:

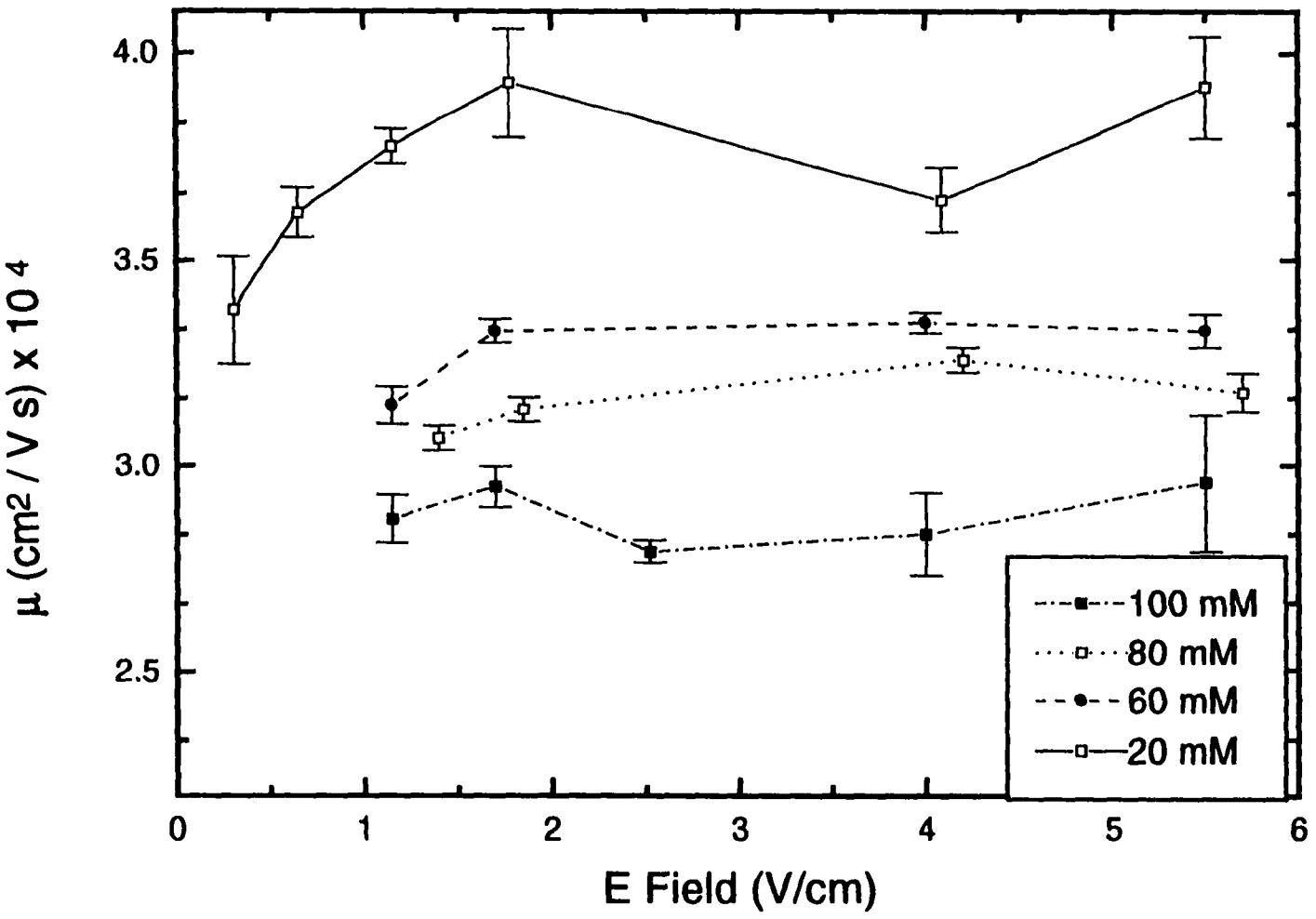

experiments. This particularly pronounced in the 20 mM data. There is no expectation for a phenomenon of this type.

Expressing the mobility data as velocity verses electric fields (Figures 7 and 8) yield mobilities (v/E) consistent with the μ_{ave}'s from the data in figure 6. The v_o's appear to be slightly negative (Table 3) indicating a possible net solvent flow. A μ_o, the mobility in absence of free counterions, can be estimated by extrapolating the plot of μ_{ave} verses the square root of the ionic strength (Debye-Hückel predicts ionic shielding to have this relationship) to zero ionic strength (Figure 9). This yields a μ_{ave} of 3.72 x 10^{-4} $cm^2/Vsec$ and, if a diffusion coefficient of 11.0 F is used, Q_{app} is calculated (Equation 26) to be 9.9 e

Steady-State Electrophoresis

Effects of Varying Cation Type on SSE Measured Charge Properties.

Figure 10 shows the experimentally determined Q_{app} of $pd(A)_{20}$•$pd(T)_{20}$ (150-350 μg/ml) in the four chloride salts conditions as a function of electric field. The individually determined Q_{app} range from approximately 3 e to 6 e. The mid-range electric fields (0.05 to 0.19 V/cm) generate consistent σ's and Q_{app}'s. There appears, however, to be an electric field dependency to the measured Q_{app} at the lowest fields (< 0.05 V/cm), with the Q_{app} at the low fields generally lower than the midrange electric field values.

The estimate of σ at low fields must be viewed with some caution since the data are nearly linear and, therefore, difficult to fit properly with the exponential function (Equation 30). A far better procedure for dealing with near linear gradients is to combine individual SSE data sets taken at different electric fields (for a given buffer condition) into a single

Figure 7. The μ_{ave} of $pd(A)_{20}$·$pd(T)_{20}$ as determined by the slope of velocity versus E field (95% confidence intervals): (a) In 100 mM KCl, 20 mM Tris, pH 8.0, 20°C. (b) in 80 mM KCl, 20 mM Tris, pH 8.0, 20°C

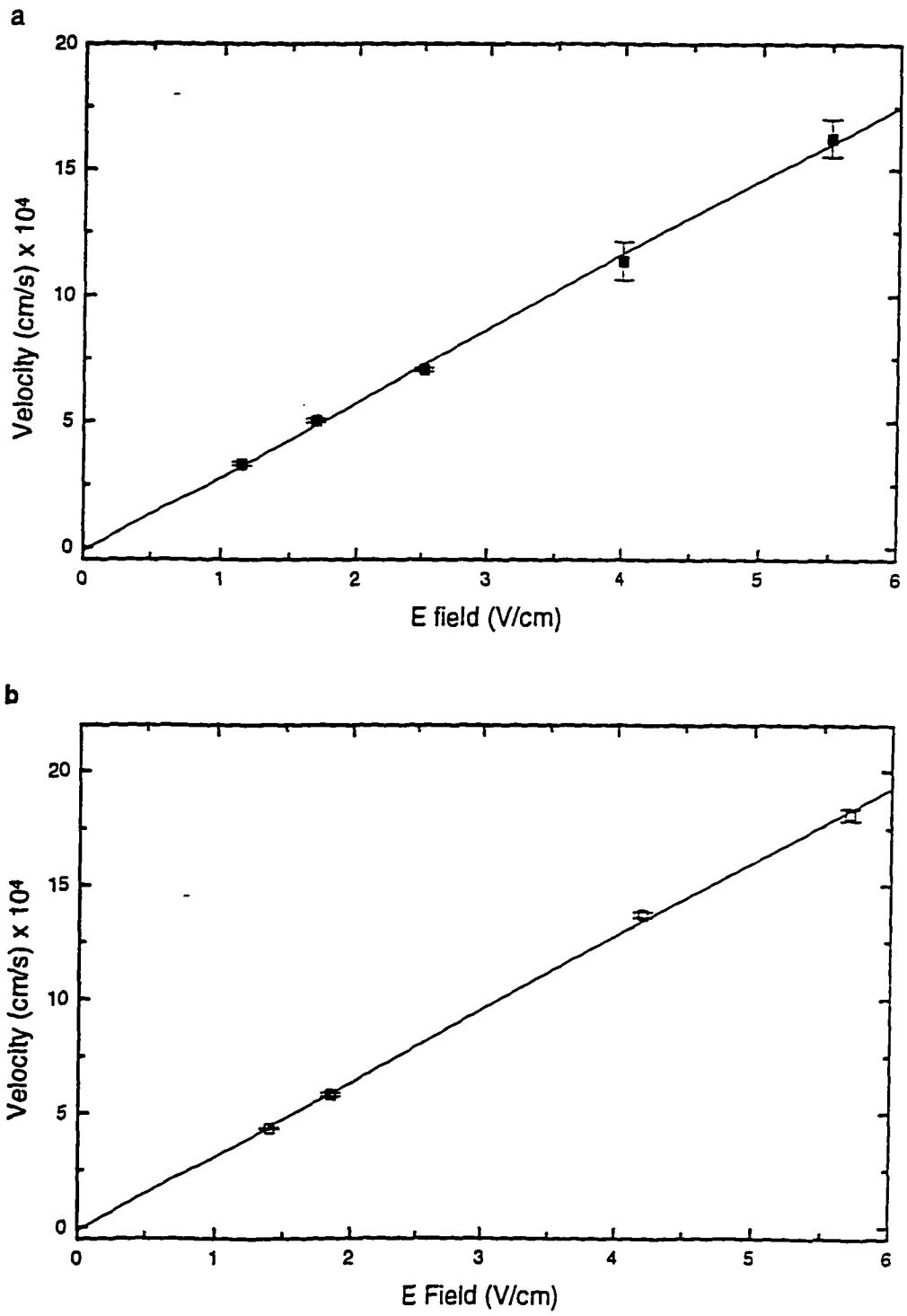

Figure 8. The μ_{ave} of $pd(A)_{20}$·$pd(T)_{20}$ as determined by the slope of velocity versus E field (95% confidence intervals): (a) In 60 mM KCl, 20 mM Tris, pH 8.0, 20°C. (b) in 20 mM KCl, 20 mM Tris, pH 8.0, 20°C

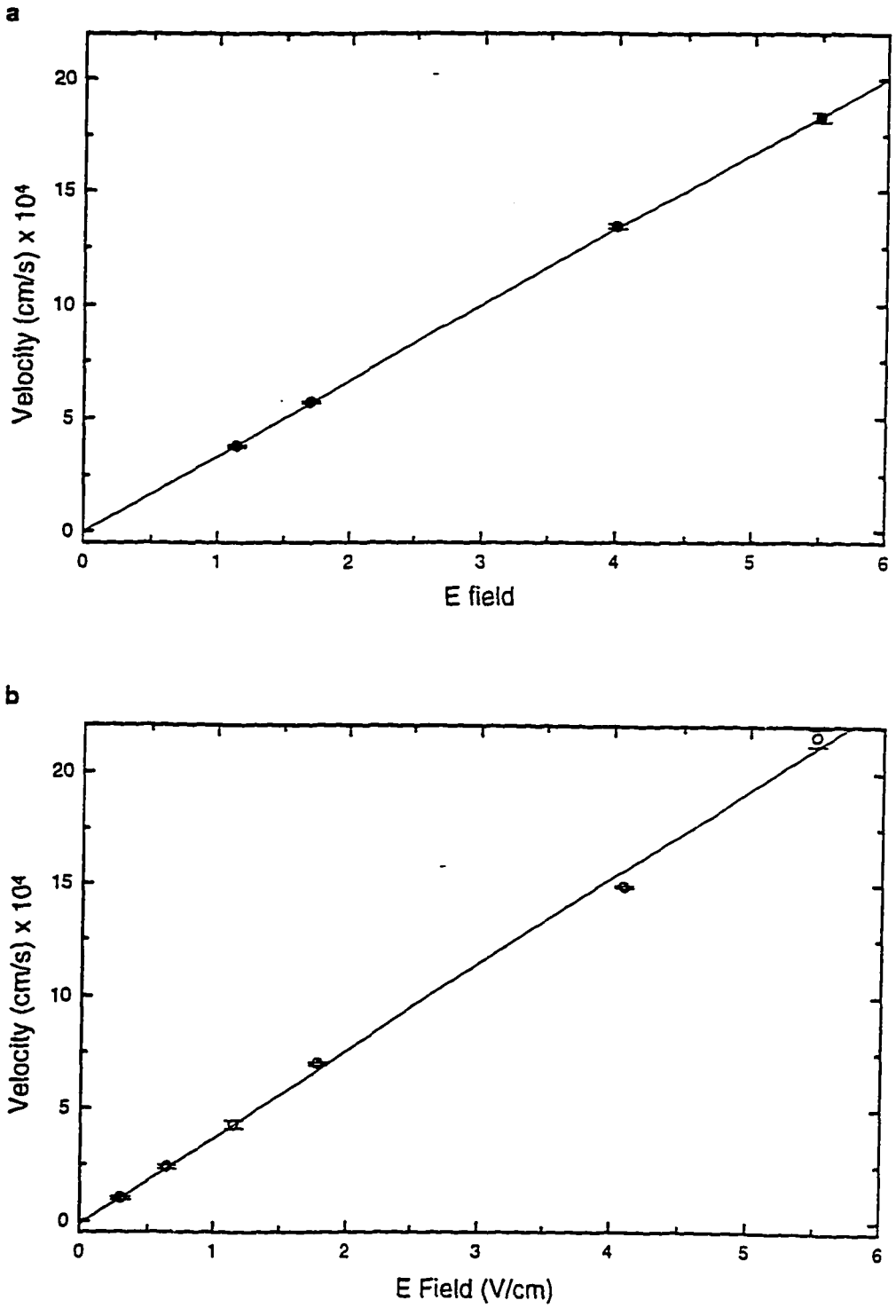

TABLE 3

ELECTROPHORETIC MOBILITY OF $pd(A)_{20} \cdot pd(T)_{20}$ IN DIFFERENT KCl CONCENTRATIONS

[a] Salt Conditions	[b] v_o (cm/s x 10^{-5})	v/E ($cm^2/V\ s \times 10^4$)	[c] μ_{ave} ($cm^2/V\ s \times 10^4$)	[d] Q_{app} (e)
100 mM KCl	-1.93 [e] (-7.28, 7.30)	2.95 (2.80, 3.11)	2.88 (2.74, 3.02)	6.62 (6.30, 6.94)
80 mM KCl	-1.55 (-6.55, 3.48)	3.23 (3.10, 3.37)	3.16 (3.00, 3.32)	7.26 (6.89, 7.63)
60 mM KCl	-0.40 (-1.81, 1.00)	3.34 (3.30, 3.38)	3.29 (3.09, 3.49)	7.56 (7.10, 8.02)
20 mM KCl	-1.5 (-7.43, 4.35)	3.87 (3.67, 3.98)	3.71 (3.29, 4.13)	8.53 (7.55, 9.50)

[a] 20 mM Tris, pH 8.0, 20 °C
[b] Zero field velocity
[c] Mean average of individually determined μ's
[d] Predicted charge from $Q_{app} = (\mu_{ave} \cdot k_b \cdot T/D)$ with D = 11 F
[e] Confidence interval are at 95%

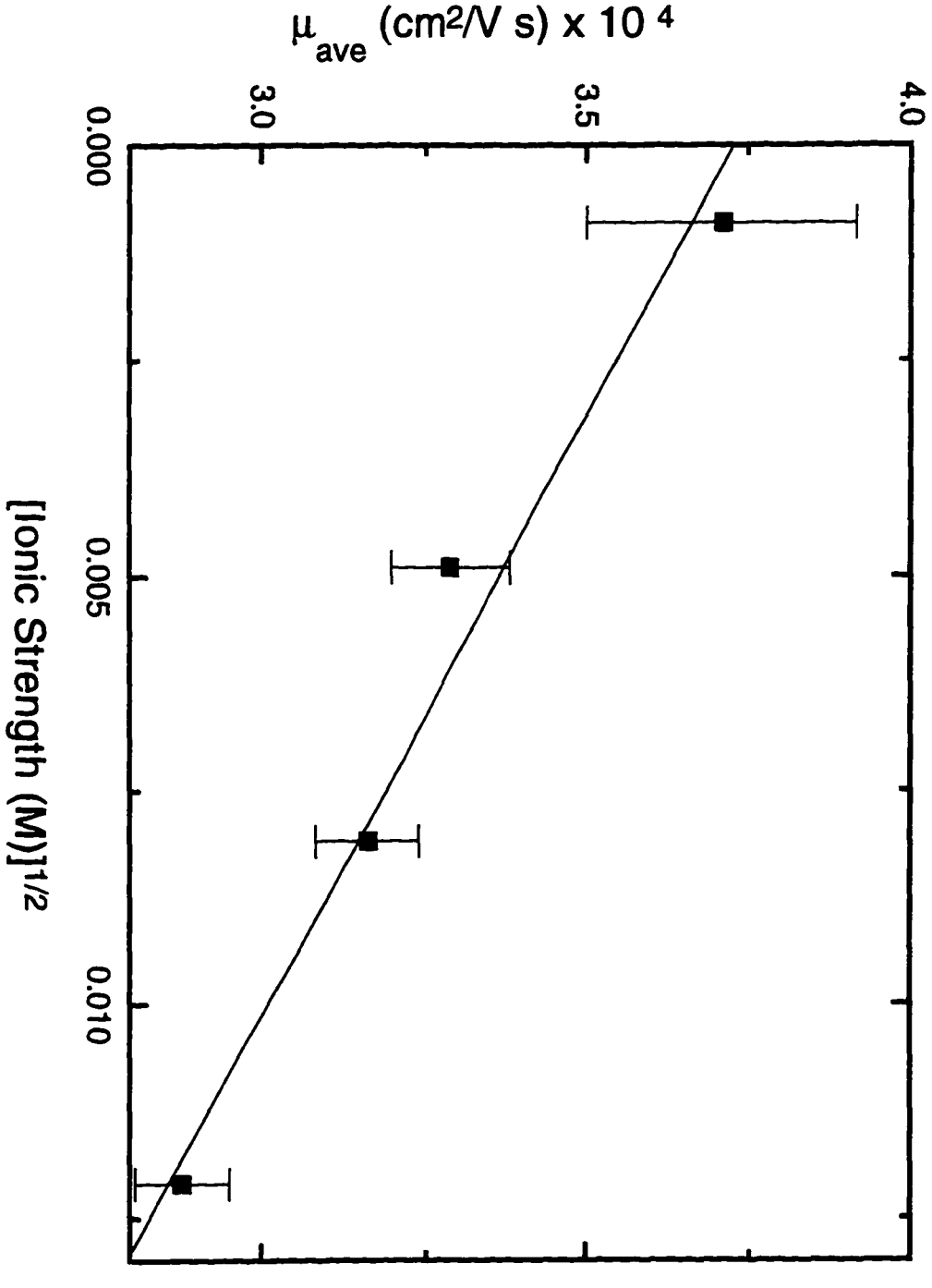

Figure 9. The μ_{ave} of $pd(A)_{20}$·$pd(T)_{20}$ as a function of ionic strength in X mM KCl, 20 mM Tris, pH 8.0, 20 °C: Extrapolation to zero ionic strength.

Figure 10. SSE determined Q_{app} (95% confidence intervals) of $pd(A)_{20}$·$pd(T)_{20}$ as a function of E field in 100 mM XCL, 20 mM Tris, pH 8.0, 20 °C: ···■··· KCL, · · □ · · NaCl, —●— LiCl, - -o- - $(CH_3)_4NCl$

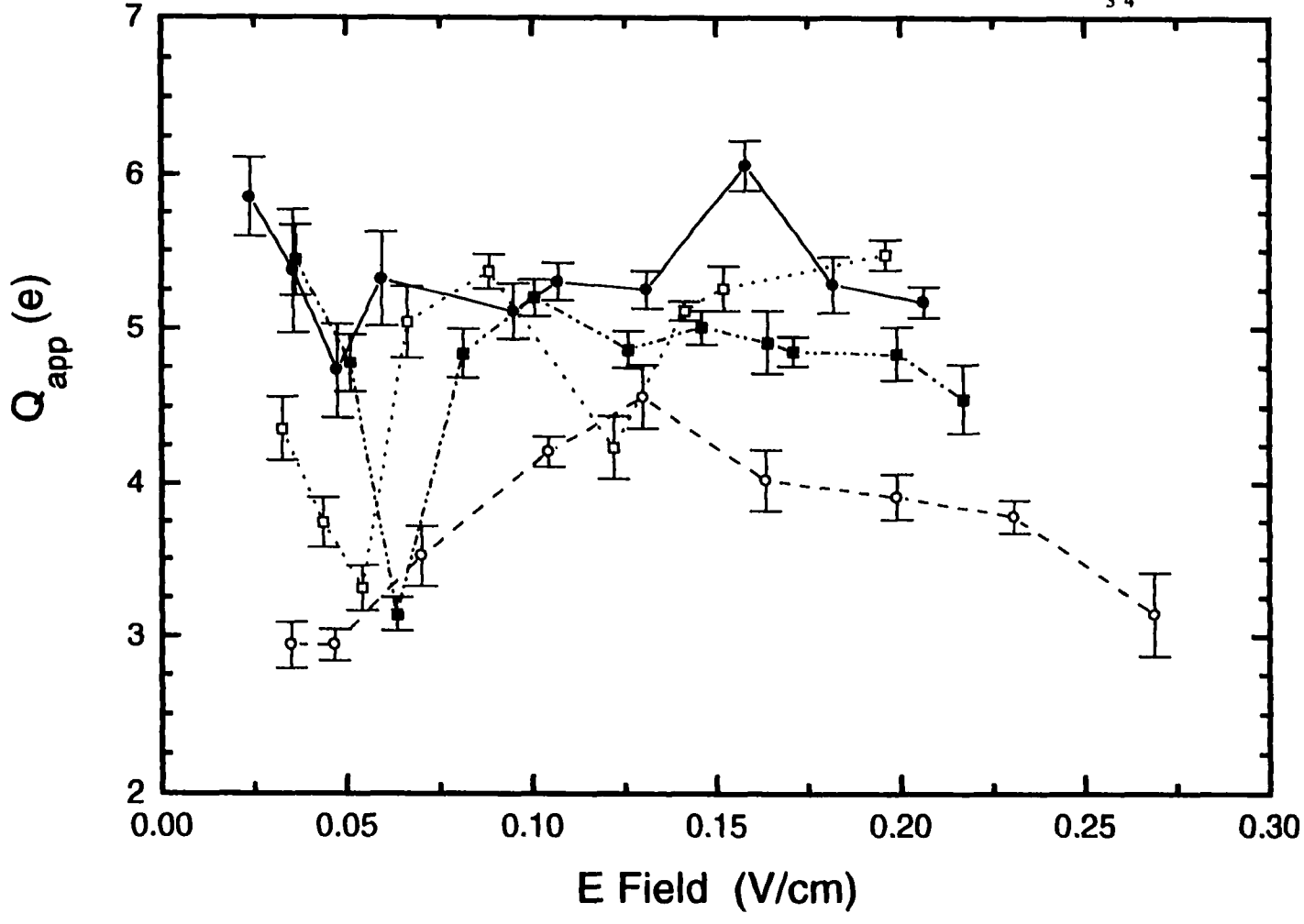

global fit Q_{app} (Table 4). This is analogous to the multi-channel, multi-speed global fit of short column sedimentation equilibrium data required to generate a more accurate description of the equilibrium gradient. Figure 11 shows a sample (100 mM LiCl) global fit of steady state gradients over an 8.5 fold range in electric field. Note that the lowest field curves, which have minimal curvature and individually give low Q_{app}'s, fit adequately to the higher σ. This could represent curve fitting limitations that allow shallow gradients to "comfortably" fit a range of σ's or the domination of the fitting algorithm by the larger high field σ's over the low field data. With the exception of $(CH_3)_4NCl$, each of the salt conditions was fit adequately to a single global σ.

The suspect behavior of low field σ's can best be seen in the plot of σ versus electric field (figure 12). The prediction is that σ is linear with E field. Comparing the rise in σ with increasing electric field indicates the range over which Q_{app} or σ/E are consistent. Over the middle and high field range, σ is linear with E field [with the exception of $(CH_3)_4NCl$ at high fields]. However, the σ's at the lowest field do not follow this line but level off instead. This could either be the result of curve fitting limitations or due to unaccounted influences (e.g. bulk fluid flow) on the concentration distribution. An averaged σ/E, σ_{ave}/E, can be determined for each buffer condition by linear regression over the constant range σ's (Figure 13, Table 4). The σ/E's can be converted to a`Q_{app}' s (making the assumption that $D_e f_e = k_b T$) to compare the different procedures for obtaining Q_{app} (Table 4).

The $Q_{app}/40e$ determined from the global fit and the average σ/E indicate that only 1/10 to 1/7 of the formal charge is capable of experiencing the electric field under these experimental conditions (Table 4).

TABLE 4

SSE DETERMINED CHARGE PROPERTIES OF $pd(A)_{20}$•$pd(T)_{20}$ IN DIFFERENT CHLORIDE SALTS

[a] 100 mM chloride salts	KCl	NaCl	LiCl	$(CH_3)_4NCl$
Q_{app} from global fit	4.91 [b] (4.80, 5.03)	5.00 (4.83, 5.17)	4.96 (4.82, 5.08)	2.83 (2.79, 2.90)
rms	0.005	0.005	0.006	0.005
Q_{app}/40e	0.123 (0.120, 0.126)	0.125 (0.121, 0.129)	0.124 (0.121, 0.127)	0.071 (0.068, 0. 072)
[c] σ_{ave}/E	205 (189, 220)	227 (207, 247)	206 (201, 211)	132 (119, 145)
[d] `Q_{app}	5.18 (4.78, 5.56)	5.74 (5.23, 6.24)	5.21 (5.08, 5.33)	3.37 (3.03, 3.67)
`Q_{app}/40e	0.129 (0.120, 0.139)	0.143 (0.131, 0.156)	0.130 (0.127, 0.133)	0.083 (0.076, 0.092)
[e] σ D/E ($x10^{-4}$ cm^2/V s)	2.25 (2.05, 2.42)	2.50 (2.28, 2.71)	2.27 (2.21, 2.32)	1.45 (1.31, 1.60)

[a] 20 mM Tris, pH 8.0, 20 °C
[b] 95% confidence interval
[c] Determined from the slope of σ vs E at 95% confidence intervals
[d] Based on σ_{ave}/E
[e] Predicted electrophoretic mobility from SSE data with D = 11F

Figure 11. Global fit analysis of the SSE gradients of $pd(A)_{20}$·$pd(T)_{20}$ in 100 mM LiCl, 20mM Tris, pH 8.0, 20 °C

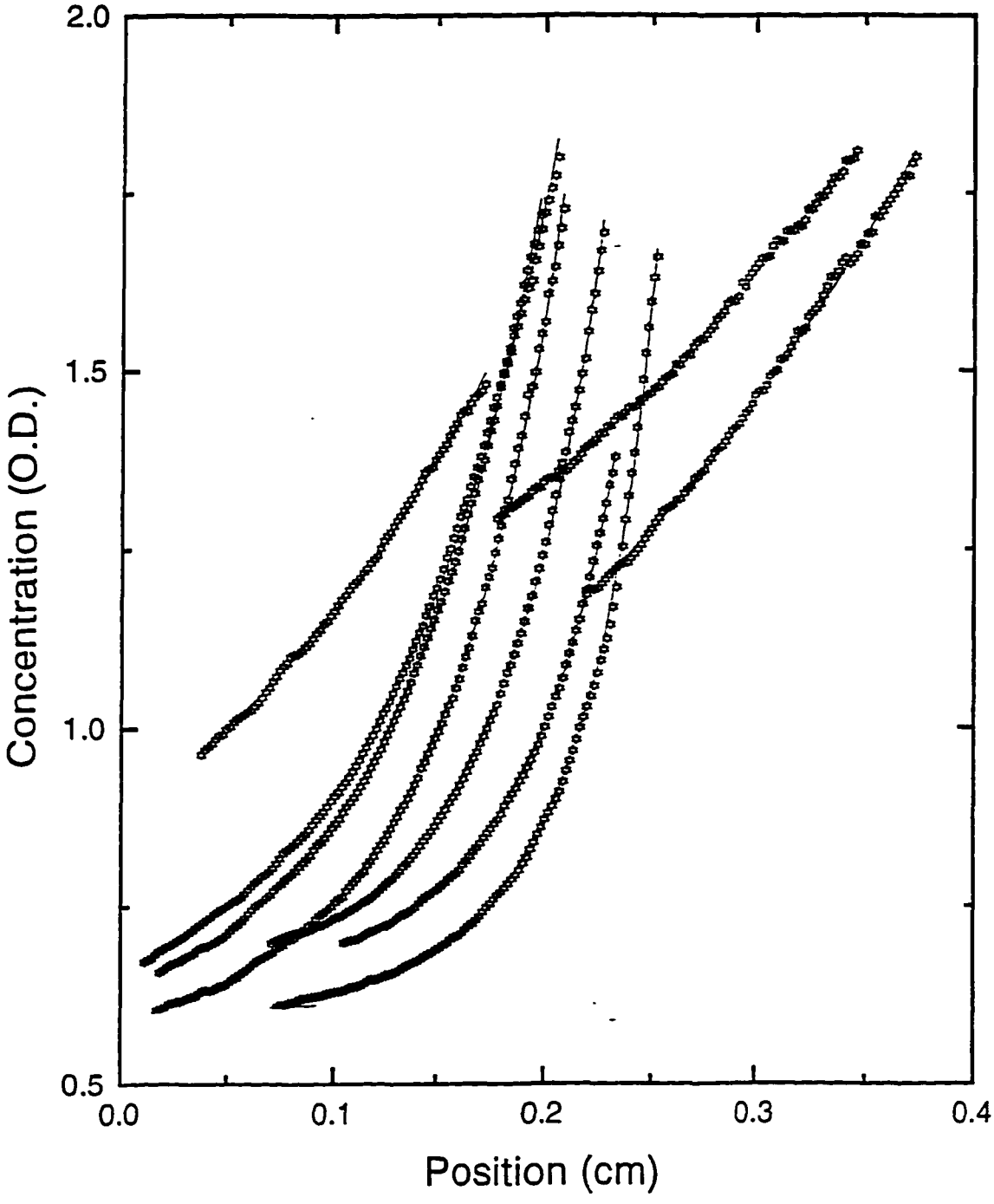

Figure 12. SSE determined σ for $pd(A)_{20}$·$pd(T)_{20}$ (95% confidence intervals) as a function of E field in 100 mM XCl, 20 mM Tris, pH 8.0, 20°C:

■ KCl, □ NaCl, ● LiCl, ○ $(CH_3)_4NCl$

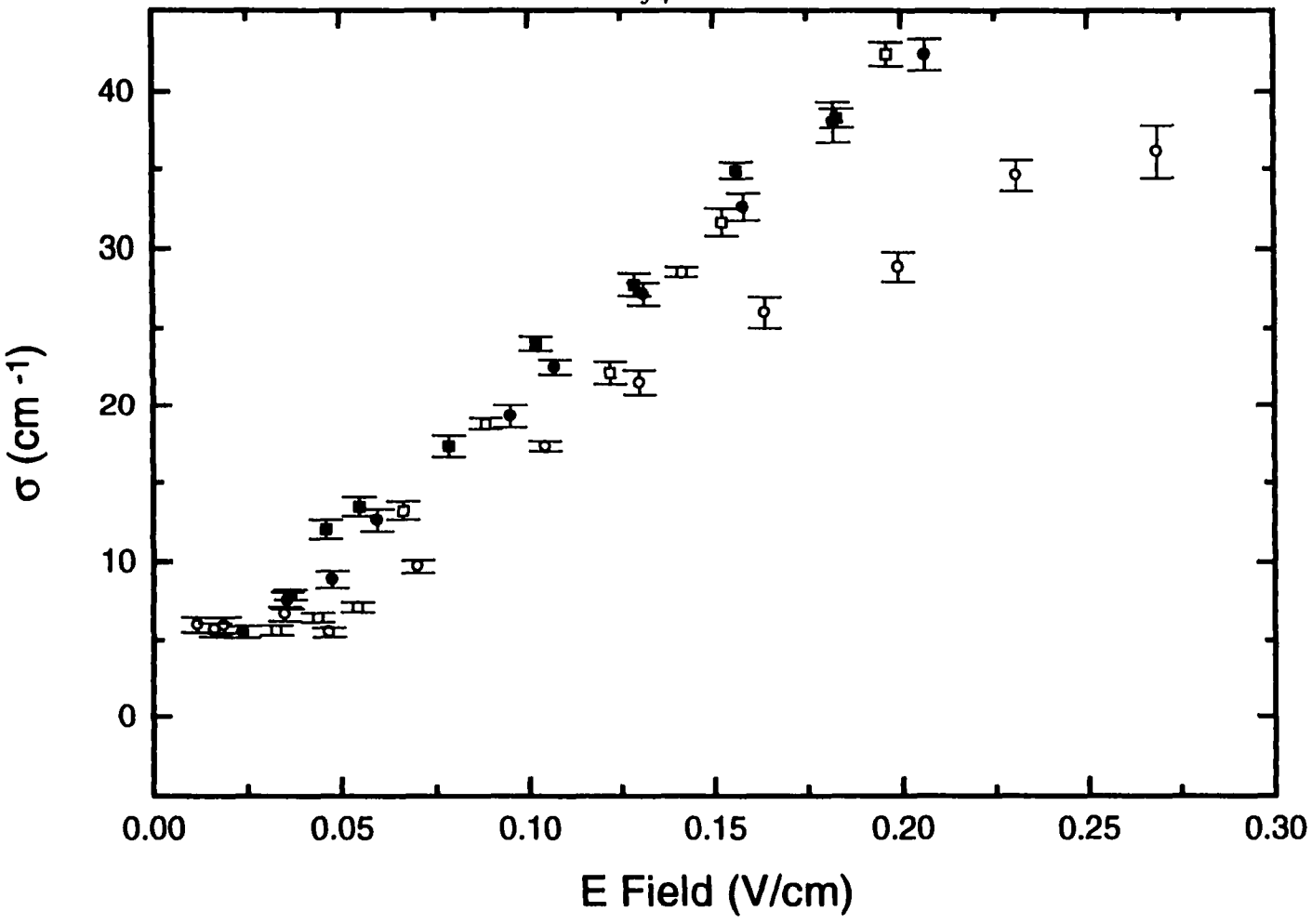

Figure 13. SSE determined σ for $pd(A)_{20} \bullet pd(T)_{20}$ as a function of E field in 20 mM Tris, pH 8.0, 20 °C, and in (a) 100 mM KCl, (b) 100 mM NaCl, (c) 100 mM LiCl, and (d) 100 mM $(CH_3)_4NCl$. The linear regression of σ versus E yields an σ/E_{ave} that is used in charge and mobility calculation in Table 4.

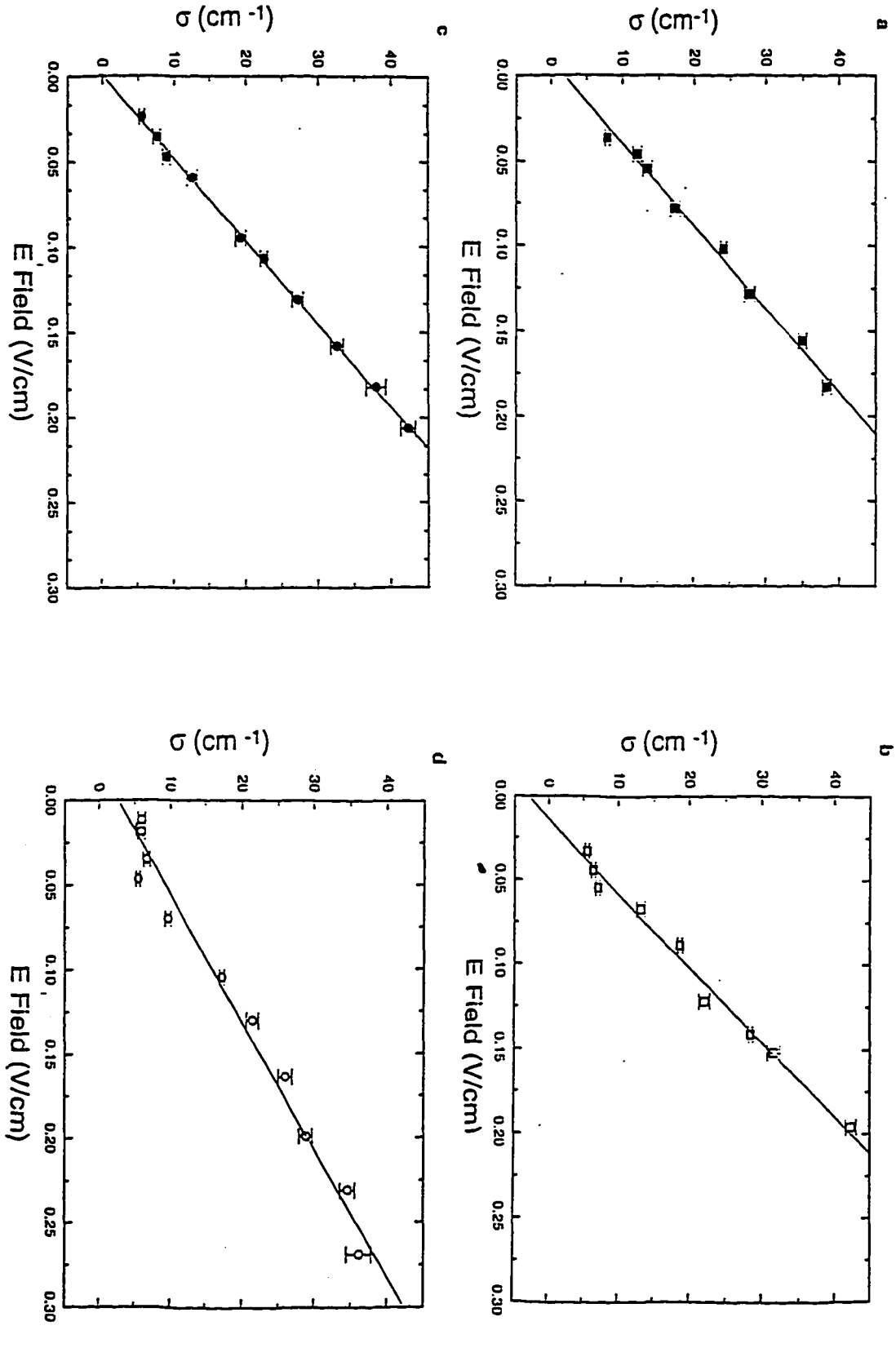

Direct comparison of experimentally determined values as a function of E field and the predicted effects of bulk fluid flow on the gradient formation can be observed with the plotting of σ/E versus electric field (Figure 14). The trends of σ/E are similar to those seen in Q_{app} versus E. The influence of a bulk fluid flow can be simulated using equation 37 and a σ_{ave}/E from either the global fit σ or from the slope of σ versus E field and compared to experimental data. Figures 15-18 compare the expected behavior of σ_{ave}/E with a net bulk fluid flow of 5×10^{-7} cm/second (effects of flow in both directions are shown) using both means of determining σ_{ave}/E. These comparisons show that a small bulk fluid flow can significantly influence the SSE data under 0.05 V/cm.

Effects of Varying KCl Concentration on SSE Measured Charge Properties.

The experimentally determined Q_{app}'s of $pd(A)_{20}$•$pd(T)_{20}$ in decreasing KCl concentration buffers are shown in Figure 19. The individually determined Q_{app}'s range from 3 e to 7 e. No clear trend is observed with the individual data sets.

Combining the individual data sets for the samples in Figure 19 into a global fit (Table 5) gives a narrower range of estimated charges, 4.6 e to 5.8 e. The fits to the data are good with the exception of 60 mM KCl (high E field σ's for the 60 mM solutions do not have a linear dependence on E). The Q_{app} appears to be increasing as the concentration drops from 80 to 20 mM. Using $Q_{app}/40e$ as an indicator of the unshielded charge (Table 5), the fraction of charge capable of experiencing the electric field ranges from 1/9 (0.115) to 1/7 (0.145).

The behavior of the exponential component σ as a function of electric field is shown in Figure 20. There appears to be anomalous behavior below 0.05 V/cm. The σ for each of the four KCl conditions apparently rises at the same rate below 0.05 V/cm but diverge slightly

Figure 14. SSE determined σ/E for $pd(A)_{20}$·$pd(T)_{20}$ (95% confidence intervals) as a function of E field in 100 mM XCL, 20 mM Tris, pH 8.0, 20 °C

■ KCl, □ NaCl, ● LiCl, ○ $(CH_3)_4NCl$

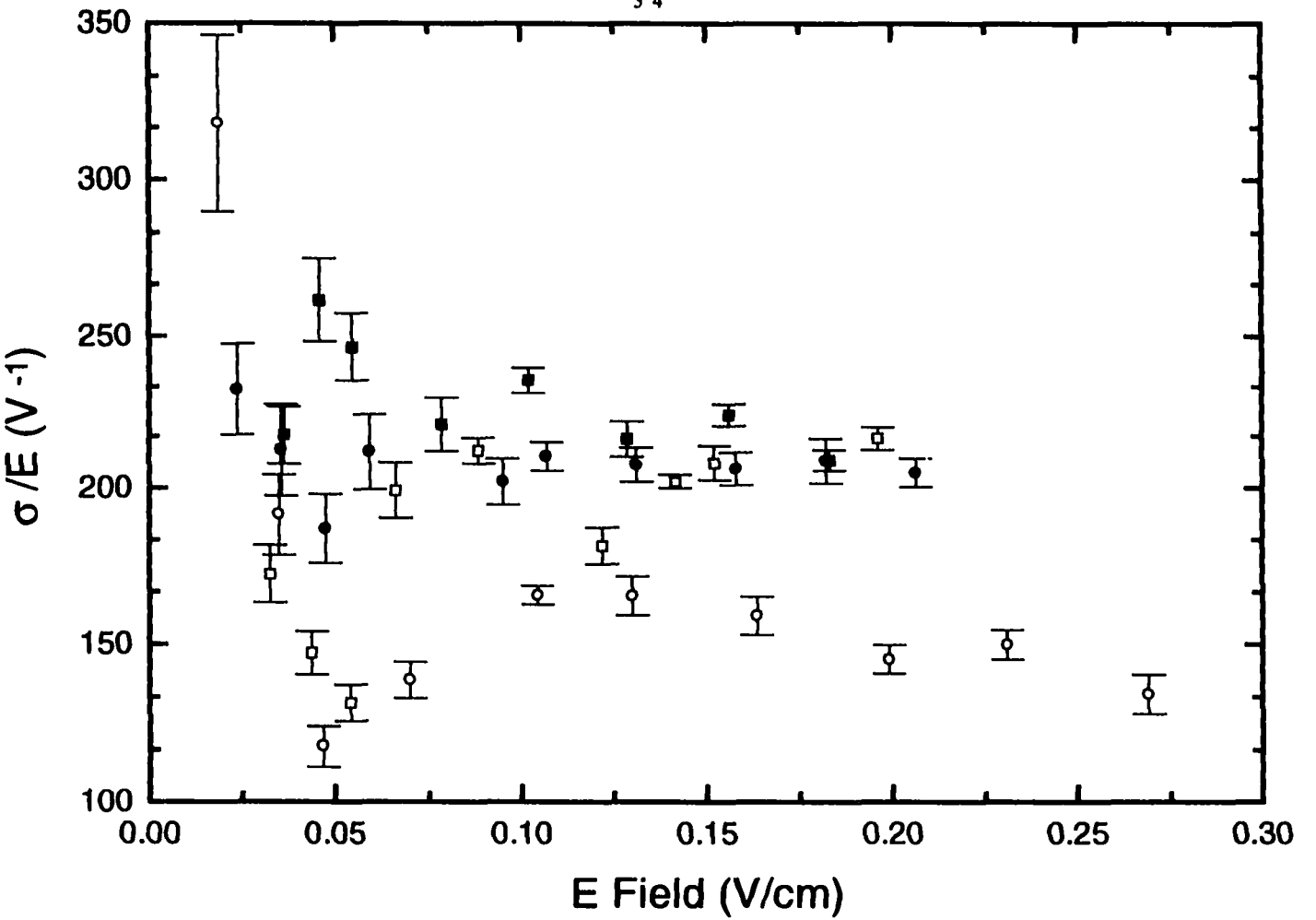

Figure 15. Comparison of the experimentally determined σ/E of $pd(A)_{20}$·$pd(T)_{20}$ in 100 mM KCl with predicted behavior ····· of σ_{ave}/E (equation 37) with a bulk fluid flow of ± 5 x 10^{-7} cm/s. The thick solid lines represents the σ_{ave}/E determined from (a) the slope of σ versus E and from (b) global fit data with - - - - - - representing 95% confidence intervals.

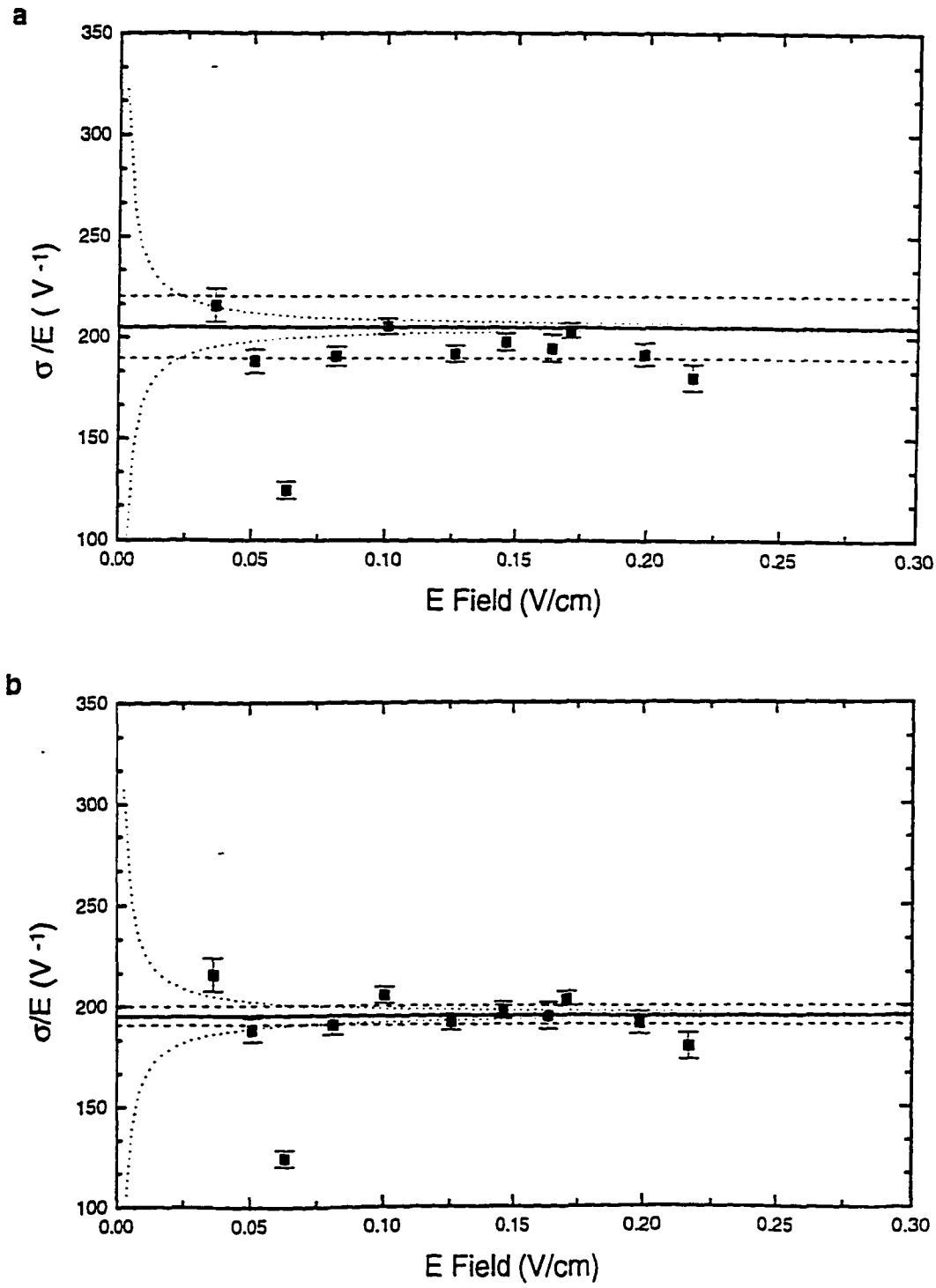

Figure 16. Comparison of the experimentally determined σ/E of $pd(A)_{20}$·$pd(T)_{20}$ in 100 mM NaCl with predicted behavior ····· of σ_{ave}/E (equation 37) with a bulk fluid flow of ± 5 x 10^{-7} cm/s. The thick solid lines represents the σ_{ave}/E determined from (a) the slope of σ versus E and from (b) global fit data with - - - - - - representing 95% confidence intervals.

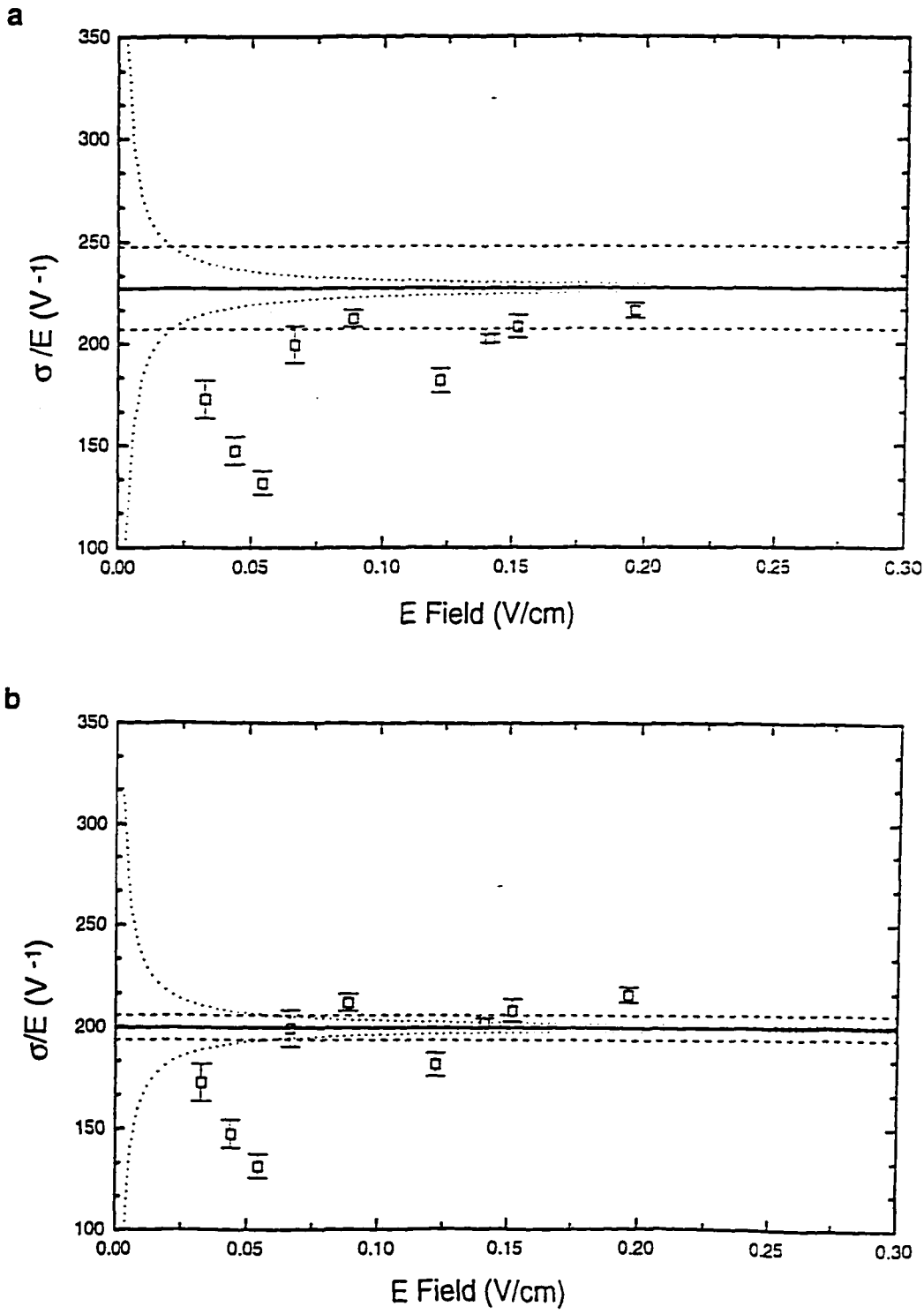

Figure 17. Comparison of the experimentally determined σ/E of $pd(A)_{20}$·$pd(T)_{20}$ in 100 mM LiCl with predicted behavior ····· of σ_{ave}/E (equation 37) with a bulk fluid flow of ± 5 x 10^{-7} cm/s. The thick solid lines represents the σ_{ave}/E determined from (a) the slope of σ versus E and from (b) global fit data with - - - - - - representing 95% confidence intervals.

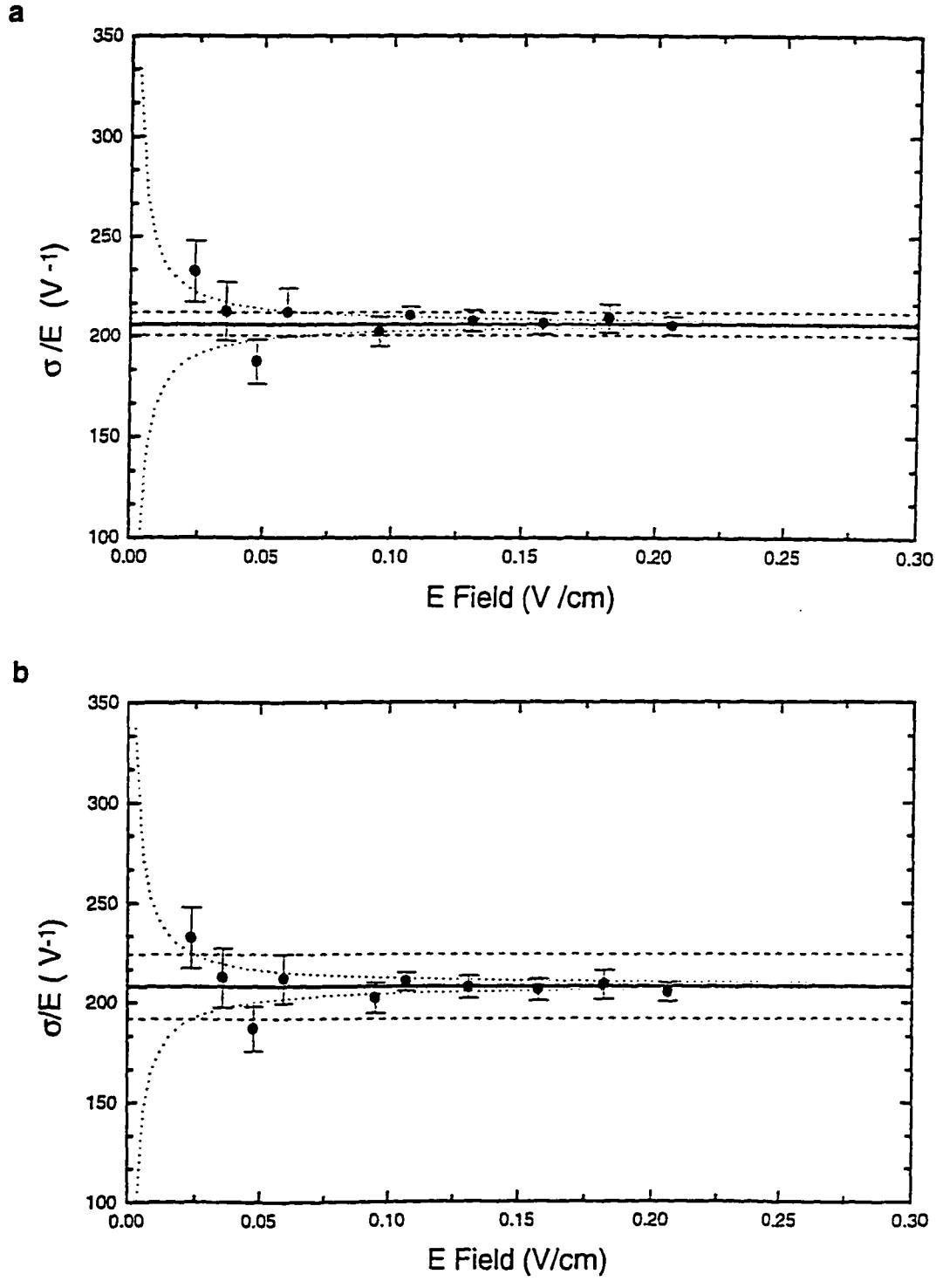

Figure 18. Comparison of the experimentally determined σ/E of $pd(A)_{20}$·$pd(T)_{20}$ in 100 mM $(CH_3)_4NCl$ with predicted behavior ····· of σ_{ave}/E (equation 37) with a bulk fluid flow of ± 5 x 10^{-7} cm/s. The thick solid lines represents the σ_{ave}/E determined from (a) the slope of σ versus E and from (b) global fit data with - - - - - - representing 95% confidence intervals.

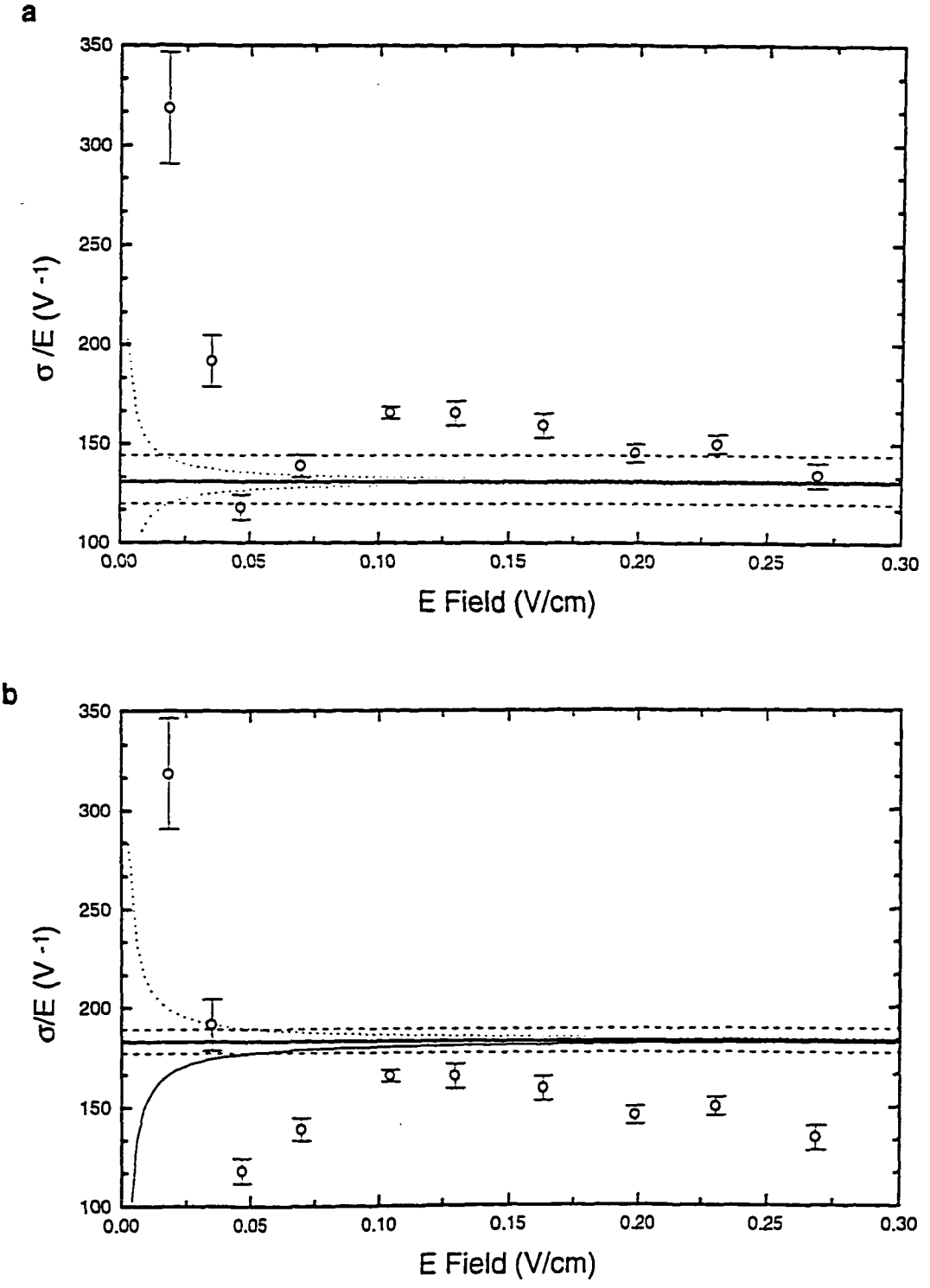

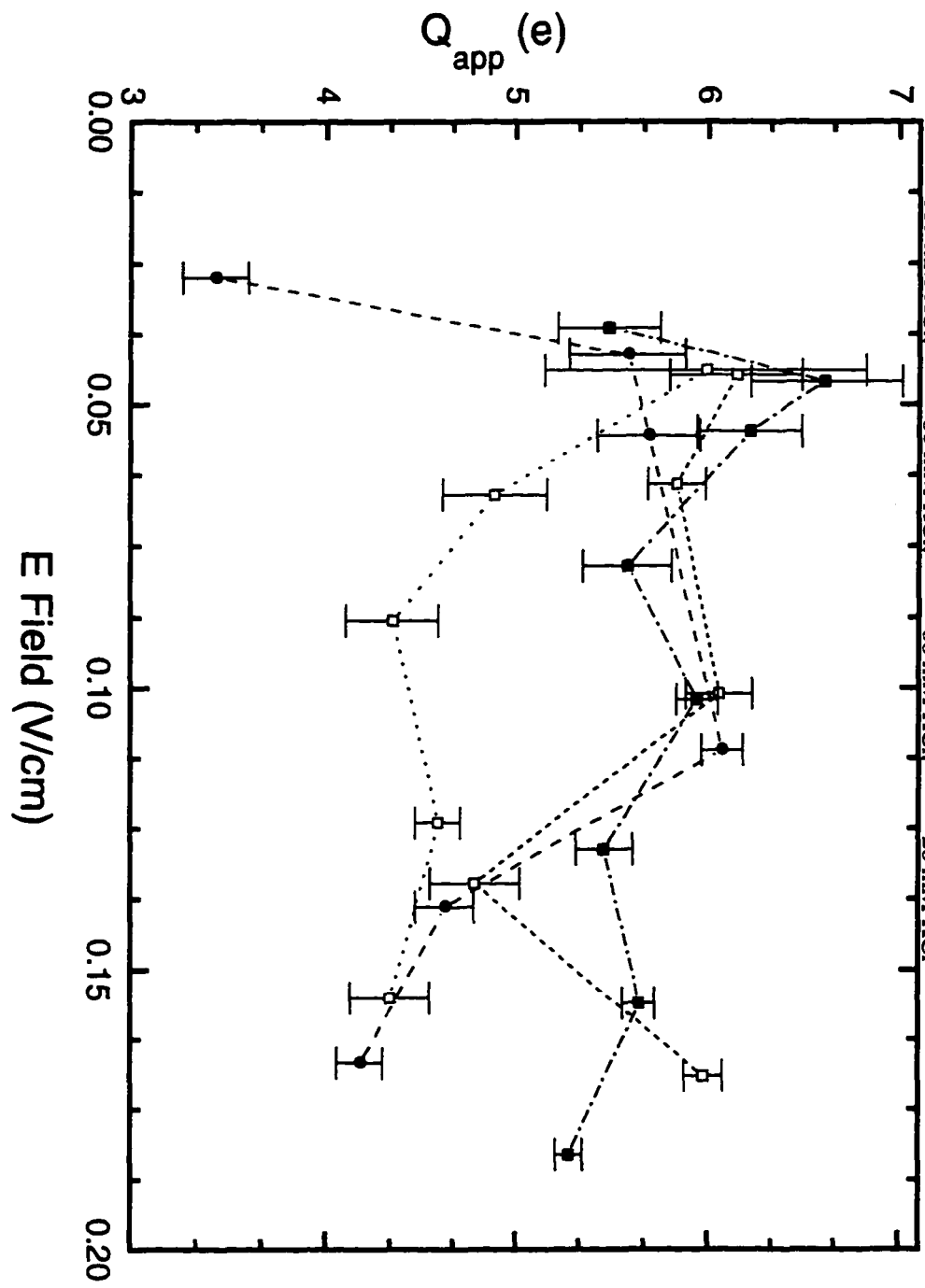

Figure 19. SSE determined Q_{app} (95% confidence intervals) of $pd(A)_{20}$·$pd(T)_{20}$ as a function of E field in X mM KCl, 20 mM Tris, pH 8.0, 20 °C:

TABLE 5

SSE DETERMINED CHARGE PROPERTIES OF $pd(A)_{20} \cdot pd(T)_{20}$ IN DIFFERENT KCl CONCENTRATIONS

[a] KCl concentration	100 mM	80 mM	60 mM	20 mM
Q_{app} from global fit	4.91 [b] (4.80, 5.03)	4.61 (4.40, 4.74)	5.03 (4.71, 5.22)	5.83 (5.68, 5.99)
rms	0.003	0.002	0.007	0.007
$Q_{app}/40e$	0.123 (0.120, 0.126)	0.115 (0.110, 0.118)	0.127 (0.118,0.131)	0.146 (0.142, 0.150)
[c] σ_{ave}/E	205 (189, 220)	151 (131, 170)	172 (116, 228)	216 (174 258)
[d] $`Q_{app}$	5.18 (4.78, 5.56)	3.81 (3.31, 4.30)	4.35 (2.93, 5.76)	5.46 (4.40, 6.52)
$`Q_{app}/40e$	0.129 (0.120, 0.139)	0.095 (0.083, 0.108)	0.109 (0.073, 0.144)	0.136 (0.110, 0.163)
[e] σ D/E ($x10^{-4}$ cm^2/V s)	2.25 (2.05, 2.42)	1.66 (1.44, 1.87)	1.89 (1.28, 2.51)	2.38 (1.91, 2.84)

[a] 20 mM Tris, pH 8.0, 20 °C
[b] 95% confidence interval
[c] Determined from the slope of σ vs E at 95% confidence intervals
[d] Based on σ_{ave}/E
[e] Predicted electrophoretic mobility from SSE data with D = 11F

Figure 20. SSE determined σ for $pd(A)_{20}$·$pd(T)_{20}$ (95% confidence intervals) as a function of E field in X mM KCl, 20 mM Tris, pH 8.0, 20 °C:
■ 100 mM, □ 80 mM, ● 60 mM, ○ 20 mM

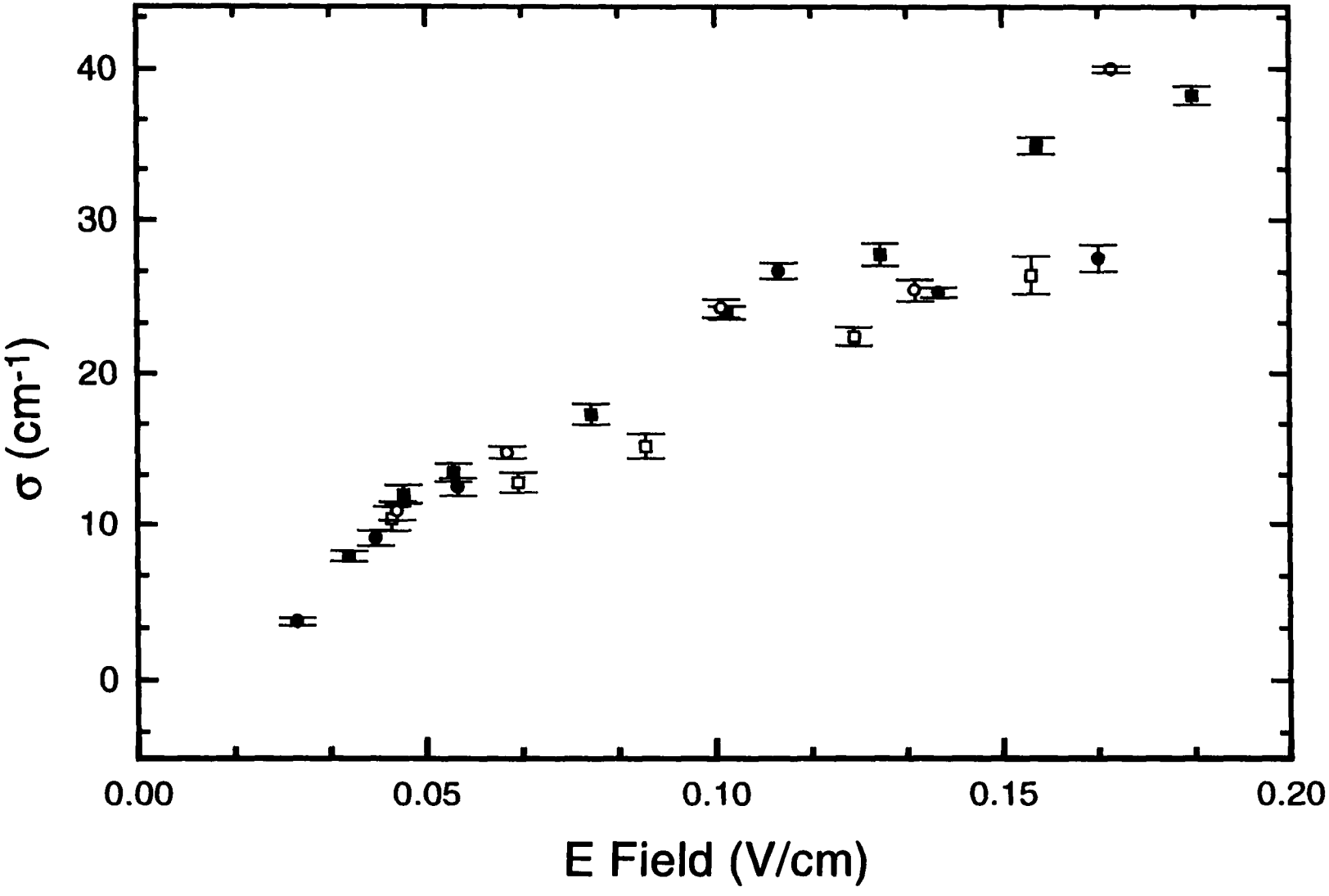

as the field increase above this value. Linear regression of the data points in the range of consistent σ (Figure 21) gives a σ_{ave}/E that, when converted to `$Q_{app}$ (making the assumption $D_e f_e = k_b T$), can be used to compare the different procedures for obtaining a more precise $Q_{app}$ (Table 4). The 60 and 80 mM global fit $Q_{app}$'s do not match up as well with their `Q_{app}'s as do the 100 and 20 mM KCl fits. The Q_{app}/40e range is larger; 1/11 to 1/6 of the charge apparently capable of experiencing the electric field.

Plotting the data as σ/E verses E field (Figure 22) displays a similar trends as those seen with to Q_{app} versus field. The value of the 20 mM KCl data appears overall higher but the variability of the individually determined Q_{app}'s prevents definitive conclusions from being drawn. The comparison of the individually determined σ/E's to the simulated behavior of σ_{ave}/E with bulk fluid flow (5×10^{-7} cm/s) are shown in Figures 15, 23, 24 and 25. The simulations suggest the possible influence of bulk fluid flow on σ/E at low fields (< 0.05 V/cm). The σ_{ave}/E from the slope of σ versus E does not appear to accurately represent the 80 mM KCl data. Analysis of both the cation type and KCl concentration data suggests that the σ_{ave}/E from the global fit offers a more precise representation.

The low salt concentration data also appears to have more variability. This can be seen more dramatically with lower DNA concentration (under 100 μg/ml). Figure 26 shows SSE data at high and low DNA concentration gradients for 60 and 20 mM KCl. Three observations can be made with this comparison. First, low concentration DNA appears to yield higher Q_{app}'s. This trend appears to be consistent for all buffer conditions but more modestly than for the 20 mM KCl data. Secondly, in contrast to the low field behavior of high concentration DNA, the Q_{app}'s for the low concentration DNA tend to increase with

Figure 21. SSE determined σ for $pd(A)_{20} \bullet pd(T)_{20}$ as a function of E field in 20 mM Tris, pH 8.0, 20 °C, and in (a) 100 mM KCl, (b) 80 mM KCl, (c) 60 mM KCl, and (d) 20 mM KCl. The linear regression of σ versus E yields an σ/E_{ave} that is used in charge and mobility calculation in Table 5.

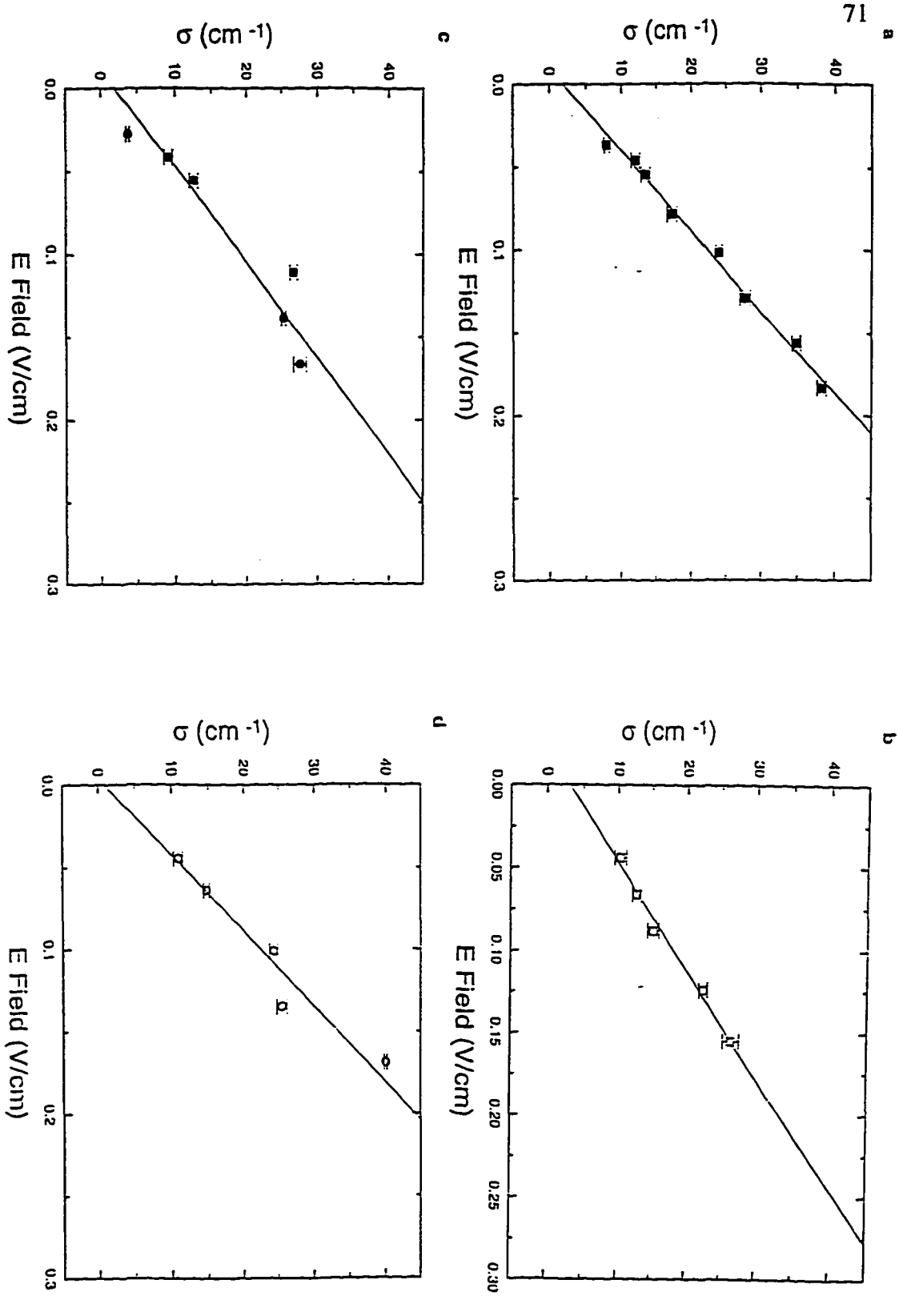

Figure 22. SSE determined σ/E for $pd(A)_{20}$·$pd(T)_{20}$ (95% confidence intervals) as a function of E field in X mM KCl, 20 mM Tris, pH 8.0, 20 °C:

■ 100 mM, □ 80 mM, ● 60 mM, ○ 20mM

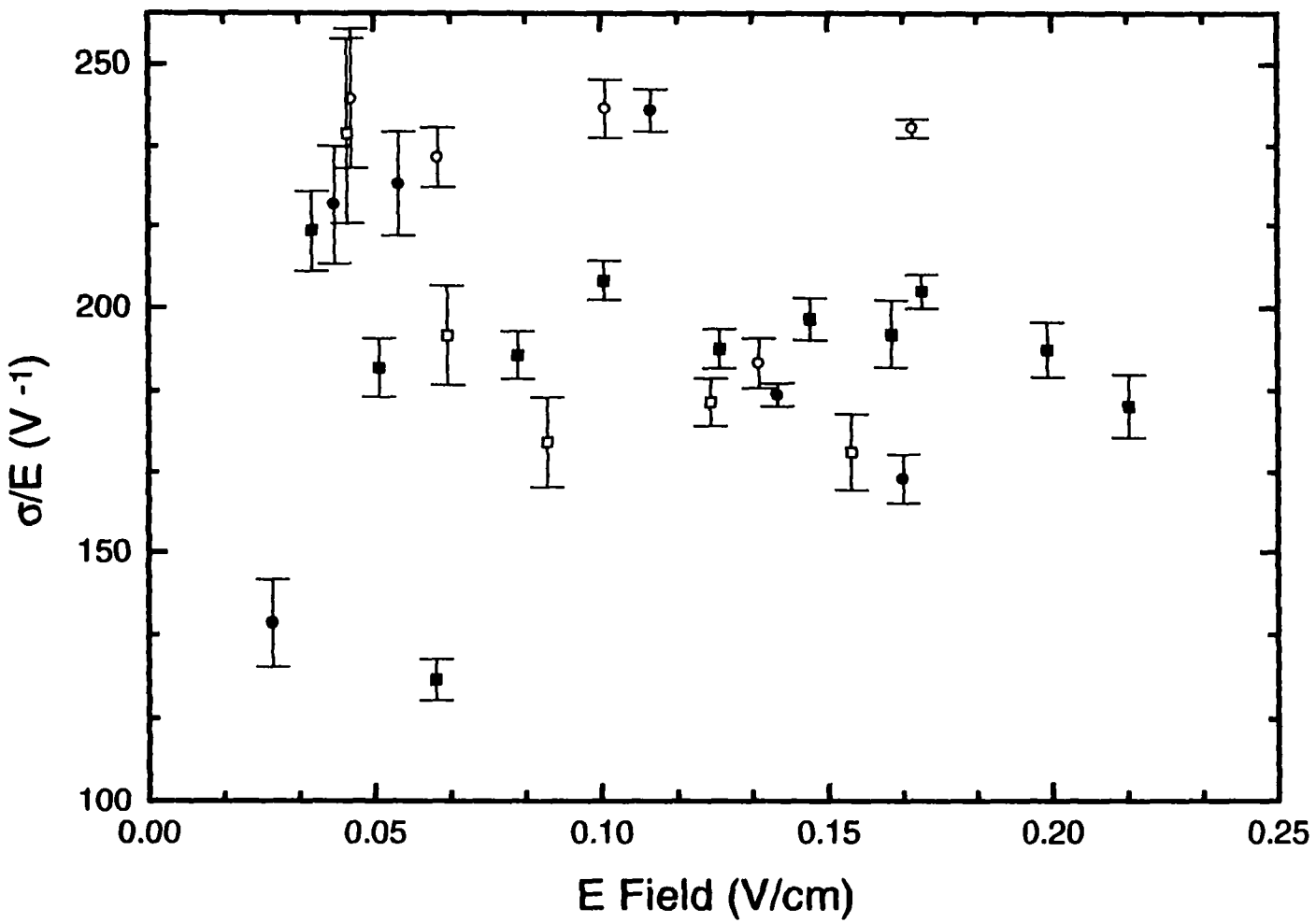

Figure 23. Comparison of the experimentally determined σ/E of $pd(A)_{20}$·$pd(T)_{20}$ in 80 mM KCl with predicted behavior ····· of σ_{ave}/E (equation 37) with a bulk fluid flow of ± 5 x 10^{-7} cm/s. The thick solid lines represents the σ_{ave}/E determined from (a) the slope of σ versus E and from (b) global fit data with - - - - - - representing 95% confidence intervals.

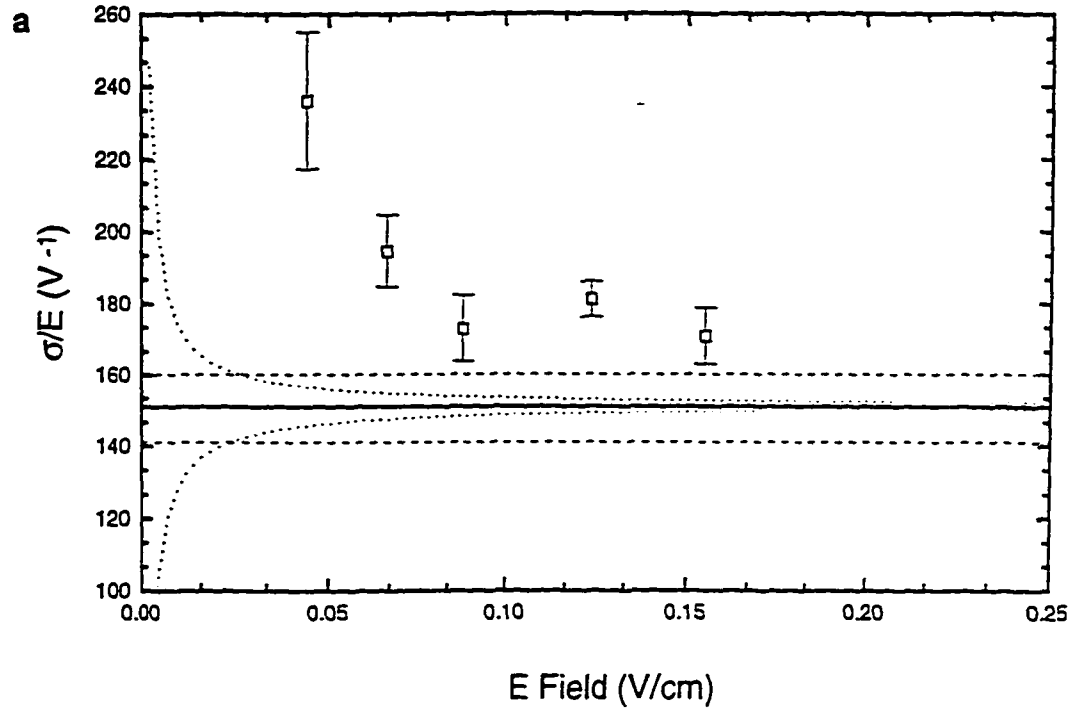

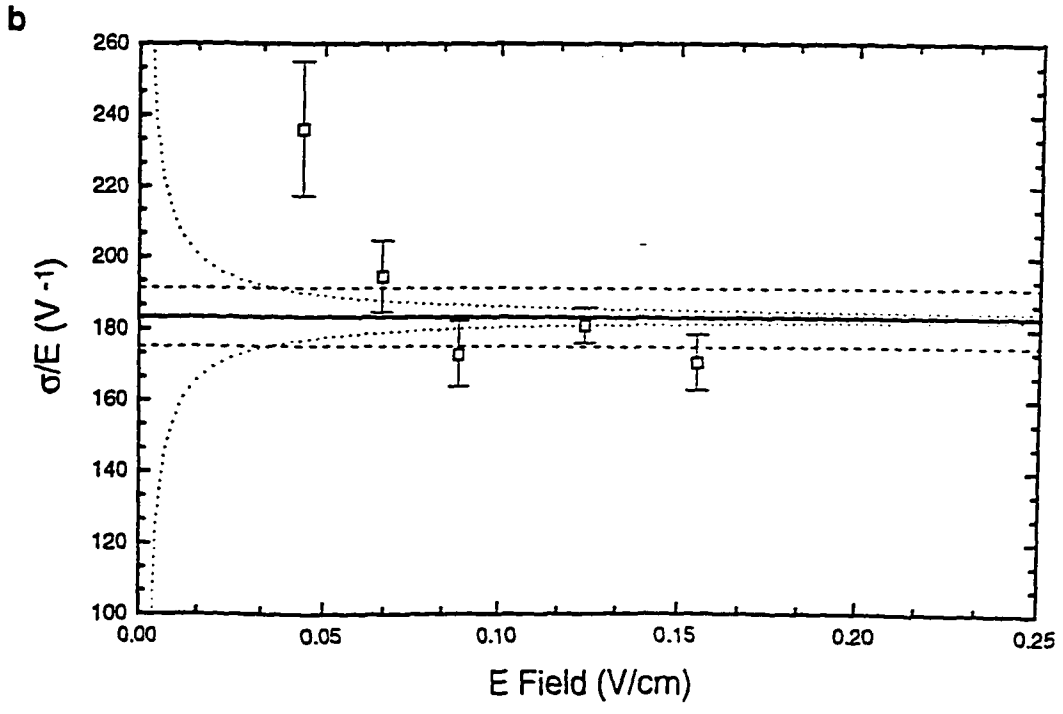

Figure 24. Comparison of the experimentally determined σ/E of $pd(A)_{20}$·$pd(T)_{20}$ in 60 mM KCl with predicted behavior ····· of σ_{ave}/E (equation 37) with a bulk fluid flow of ± 5 x 10^{-7} cm/s. The thick solid lines represents the σ_{ave}/E determined from (a) the slope of σ versus E and from (b) global fit data with - - - - - - representing 95% confidence intervals.

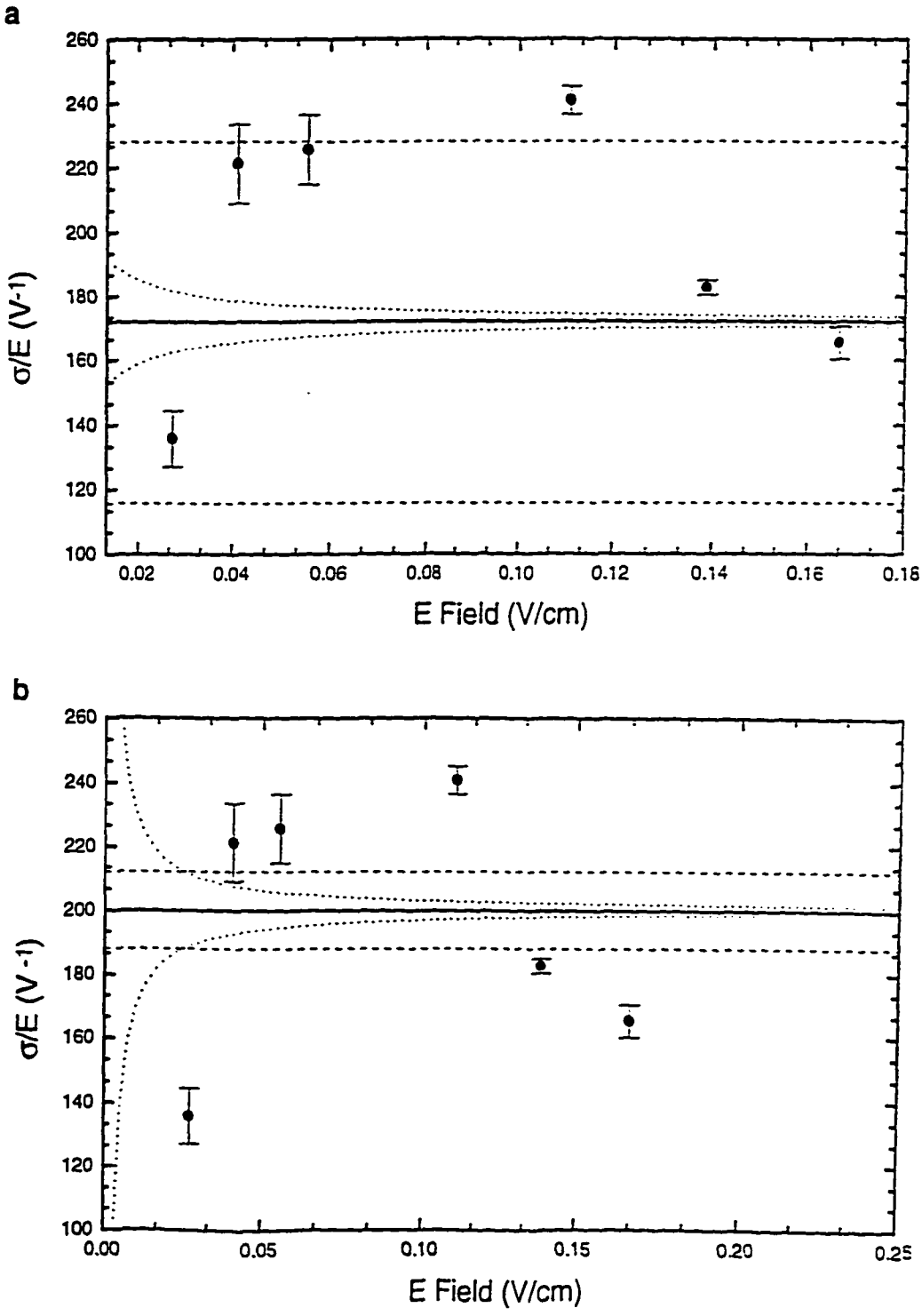

Figure 25. Comparison of the experimentally determined σ/E of $pd(A)_{20}$·$pd(T)_{20}$ in 20 mM KCl with predicted behavior ····· of σ_{ave}/E (equation 37) with a bulk fluid flow of ± 5 x 10^{-7} cm/s. The thick solid lines represents the σ_{ave}/E determined from (a) the slope of σ versus E and from (b) global fit data with - - - - - - representing 95% confidence intervals.

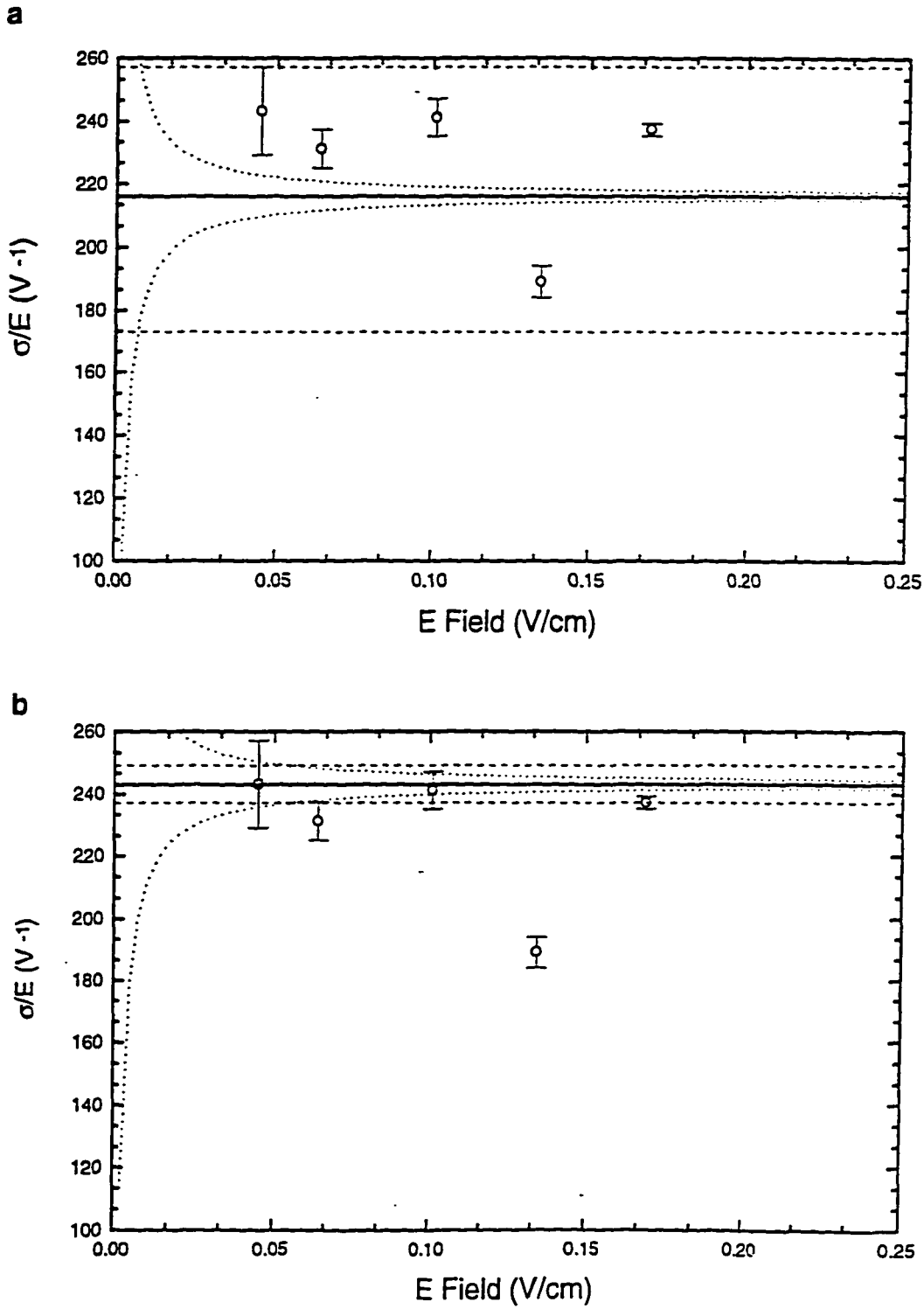

Figure 26. SSE determined Q_{app} (95% confidence intervals) of $pd(A)_{20}$·$pd(T)_{20}$ as a function of E field and DNA concentration in X mM KCl, 20 mM Tris, pH 8.0, 20 °C:

▲ 20 mM (200 μg/ml), △ 20 mM (25 μg/ml),

● 60 mM (260 μg/ml), ○ 60 mM (75 μg/ml)

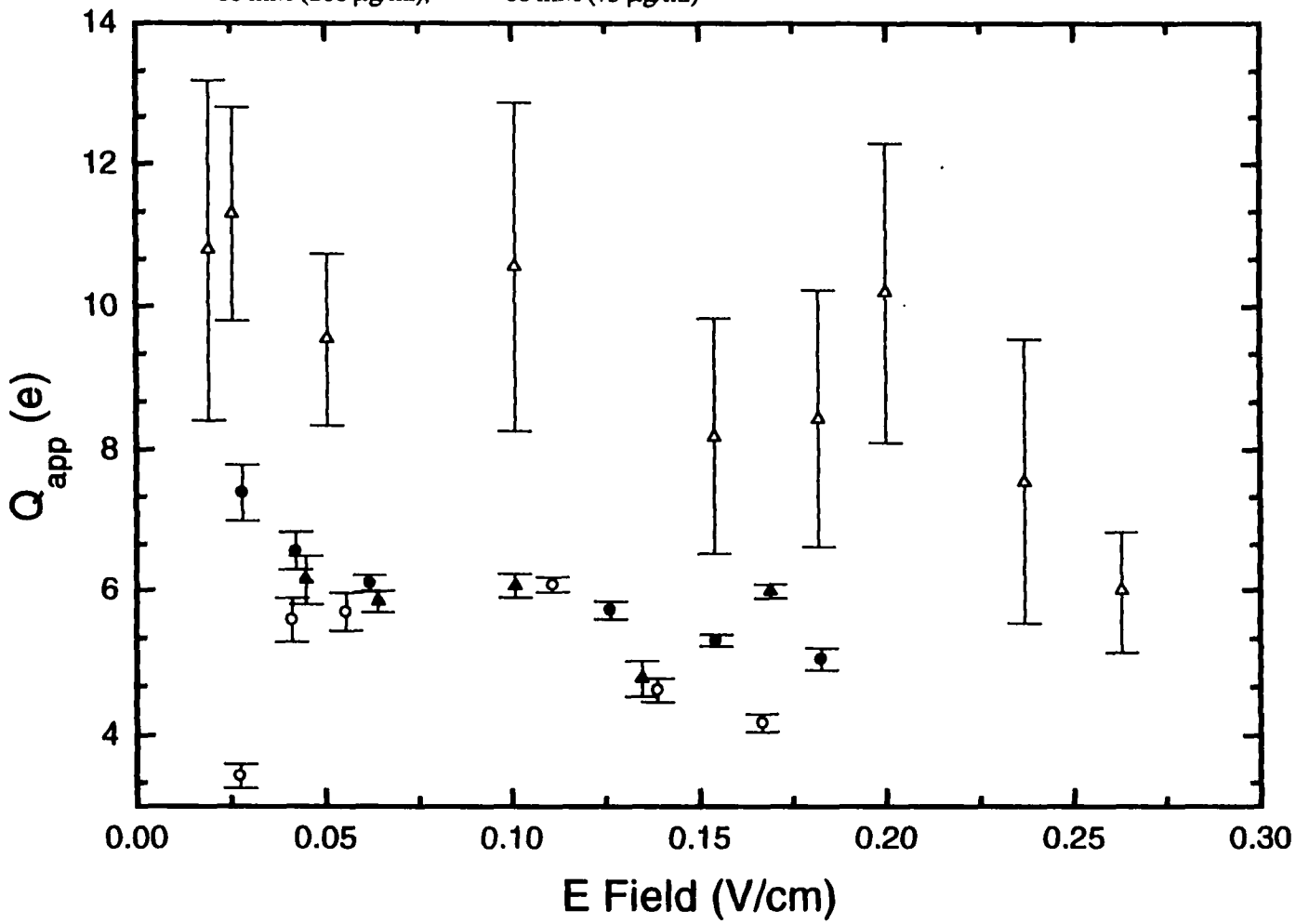

decreasing electric fields. Finally, DNA concentrations under 100 μg/ml (0.2 O.D. with the 0.2 cm cells) yields data that are more variable and less reproducible than at higher concentrations.

An important observation from the KCl concentration experiments is the inability to form gradients or clear mobility boundaries of $pd(A)_{20} \cdot pd(T)_{20}$ in 40 mM KCl. The DNA can be made to migrate under an E field but convection prevents stable patterns. The reasons for the convection are unclear. Both 20 and 60 mM KCl solutions form DNA gradients and mobility boundaries. The unexpected behavior of the DNA in 40 mM KCl underlies sensitivity of the AEA to convection and the modest changes in solution conditions to produce it.

Diffusion Coefficient Determination

Diffusion Coefficient in the Absence of an Electric Field

The diffusion coefficient of the $pd(A)_{20} \cdot pd(T)_{20}$ has been determined in the AEA and by analytical ultracentrifugation. In the AEA, the zero field diffusion coefficient, D_o, was measured by monitoring the decay of a concentration gradient (Figure 27). Presented in Tables 6 and 7 are the statistical averages of a number of D_o determinations of the DNA in the four different 100 mM chloride salts and in the different KCl concentrations respectively. The limited precision of this procedure prevents direct comparison of D_o as a function of cation type or ionic strength.

Also shown in Table 6 are the diffusion coefficients, D_s, calculated from sedimentation velocity data as analyzed by the g(s)* program. The precision of this method is considerably higher than D determination in the AEA.

Figure 27. Decay profile of a concentration gradiant of $pd(A)_{20}pd(T)_{20}$ after the electric field has been removed: - - - - 0 min, ····· 30 min, -·-·-· 121 min

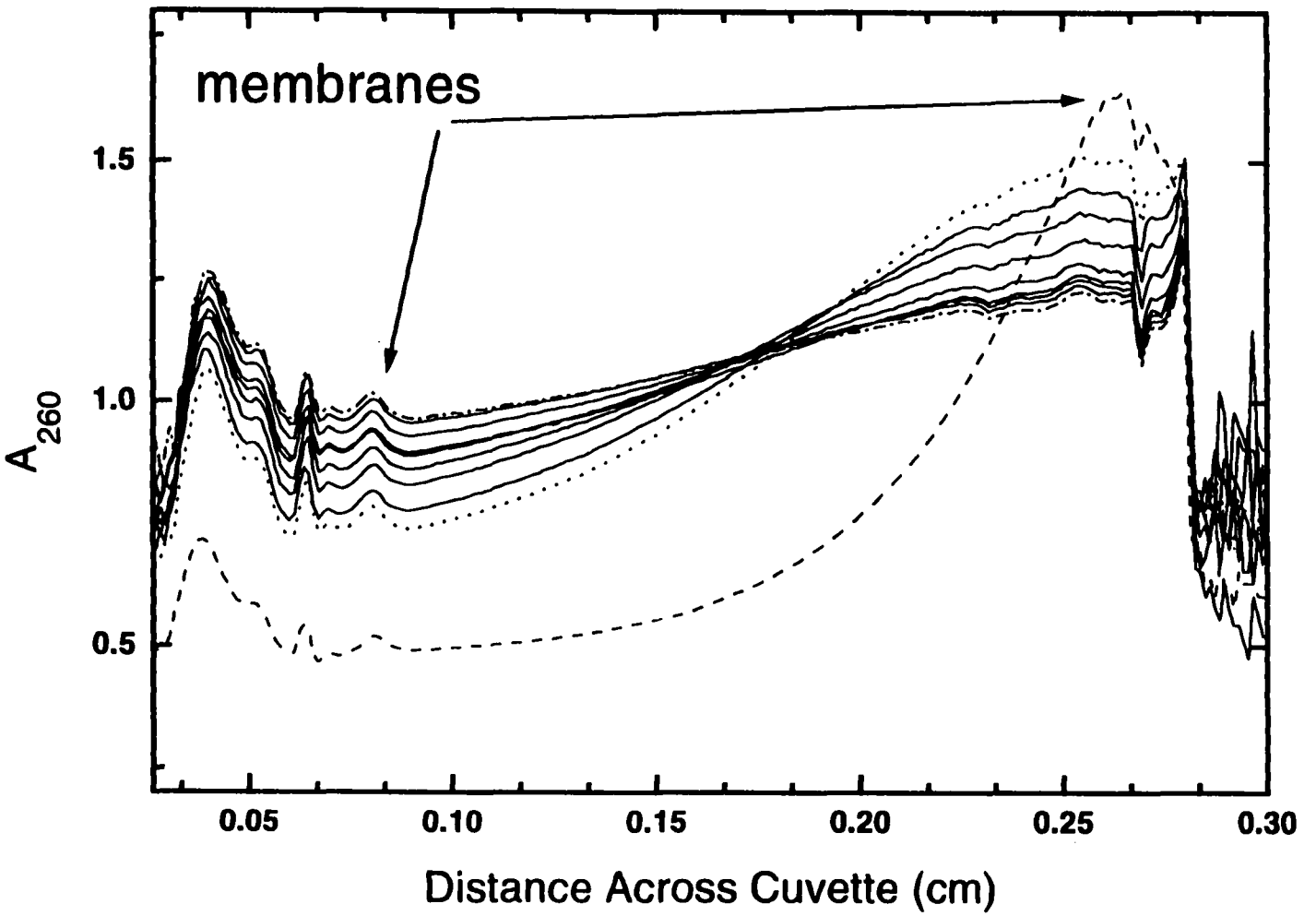

TABLE 6

THE DIFFUSION COEFFICIENT IN THE ABSENCE OF AN ELECTRIC FIELD OF $pd(A)_{20}$•$pd(T)_{20}$ IN DIFFERENT CHLORIDE SALTS

[a] 100 mM chloride salts	KCl	NaCl	LiCl	$(CH_3)_4NCl$
AEA ($\times 10^7$ cm^2/s)	9.6 [b] (8.5, 10.7)	7.8 (6.6, 8.9)	7.5 (6.4,8.5)	8.5 (8.1, 8.9)
Sedimentation Velocity ($\times 10^7$ cm^2/s)	10.4	[c] NA	NA	NA

[a] 20 mM Tris, pH 8.0, 20 °C
[b] Confidence interval are at 65%
[c] Not available

TABLE 7

THE DIFFUSION COEFFICIENT IN THE ABSENCE OF AN ELECTRIC FIELD OF $pd(A)_{20}$•$pd(T)_{20}$ IN DIFFERENT CHLORIDE SALTS

[a] KCl Concentration	100 mM	80 mM	60 mM	20 mM
AEA ($\times 10^7$ cm^2/s)	9.6 [b] (8.5, 10.7)	9.25 (9.0, 9.5)	9.51 (8.74, 10.28)	8.95 (7.55, 10.29)
Sedimentation Velocity ($\times 10^7$ cm^2/s)	10.4	[c] NA	NA	NA

[a] 20 mM Tris, pH 8.0, 20 °C
[b] Confidence interval are at 65%
[c] Not available

The values for D determined by the AEA and sedimentation velocity are similar. Additionally they both fall between the theoretical estimates from the models (see THEORY) of between 6.4 and 13.6 F (touching beads and generated prolate ellipsoid respectively).and near the Tirado and de la Torre estimated value of 10.9 F and measured value of 11.0 F.

The hydrodynamic friction coefficient obtained from D can be used to calculate a predicted electrophoretic mobility from the SSE data (Tables 4 & 5). Table 4 shows that the mobilities predicted from SSE measurements are a factor of 1 ½ lower than the measured μ in figures 4 and 7. This observation is of great interest. At present, no theory predicts this wide a disparity and none of our observations can resolve it.

Diffusion Coefficient in the Presence of an Electric Field

Figures 28 and 29 show the D_e of $pd(A)_{20} \cdot pd(T)_{20}$ as a function of electric field for the four different cation conditions and the different KCl concentrations. There is a distinct increase in D_e over the range of electric fields. The variability of individually determined D_e, especially at lowest and highest fields, is due in part to the limited number of measurements of the moving boundaries that can be free from interference with the membranes. This inhibits describing the relationship between D_e and electric field as linear. It is interesting to note however, that the best fit line through D_e versus electric field gives a zero field intercept comparable to the gradient relaxation determined D_o for all conditions except 100 mM LiCl (4-11 in different cation solution and 8-17 in the various KCl concentrations).

Sedimentation Equilibrium

An estimation of the charge on a macroion can be obtained from the second virial

Figure 28. Diffusion coefficient in the presence of an electric field of $pd(A)_{20}$· $pd(T)_{20}$ in 100 mM XCl, 20 mM Tris, pH 8.0, 20 °C:

■ KCl, -·-■-·- KCl linear fit; □ NaCl, ···□··· NaCl linear fit;

● LiCl, ——●—— LiCl linear fit; ○ $(CH_3)_4NCl$, - - ○ - - $(CH_3)_4NCl$ linear fit

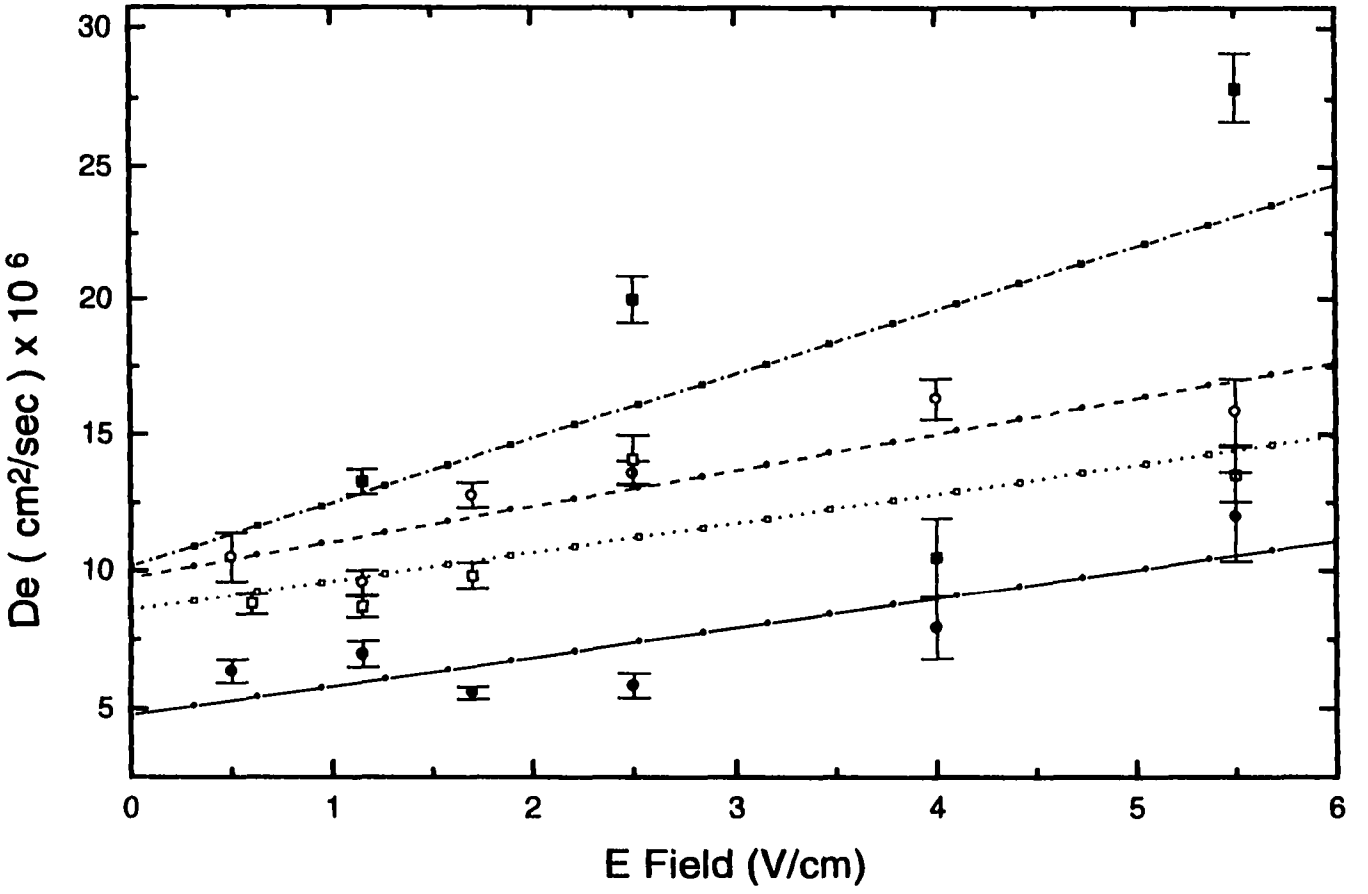

Figure 29. Diffusion coefficient in the presence of an electric field of $pd(A)_{20}pd(T)_{20}$ in X mM KCl, 20 mM Tris, pH 8.0, 20 °C:

■ 100 mM KCl,·····100 mM linear fit; □ 80 mM,····· 80 mM linear fit;

● 60 mM, - -·- - 60 mM linear fit; ○ 20 mM ,—·— 20 mM linear fit

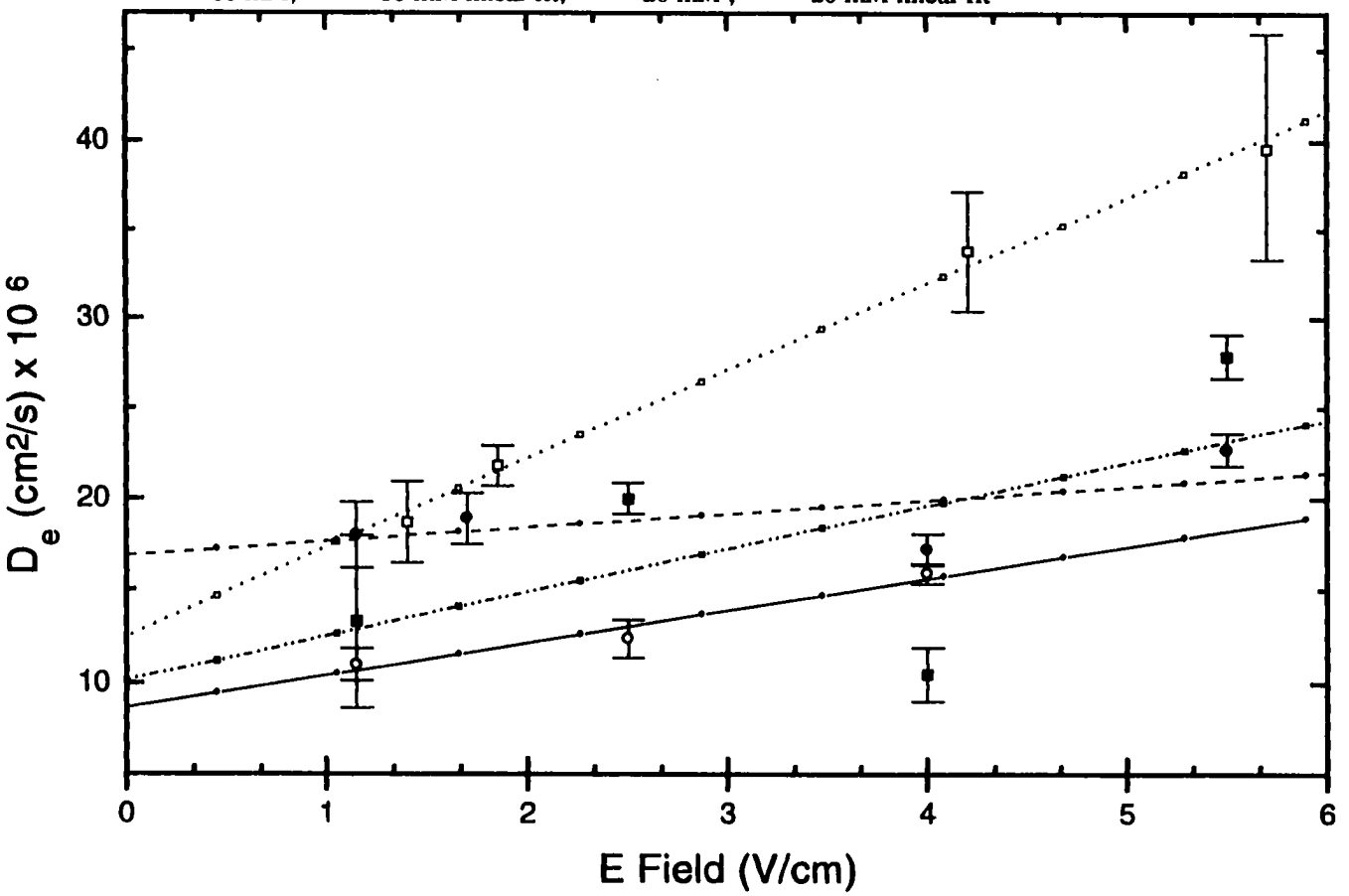

coefficient determined in sedimentation equilibrium. As described in Equations 48, 49, and 50, the nonideal behavior of a charged species will produce increased dispersion in an equilibrium experiment. This will be manifested as a lower apparent molecular weight. Using the known molecular weight of the macroion in the analysis of the gradient yields an estimation of the second viral coefficient. Experiments with $pd(A)_{20} \cdot pd(T)_{20}$ in 100 mM KCl, 20 mM Tris, pH 8.0, at 20 °C generated a B of 0.085 ±.035. This corresponds to a Q_{app} of ~3.2 e. The sensitivity of B to factors such as mass homogeneity limits the confidence in charge determination from sedimentation equilibrium.

DISCUSSION

Introduction

Assessment of Charge Determination Procedures in the AEA

The AEA offers new and enhanced procedures for investigating polyelectrolyte theory and the solution behavior of charged macromolecules. Development of the AEA as a viable biophysical instrument requires exploration into the range and accuracy of the four types of measurements made in it. In particular, it is necessary to address the potential influences on electrophoresis due to the membranes at either end of the cuvette. The use of $pd(A)_{20}$•$pd(T)_{20}$ as a model compound allows the soundness of the simple theory under various solvent conditions to be tested. The four types of measurements can be combined to evaluate electrostatic behavior and address the roles of ion condensation and counterion shielding in electrophoresis.

One goal of the AEA has been to obtain the charge properties (Q_{app} and μ) of a macroion using different procedures. However, the four procedures lead to significant discrepancies in the determined charge properties. For instance, the electrophoretic mobility can be determined experimentally from a moving boundary or it can be predicted from SSE data (σ/E) combined with a D from either experiment or literature. Comparing the predicted mobilities in Tables 2 and 3 to the measured μ's in Figures 3 and 6 reveals the discrepancy, with the experimentally determined μ being 1 ½ to 2 times higher than the predicted value. An evaluation of the Q_{app} obtained from SSE and predicted from μ data yield a similar

discrepancy. Currently, there is no theoretical basis to account for the magnitude of the differences in these properties. Further investigation of possible optical problems and the possible influence of bulk fluid flows are necessary steps in addressing the discrepancy.

While the SSE and μ determined charge properties of the DNA do not appear to directly correspond, they can be used individually to assess the impact on the charge of the DNA from solutions of different ionic compositions.

Evaluation of the Range and Behavior of the AEA Measurements

AEA measurements are taken over the broadest range of E fields and evaluated for consistency and precision. Certain behavioral trends appear to reflect an electric field dependence. It is important to determine whether these behaviors are experimental artifacts that indicate apparatus limitations (possibilities are discussed below) or whether they represent behavior unaccounted for in the simple theories.

Figures 10 and 19 show that the Q_{app} determined from SSE experiments are generally constant over a significant range of electric fields. Two areas that exhibit possible anomalous behavior are the data at the highest and lowest E fields.

Previous analysis of SSE data (25) postulates that curve fitting limitations are one probable cause. Consistent with this contention, the global fit of gradients taken over the full range of E fields yields values similar to the constant range Q_{app}'s with only a slight increase in the root mean of the fit and with comparable residuals. A representative example (Figure 11) shows that low field gradients can easily fit to a global σ. This supports curve fitting limitations as a valid explanation of the behavior at low fields but does not prove it.

As shown in figures 15-18 and 23-25, bulk fluid flows as low as 75 nL/hour are capable of altering macroion gradients. Influences from the apparatus are discussed below as possible explanations for the low field behavior.

The precision of the SSE measurements can be seen in Figure 30. The Q_{app} of $pd(A)_{20}$•$pd(T)_{20}$ was determined in five different set-ups using the same DNA stock solution. The high and low E field data shows variability but the mid-range fields are generally consistent. It appears that the SSE determined Q_{app} of $pd(A)_{20}$•$pd(T)_{20}$ cannot be determined better than ± 1 e. The variability in the measurements can be attributed partially to the flicker and wander in the mercury arc-lamp light source.

The moving boundary in an electrophoretic mobility experiment appears to have a constant velocity. The fitting of the modified Gaussian to the $\Delta c/\Delta t$ profiles yield consistent changes in the position of the centroid of the boundary (peak of the profile) with time. The precision of the procedure and the relationship between the migration of the boundary and the applied E field can be see in Figures 31 (1.7 V/cm μ determinations from different set-ups) and 32 (same set-up, different E fields). The reproducibility of the mobilities, and the consistency of the migrating centroid, shown in Figure 31 suggest that this procedure effectively generates and monitors electrophoretic flux based on the charge characteristics of the macroion.

One important observation from Figure 32 is the consistency of the velocity of the boundary at each E field. The velocity of the moving boundary at the early stages of the experiment is the same as the boundary at the latter stages. The decrease in μ at low E field seen in Figures 3 and 6 is reproducible but still unexplained. The apparent lower velocities

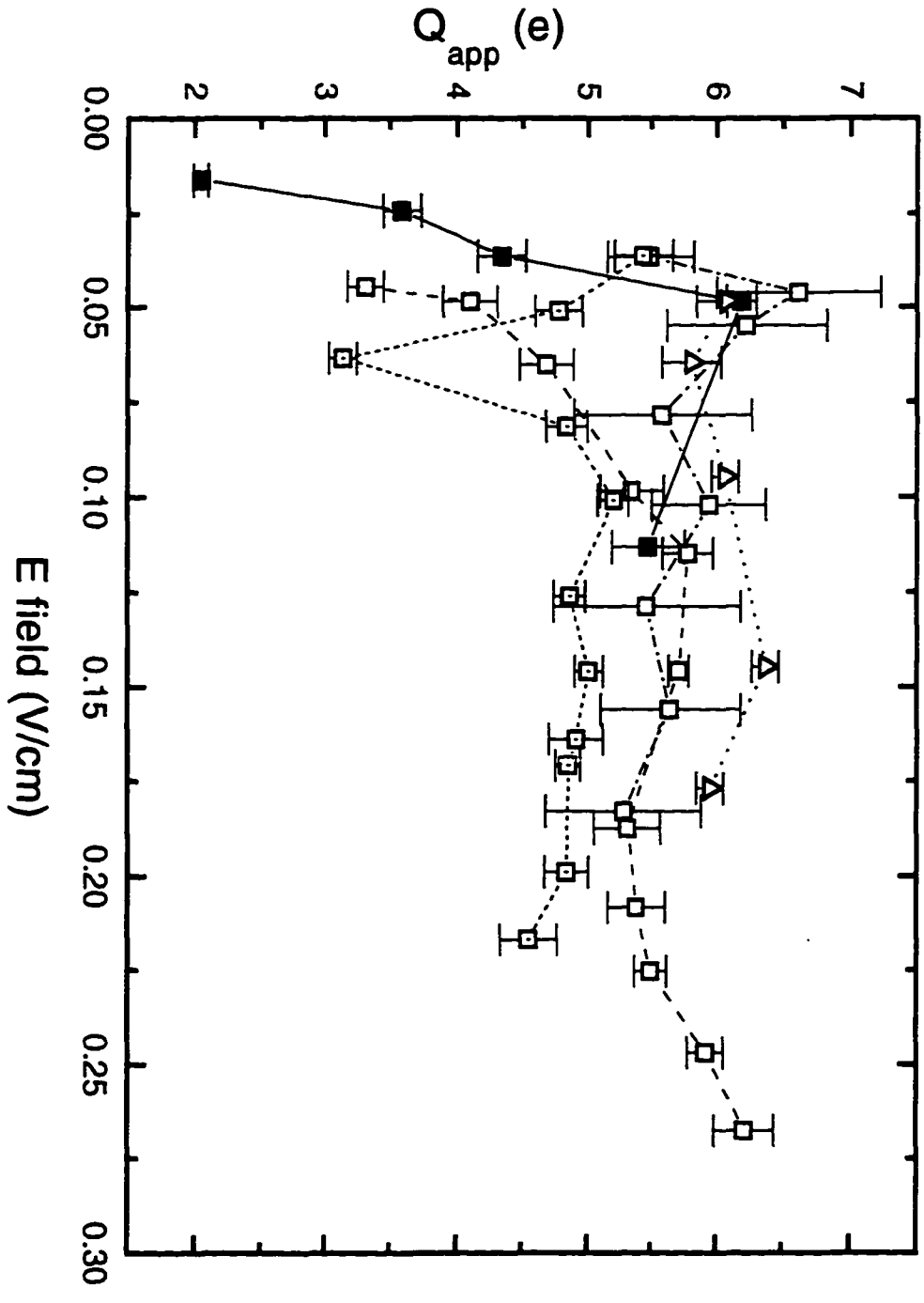

Figure 30. Five independently determined Q_{app} (95% confidence intervals) of $pd(A)_{20}$·$pd(T)_{20}$ as a function of E field in 100 mM KCl, 20 mM Tris, pH 8.0, 20 °C

Figure 31. Reproducibility of 1.7 V/cm μ experiments using four different set-ups of $pd(A)_{20}$·$pd(T)_{20}$ in 100 mM KCl, 20 mM Tris, pH 8.0, 20° C. Offsets of the individual data set reflect different frames of reference

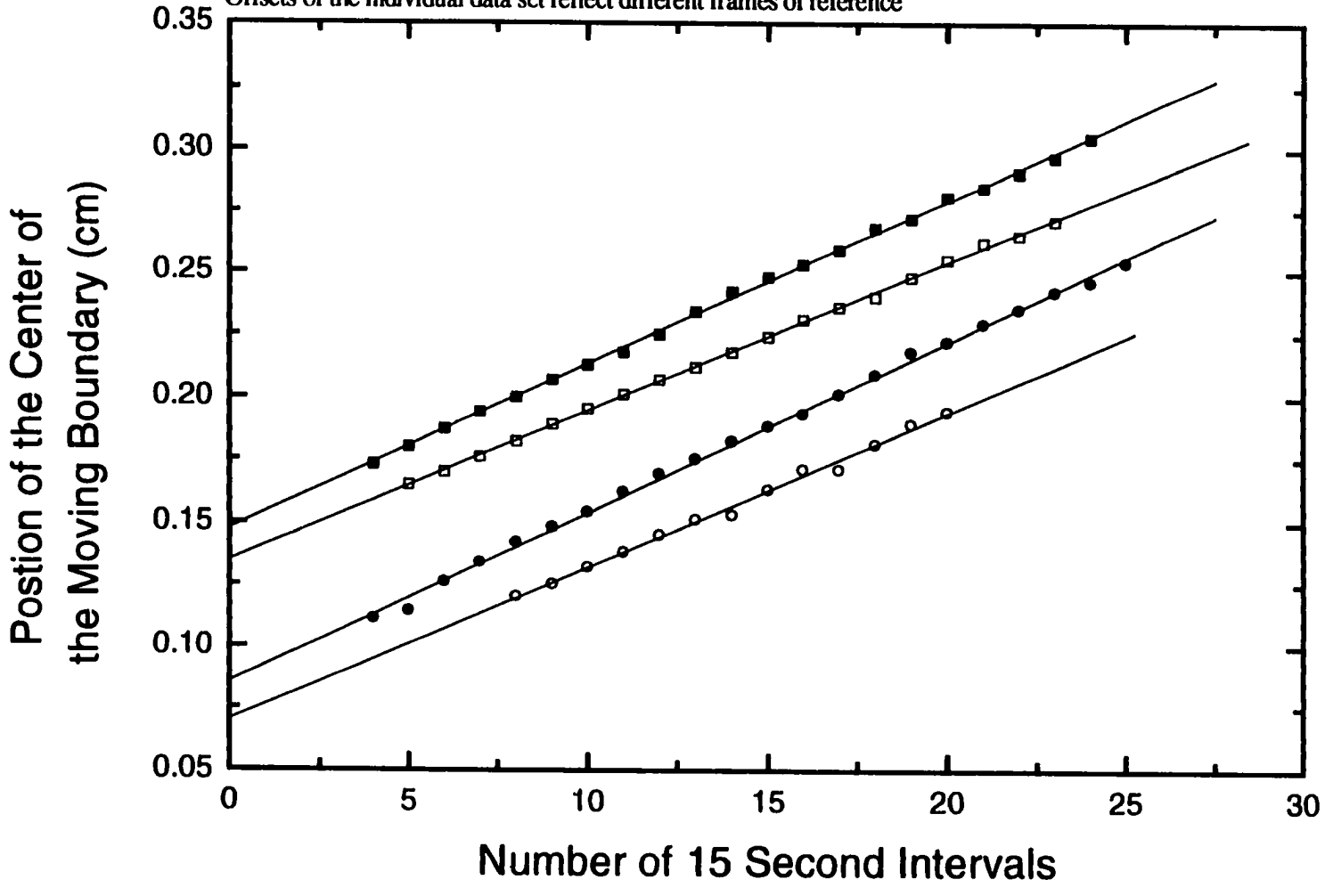

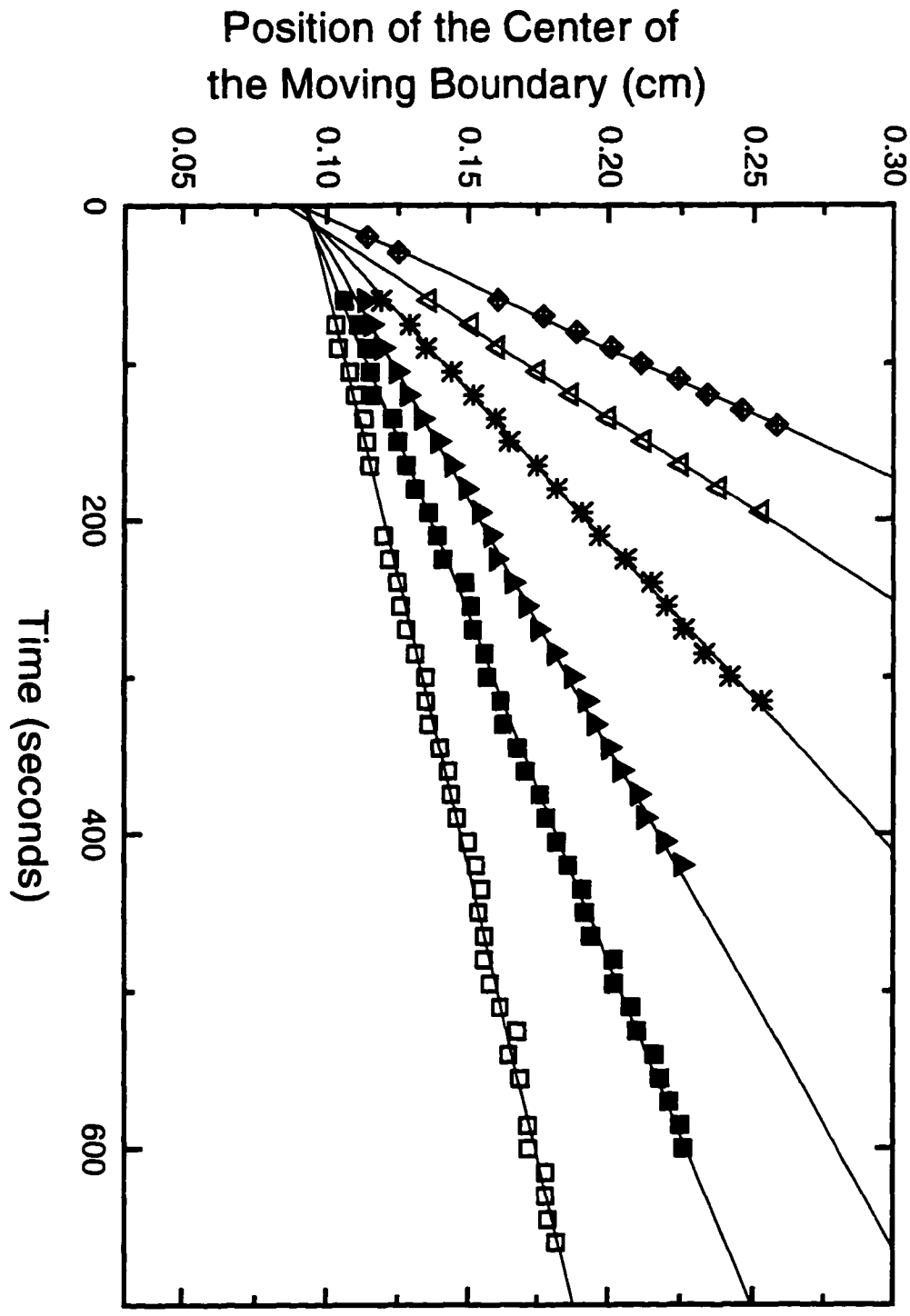

Figure 32. Velocity determination of $pd(A)_{20}$-$pd(T)_{20}$ as a function of E fields in 100 mM KCl, 20 mm Tris, pH 8.0, 20 °C
□ .508, ■ .813, ▲ 1.15, ✱ 1.71, ▽ 3.05, and ◆ 4.06 V/cm

at these field are still consistent throughout the experiment.

The spreading of the migrating boundary appears to be E-field-dependent. The D_e derived from the boundary spreading increases with E field and can show significant variation from experiment to experiment. Electric-field-dependent flows (those linearly dependent on E) are expected to act like an additional velocity term and not increase dispersion unless they promote convection.

Charge heterogeneity and structural fluctuations (end fraying, base pair openings) would lead to increased spreading like that observed here. However, simulated data suggests that the extent of inhomogeneity and fluctuations need to produce spreading of this magnitude far exceeds their expected levels (Thomas Moody and Thomas Laue personal communication). A sufficient explanation of the increased spreading is currently unavailable.

The decay analysis in D_o experiments generally yield data that is consistent with the mathematical model of diffusion (Equation 40) in the AEA (Figure 33). There can be however, up to a 20% differences in the D_o obtained in different experiments under similar conditions. The variation is not easily explained. Experiments using 0.4 cm length cuvette have yielded more consistent data. Full analysis of a macromolecule in the AEA may require the use of cuvettes of different dimensions.

Assessment of the Contributions to the Observed Concentration Distribution That Are a Consequence of the Apparatus or the Process of Electrophoresis

Development of the AEA requires the identification and analysis of potential processes and properties that affect the concentration distribution that are not properties of the

Figure 32. Diffusion coefficient determination of $pd(A)_{20}$·$pd(T)_{20}$ in 100 mM KCl, 20 mM Tris, pH 8.0, 20 ° C. The slope of the best fit line is an estimation of D_o

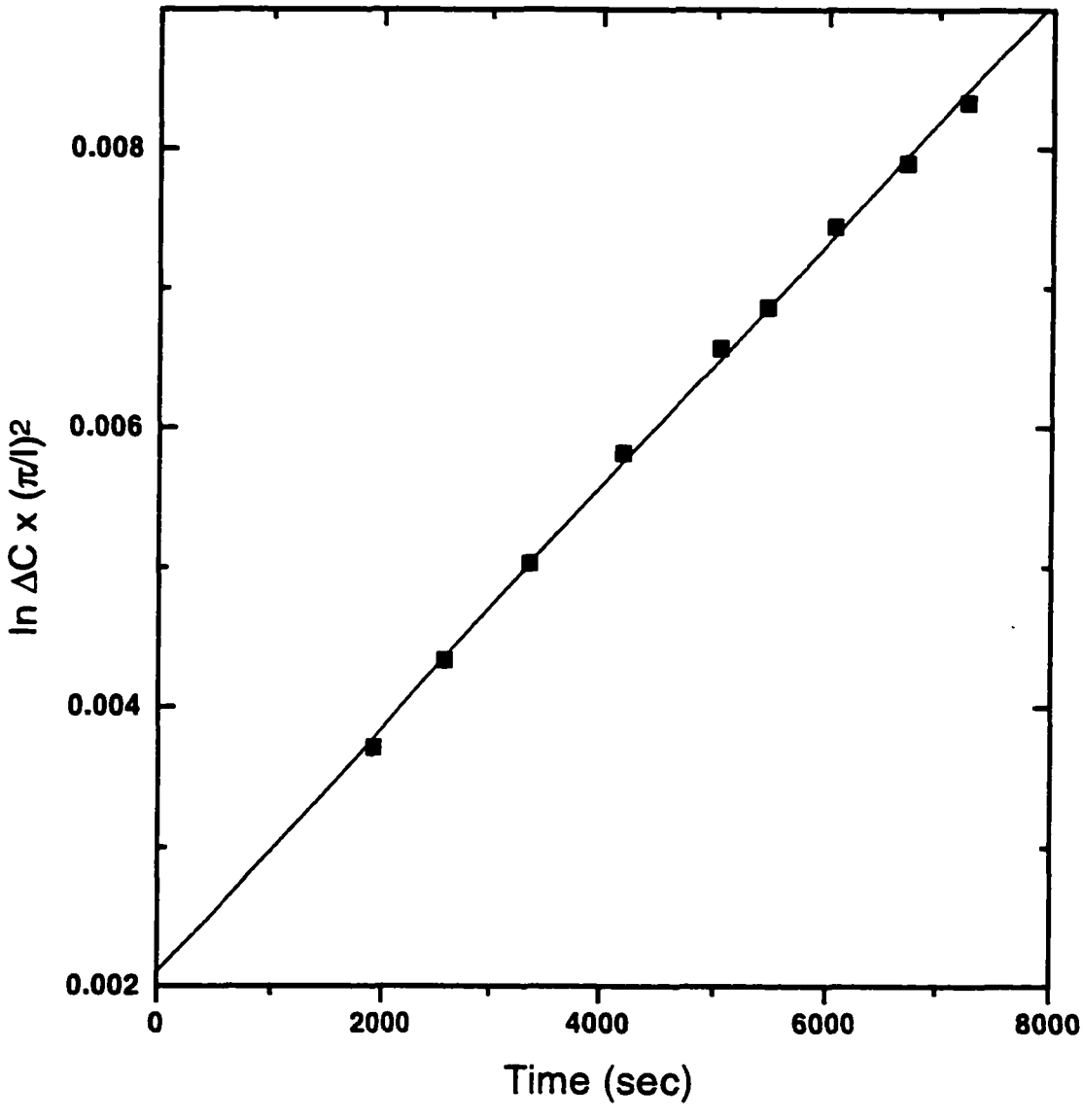

macroion. Nonuniformity of the E field and altered migration due to electroosmosis can distort the laminar concentration distribution leading to inaccurate optical profiles. These processes should reveal their significance in an E-field-dependent manner. Bulk fluid flow acts like a force term that is not accounted for in simple theory. The significance of its effects should be observed in the advancement or impediment of the electrophoretic flux in SSE and μ determination experiments.

Potential Influences on the Optical Detection of the Concentration Distribution Due to a Nonuniform Field at the Cuvette Wall

All interpretations of AEA data are premised on laminar flow through the cuvette and a laminar concentration distribution across the cuvette that is driven by a uniform E field. The Reynolds number determined for the $(0.2\ cm)^3$ cuvette strongly suggests that the solvent flowing thought the AEA is indeed laminar (INTRODUCTION). The extent to which the E field through the cuvette is uniform is difficult to gauge. Figure 1 demonstrates how the nonuniform E field at the cuvette wall can result in non-laminar concentration distribution and potentially influence the accuracy of the optical detection. Significant distortion of the optical profile will invalidate the simple theory used in these investigations.

The electric potential that drives ionic migration must go from a finite value inside the cuvette to a value of zero at the wall. In the AEA, the E field is calculated from measurements substituted into Ohm's Law (E field = $I / \kappa a$). Previous investigations have shown this procedure to provide an acceptable description of the potential between the two membranes. (25). However, an accurate description of the E field near the wall of the cuvette is not possible in the AEA. Assuming an exponential decay, the significance of any transition

region to the accurate optical detection can be assessed with two parameters. The exponential describes how far the E field transition region extends in towards the middle of the cuvette and, thus, defines the shape of the distortion. The second defines the length of time required for a macromolecule to diffuse out of the transition region. Addressing these parameters allows a comparison of the distance that molecules in the rest of the cuvette migrate while others are trapped in the transition region. While the actual behavior of the transition regions remains unclear, it is expected that the potential influence can be quantified.

Expectations are for the E field transition region to occur within 10 to 20 nm of the cuvette wall. This encompasses an area of significantly less than 0.01% of the cuvette. A concentration discrepancy in this small of an area would not be detected. This is true even if the transition region extends out a micron (still less than 1% of the total area of the cuvette). It is not until the transition region is projected to extend 0.1 mm into the 2 mm cuvette that there is a significant amount of area (10%), and potential non-laminar concentration distribution, capable of altering the analyses.

The longer a macromolecule stays in the nonuniform E field region the greater the potential for altering the laminar concentration distribution. The time it takes a macromolecule to diffuse back into the region of laminar migration from the transition region can be estimated from Einstein's equation describing a *random walk*:

$$\Delta t = \frac{\overline{x^2}}{2D} \tag{53}$$

where $\overline{x^2}$ is the mean square distance traveled in time Δt (time of flight) for a molecule of

diffusion coefficient D. Using a D of 11 F for 20 base pair DNA, it would only take 1.8 μs to diffuse out of a 20 nm transition region. The relationship between the thickness of the transition region and the time it would take to diffuse out is shown in Figure 34. Even with a transition region of 1 μm it takes only 4.5 milliseconds for the DNA to return to the laminar concentration region. Simulations suggest that millisecond time scales are too short to account for the trends found in the AEA data (Thomas Laue personal communication).

It is important to relate the time of flight from the transition region to the velocity of migrating boundaries in order to put the consequences of a nonuniform E field into perspective. In SSE experiments, the low fields ($0.02 < E < 0.3$ V/cm) generate DNA velocities on the order of 0.1 to 1.0 μm per second. This means that a molecule in a 1 μm E field transition region would diffuse out before a similar molecule in the center of the cuvette had migrated an additional 4.5 nm. In μ determination experiments ($0.3 < E < 5.5$ V/cm), the molecules at the center of the cuvette molecules would migrate less than 75 nm before a molecule diffused out of the 1 μm transition region. Both scenarios assume the macroion to be diffusing from the wall and that the electrophoretic migration in the entire transition region is zero.

Analysis of the AEA data suggests that the field transition region does not significantly alter the absorbance profile. Optical problems due to altered migration in the transition region are presumed to be E field dependent. High field data would be the most susceptible to influences from the nonuniform field because of the higher electrophoretic velocities and the greater extent of the E field transition. But, SSE and μ data are consistent over a 2 to 3 fold range of the higher E fields. The anomalous behavior seen at the low fields in SSE is not

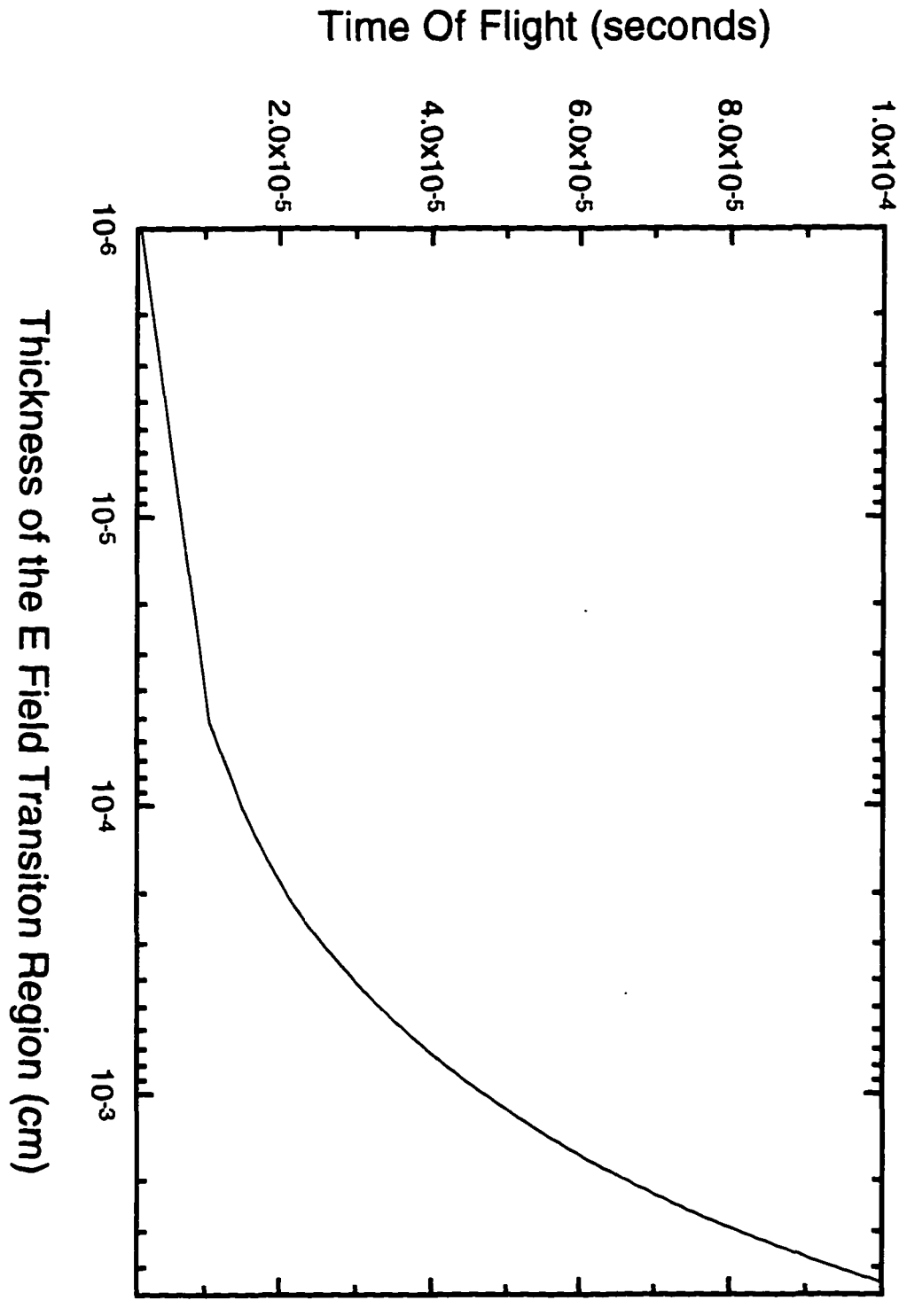

Figure 34. The relationship between the thickness of the E Field transition region and the time it would take for a molecule to diffuse out according to Equation 53

believed to be a product of the nonuniform E field because of the lower velocities and the shallowness of the gradients.

Taken together, it seems reasonable to deduce that the anomalous behavior seen in the AEA data is not a manifestation of an E field transition region as long as these regions are less than 1 μm in extent.

Electroosmosis

Perturbation of migrating ions can occur at the interface between the solution and the cuvette due to the slight negative charges present on the quartz surfaces. The preferential flow of positive ions along the stationary quartz interface (electroosmosis), combined with surface repulsion of the DNA, has the potential of creating local regions of altered mobilities, thereby distorting the electrophoretic flow and creating a non-laminar concentration distribution. Figure 1 can be used to describe the potential influence on the optical profile due to electroosmosis in a manner similar to the argument for the nonuniform E field transition region. Electroosmosis also is expected to have the property of E field dependence. Fortunately, electroosmosis is known to occur within a few molecular diameters (< 20 nm) of an interface (55).

The same dimensional arguments that were applied to the nonuniform E field transition (limited thickness of the region, brief time of flight out of the region, and the limited general migration) can be applied to electroosmosis. Additionally, the extent of the interaction at the interface has been investigated by treating the surface of the cuvette with a siliconizing agent to make it non-wetting. The siliconizing agent applied to the cuvette forms a hydrophobic surface that is believed to eliminate preferential interactions. The results of the measurements

taken before the coating have been compared to those taken after the coating and analyzed for reproducibility and E field dependence. Within the sensitivity of the apparatus, there appears to be no difference using the siliconized cell. SSE and μ data still show anomalous low field behavior. Experiments measuring D_o and D_e yield results in the expected ranges.

Electroosmosis does not appear to be the reason for the observed trends. The flow of positive ions along the wall of the cuvette does not appear to generate a significant alteration to the laminar concentration distribution. In future AEA experiments, the significance of electroosmosis may need to be verified for certain types of macromolecules and solvent conditions that lead to preferential interactions with quartz.

Potential Influence of Solution-Membrane Interactions

A fundamental concern in all AEA experiments is the role of the membrane. One of the earliest steps in the development of the AEA was the testing of various types and sizes of membranes (25, 51) using macromolecules such as cytochrome c and lysozyme. The regenerated cellulose membranes were found to provide minimal charge and molecular interaction. Still, each macromolecule has its own set of properties which are sensitive to factors such as salt concentration and E field. Electrostatic interactions of the $pd(A)_{20}$•$pd(T)_{20}$, or components of the buffer solution, with the slight negative charges of the membranes can potentially alter laminar flow and the laminar concentration distribution.

Dialysis membranes have pores that limit the size of a particle able to pass through them. The membrane casting procedure is such that the amount of regenerated cellulose per unit of area decreases with increasing pore size. If migrating ions interact with the membrane bound charges, then varying the pore size and, therefore, the amount of membrane material, will

affect measurements in the AEA.

Membranes of various molecular weight cut offs (MWCO) were used in SSE and mobility experiments under a variety of conditions and compared for reproducibility. Three MWCO pore sizes (3500, 6-8 K and 14 K) of regenerated cellulose dialysis membranes were used in investigations conducted at electric fields of 0.05 to 0.3 V/cm (SSE) and 0.3 to 8 V/cm (μ) in 10, 20, and 100 mM KCl. Within the precision of the measurement, all three membranes behaved identically (with the exception of an increased loss of DNA with the 14 K MWCO). These results, combined with the earlier membrane studies (25), indicate that the porosity of the dialysis membrane used in our experiments with $pd(A)_{20} \cdot pd(T)_{20}$ does not significantly affect the results.

Assessment of the Influence on the Observed Concentration Distribution Due to Bulk Fluid Flow

The aim of the AEA is to monitor the migration of macroions attributed to an applied E field and diffusion. Simple theory may then be used to obtain the charge and hydrodynamic properties of the migrating species. But, an apparatus that produces crossing currents of migrating ions, macromolecular gradients, and employs a constant flow buffer system is highly susceptible to the generation of bulk fluid flows capable of influencing the distribution of the macroion. Determining the circumstances in which bulk fluid flow significantly colors analysis of AEA measurements is imperative in the development of the apparatus.

Bulk fluid flow can be thought of as contributing an extra velocity term (either positive or negative) to the theories used to describe electrophoresis and diffusion. This term may be E field dependent such as those produced if the sum of the flows of current carrying hydrated

ion is not zero or from osmotic pressure differences generated by developing concentration gradients at the two membranes. The velocity term may also be E field independent, an example being one generated by a hydrostatic pressure difference across the cuvette. Simulated data suggest that the minimum rate of bulk fluid flow capable of influencing AEA measurements is on the order of 75 nL/hour which is well below the ability of simple quantitative measurements. Its significance, however, can be deduced from AEA measurements showing characteristics of the those flows.

A linear E field dependent bulk fluid flow should influence AEA measurements as the addition or subtraction of a constant to the true values ($J_e = c\ Q\ E/f_e + `F\ E$). In other words, E field dependent bulk fluid flow acts like an additional velocity term (positive or negative) that is a function of the applied field and will enter into the determined values as a modified electrophoretic velocity.

The importance of E field dependent bulk fluid flow can be addressed by monitoring AEA measurements at conditions which maximize the extent of a flow or accentuate a difference in flows. The significance of an excess of water being carried in the hydration sphere of one of the salt ions can be approached by alternating the direction of the bulk fluid flow and observing the change in the magnitude of the measurements or the reversal of a trend. Osmotic pressure effects should increase with the increase of the concentration difference at the two membranes. Both SSE and μ data contain large macroion concentration difference at the membranes and can be used to probe for osmotic influences.

The significance to AEA measurements of a hydrostatic pressure difference across the cuvette was investigated by mismatching the buffer flow rates and observing the effects.

These potential influences to the AEA measurements are discussed in turn below.

Evaluation of AEA Measurements for the Significance of Hydration Sphere Induced Bulk Fluid Flow on the Observed Concentration Distribution

The laminar flow of 100 mM hydrated ions through the AEA cuvette are on the order of pL/s to nL/s. Bulk fluid flow produced by the non equal hydration of the cations and anions will also be of this magnitude. The extent that such low flows influence the charge measurements of $pd(A)_{20}$•$pd(T)_{20}$ was investigated by using chloride salts with cations exhibiting either a larger (Li^+) or smaller [$(CH_3)_4N^+$] number of waters in their hydration sphere (compared to chloride's 4 waters).

Li^+ has a hydration sphere of 6 waters while $(CH_3)_4N^+$ has only 2 waters. The bulk flow produced by the LiCl should impede the electrophoretic flow of $pd(A)_{20}$ •$pd(T)_{20}$ while $(CH_3)_4NCl$ induced flow should augment it. The expectation for the influence of bulk fluid flow on AEA measurements is either an E field dependent increase or decrease depending on the direction of the flow.

Figure 35a shows the μ's of $pd(A)_{20}$ •$pd(T)_{20}$ in the two salt conditions as a function of E field. For an E-field-dependent flow, a constant offset in mobilities is predicted. While the difference in the magnitude of the mobilities are primarily a function of the cation type, the maximum difference that could be attributed to the hydration sphere induced bulk fluid flow (but probably significantly less considering the bulk fluid flows are in opposite directions) is about 15%. The similarity in the low E field trend (decreasing μ with decreasing E field) suggests that the phenomenon responsible for that behavior is not a linear E-field-dependent

Figure 35. Comparison of the AEA determined (a) electrophoretic mobility and, (b) σ, of $pd(A)_{20}$·$pd(T)_{20}$ (95% confidence intervals) as a function of E field in 20 mM Tris, pH 8.0, 20 °C and in • 100 mM LiCl or ○ 100 mM$(CH_3)_4NCl$

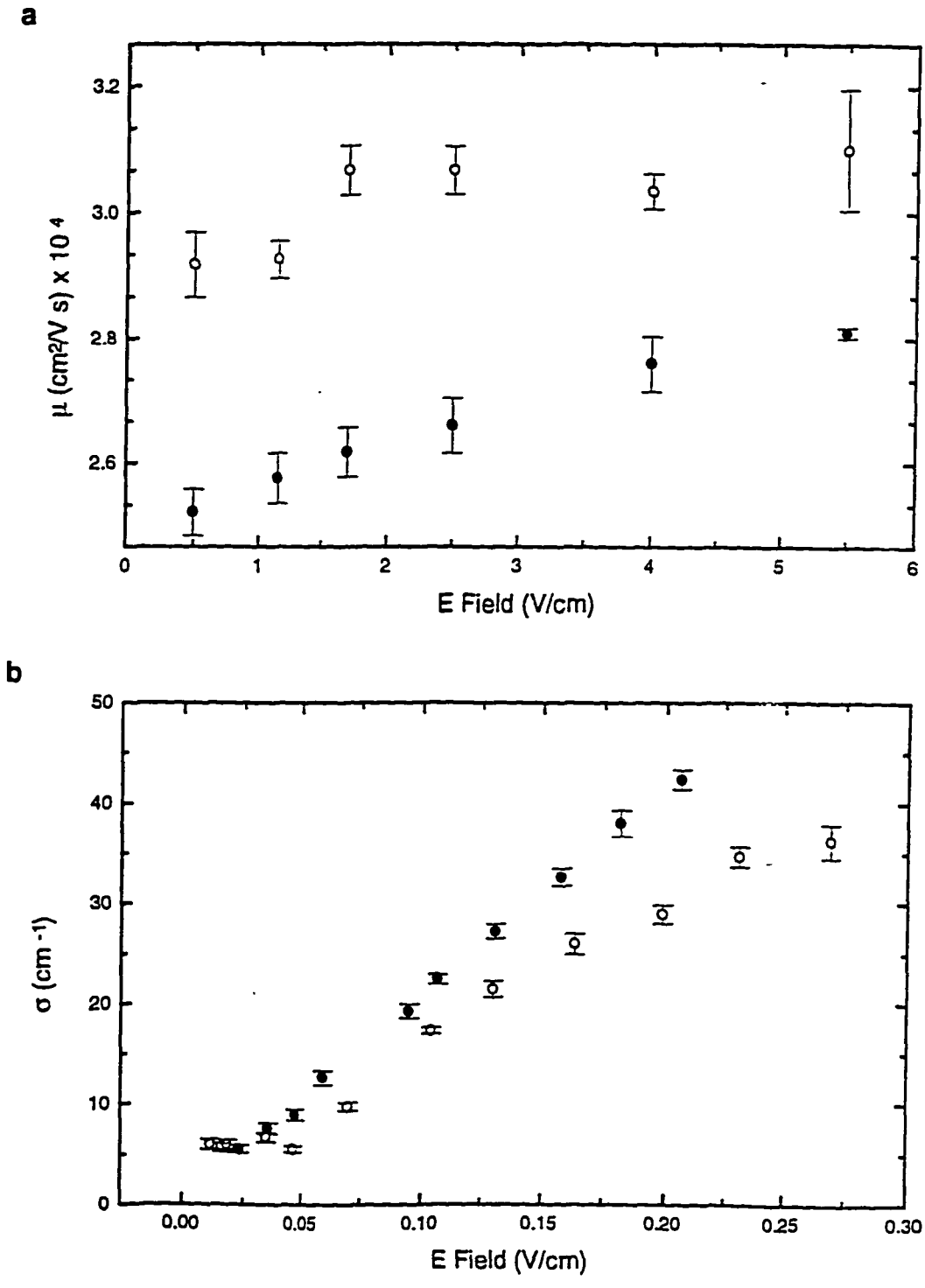

bulk fluid flow but a flow that depends on polarization which goes as E^2 ($J_e = c\ Q\ E/f_e + `F\ E + ``F\ E^2$).

The excess spreading of the μ boundaries that translates into increasing D_e's with increasing E field is not likely to be produced by hydration sphere induced bulk flow unless the flow leads to convection. A preferential flow through the AEA cuvette in a mobility experiment would be expected to act like an additional velocity term. From the frame of reference of the migrating boundary, a laminar bulk flow (especially the nL/s flows experienced in the AEA) would not promote the dispersion of macromolecules seen in the mobility experiments.

The same argument for the influence of hydration sphere induced bulk flow on electrophoretic flux can be made with SSE data although the low electrophoretic flows suggest a lesser potential impact. Figure 35b shows the similarity of σ's of $pd(A)_{20} \bullet pd(T)_{20}$ in LiCl and $(CH_3)_4NCl$ over the low and mid-field E fields. The magnitude of the difference in the σ's is less than 10%.

The most likely explanation for the high field $(CH_3)_4NCl$ behavior is in the chemistry of $(CH_3)_4N^+$ with the membranes and the DNA. $(CH_3)_4N^+$ is well known to behave atypically under certain circumstances (38, 54).

The relationship between the anomalous behavior of Q_{app} at low electric fields (Figures 10 and 20) and hydration sphere induced bulk fluid flow, if it exists, cannot be established. Simulated data predicts that the lowest flows capable of being detected as forming a gradient from a uniform concentration distribution is 75 nL/hour. But it is also a reasonable conjecture that, *in the AEA*, the nL/hour flow rates of the hydrated ions at the lowest fields are subjected

to real solution dynamics and do not produce distinct alterations in the gradients. However, if ion-induced bulk fluid flow is an influence on the electrophoretic velocity of the macromolecule, then its prominence may require these very low macromolecular velocities to become detectable.

Assessment of Osmotic Pressure Induced Bulk Fluid Flow On the Observed Concentration Distribution

The osmotic pressure, π, across a semi-permeable membrane is proportional to the concentration of the macromolecule on the one side. The argument for osmotic pressure induced bulk fluid flow in the AEA is considered for a steady state gradient in which the concentration of the macromolecule at the two membranes is different. If the π is a function of the *total* concentration inside the cell, then both membranes experience the same pressure and there is no net flow. If, however, π is a micro or local phenomenon, then the areas adjacent to the membranes will generate unequal osmotic pressures. Experimentally, this would be manifested as E field dependent osmotic pressure flow (Equation 30 reveals the E field dependence to be exponential). At high fields, the gradients are steeper and consequently would generate larger flows. The osmotic flow would act to reduce the electrophoretic flux thereby yielding lower σ's. This argument is particularly relevant during the establishment of an SSE gradient and can be extended to concentration gradients in mobility and diffusion experiments.

An important consideration in assessing the significance of osmotic pressure on the concentration distribution is the defining the magnitude of the π under the conditions of these experiments. The force due to osmotic pressure in the AEA can be expressed as:

(54) $$F = \frac{\Delta c_1 RT}{K_1} + \frac{\Delta c_2 RT}{K_2}$$

where Δc_1 and Δc_2 are the concentration differences at the two membranes that exhibit permitivities of K_1 and K_2 respectively. Assuming no inhibition to flow at the membranes and 300 μg/ml of $pd(A)_{20}$ •$pd(T)_{20}$ the upper limit of π in SSE is on the order of 10^{-3} atmospheres. Any appreciable resistance at the membranes will reduce the flow through them. It is difficult to quantify this pressure because the resistance to flow of the membranes is not known.

An argument can be made against osmotic flow at steady-state in SSE experiments. Figure 36 represents an SSE gradient divided up into numerous boxes. The osmotic pressure at the top membranes is directed into the first box of the cuvette. The macroion concentration in the second box is higher than that in the first, thereby creating an osmotic pressure directed into the second box. This argument can be propagated all the way to the last box (bottom membrane). The concentration in the last box creates an osmotic pressure into the box. The sum of the osmotic pressures in all but the last box is equal and opposite to the osmotic pressure into the last box. The two osmotic flows cancel each other and do not produce a bulk fluid flow.

Analysis of the AEA data suggests that osmotic flow does not significantly influence electrophoretic flux. Two lines of evidence support this contention. First, σ versus E data is linear over a broad range of fields and, therefore, a broad range of macroion concentration differences (Figures 12 and 21). With the exception of 60 mM KCL and 100 mM $(CH_3)_4N^+$

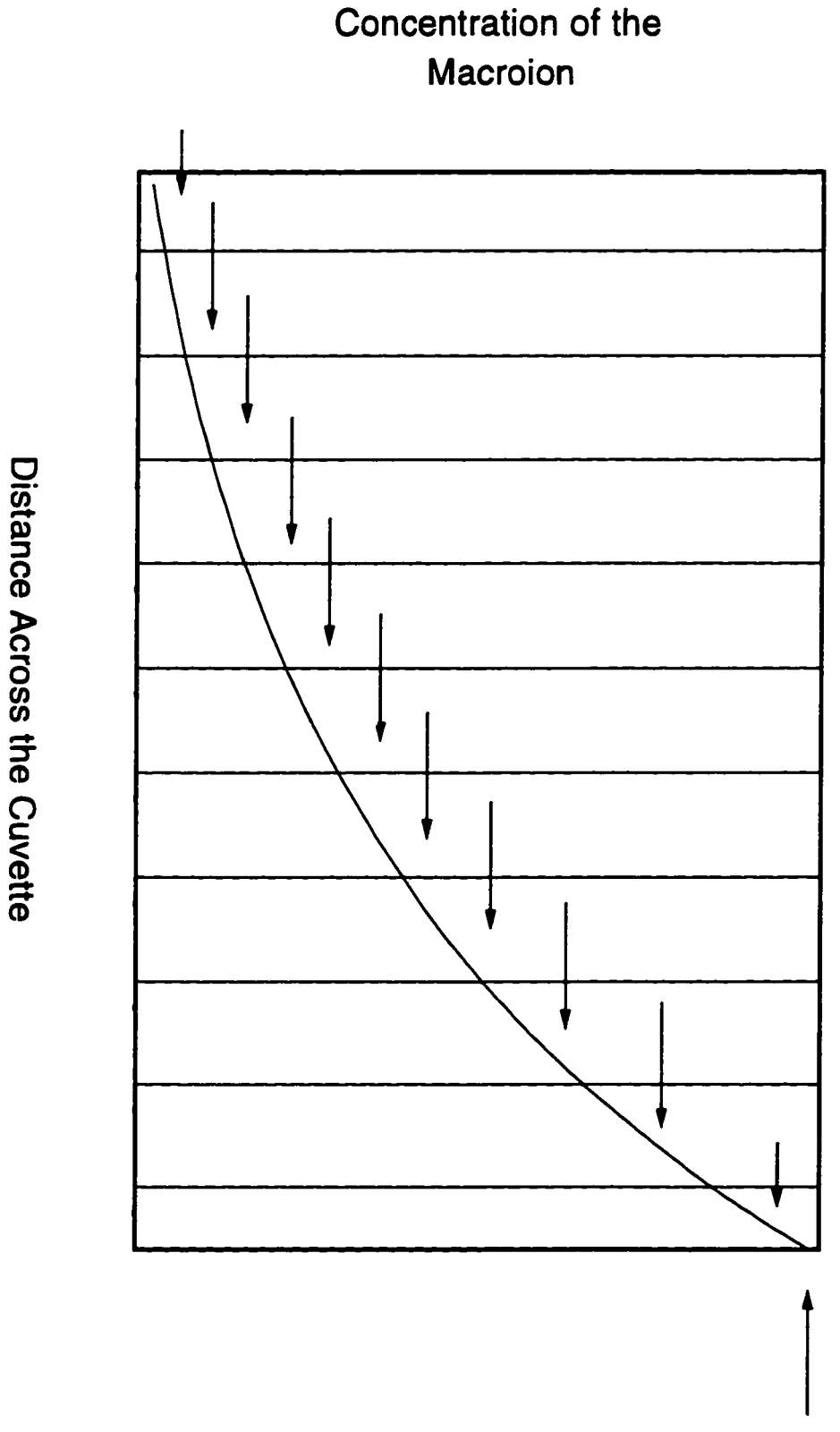

Figure 36. A representation of the argument against osmotic induced bulk fluid flow through the AEA in a SSE experiment. The arrows indicate the direction of the osmotic flow through sections of the cuvette

data (the two conditions that do not behave well at high SSE E fields), there is no evidence (curling down of σ's at high E fields) for significant retardation of the electrophoretic flux. Secondly, in μ determinations the centers of the moving boundary (the peak position of $\Delta c/\Delta t$ analysis shown in figure 2b) are equally spaced (Figure 2c, 31, and 32) over the detectable region of the cuvette even though the concentration differences of $pd(A)_{20} \cdot pd(T)_{20}$ at the two membranes becomes increasingly different (20-fold or more) at the later times.

Osmotic pressure induced flow is most likely not a factor for the decreasing μ with decreasing field. Velocity determinations start with a homogeneous concentration distribution of macroions. Velocities taken at the beginning of the experiment in which little to no gradients have formed are the same as velocities at the end of the experiment indicating no significant impediment to electrophoretic flux.

Similar to the argument against the spreading of the μ boundary (D_e) due to hydration sphere induced bulk fluid flow, osmotic induced flow should act like an additional velocity term and not promote dispersion of the macromolecules Unless osmotic-induced flow leads to convection, the large E field dependent spreading in mobility experiments is probably a result of a different phenomenon.

In D_o experiments, the concentration difference at the membranes is considerably less than in most SSE and in all μ determinations. Considering the requirement of allowing ~2000 seconds to pass in D_o determination before taking data, the expectation is for the gradient to relax significantly and the difference in π to be small. The decay profile in Figure 27 and the representative fit shown in Figure 33 suggest that decay of the gradient fits Equation 40 over a broad range of times and concentration differences at the membranes. It should be noted

that a roughly exponential decrease in a bulk flow with time will lead to an analysis that fits a straight line and yields a wrong D_0 (Tim Wilson and Harvey Shepard personal communications). The significance of osmotic induced bulk flow in diffusion experiments appears to be small but cannot be ruled out.

The Effects of Hydrostatic Pressure Differences on the Observed Concentration Distribution

In the AEA, buffer is pumped continuously past the membranes at rates of 20-40 ml/hour in order to flush out electrolysis products and to minimize ion gradients in the cuvette due to electrodialysis. The flow rates in the upper and lower buffer chambers are matched to prevent a hydrostatic pressure difference from being formed across the cuvette. Exact matches are not always possible due to limitations of the tubing and peristaltic pump. The significance to AEA measurements of a hydrostatic pressure difference across the cuvette has been investigated by purposely mismatching the flow rates in the two chambers. Steady state gradients were formed with the top chamber having no flow or ½ the flow of the bottom chamber. Similar experiments were performed with the lower chamber having the reduced flows.

Figure 37 shows the σ's of SSE gradients of $pd(A)_{20} \bullet pd(T)_{20}$ in 100 mM KCl, 20 mM Tris, pH 8.0 at 20° C formed in low and mid range E fields (0.026 and 0.065 V/cm respectively) under the different flow conditions. The σ's from the mid range E field were within 5% of each under all flow conditions. The low field σ's were completely dependent on flow conditions. Flows favoring electrophoretic migration increased σ while flows opposing decreased σ. While the magnitude of the change in σ was similar at both fields, the ratio of change was distinct. This evidence indicates that the range of E fields that yield

Figure 37. The significance of hydrostatic pressure in gradient formation in the AEA. Hydrostatic pressures across the cuvette were created by mismatching the buffer flow rates through the top and bottom buffer chambers. The σ's were measured for $pd(A)_{20} \cdot pd(T)_{20}$ in 100 mM KCl, 20 mM Tris, pH 8.0, 20 °C at □ 0.026 V/cm and ■ 0.065V/cm in which there was either no flow through the chamber or the flow rate was half of the other chamber. This was done for both the top and bottom chambers

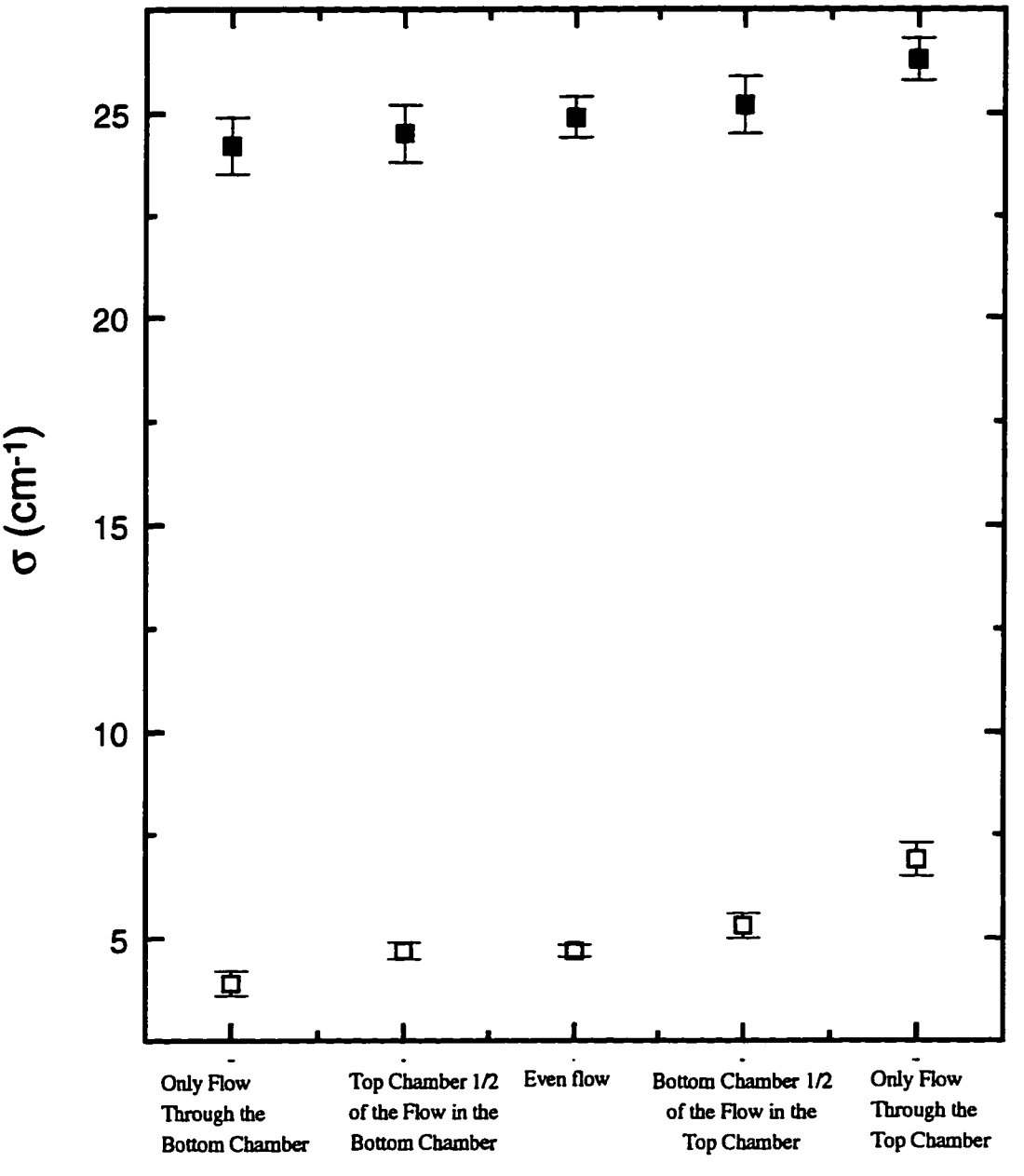

higher, consistent σ's are not significantly influenced by the applied bulk fluid flow but that the low field data can be influenced.

While it is evident that hydrostatically induced bulk fluid flow is capable of influencing the concentration distribution it is not proof that the anomalous behavior at low field is the result of this flow. Effects on σ required large discrepancies in the flow rates and efforts are made to match the flows. More quantitative studies have been proposed (Tim Wilson personal communication) in order to better characterize the effects of hydrostatic pressure. A back pressure can be produced by preferentially reducing the sizes of the tubing leading from the apparatus. Monitoring the effects of the tube size on the measured σ may offer additional insights

Effects of Varying Monovalent Cations on the Electrophoretic Properties of $pd(A)_{20}$•$pd(T)_{20}$

Most theoretical predictions (see THEORY) for the charge, and the ionic shielding, of macroions have little to no dependence on the type of monovalent counterion used. Roles for affinity of the counterion to the macroion, radius of the counterion and size of the hydration sphere of the counterion are not incorporated. Only the DH theory integrates the radius of the counterion in its calculation of the center to center distance of closest approach. With $pd(A)_{20}$•$pd(T)_{20}$ in chloride salts of either KCl, NaCl or LiCl, the distance of closest approach changes by less than 10%. According to equation 15, this should lead to changes in the Q_{eff} of less than 3%. Even with a cation 2 to 3 times larger, $(CH_3)_4N^+$, the difference in Q_{eff} for $pd(A)_{20}$•$pd(T)_{20}$ is less than 10%.

The MCC theory does not predict a cation type dependence in charge shielding. Manning argues (38) that the differences in the magnitude of the mobility of a polyelectrolyte in the

different chloride salts would be a function of the "..different transport characteristics of different small-electrolyte solutions....". In other words, the mobility (Table 1) of the cations (Manning uses the term *equivalent conductance*) directly influences the overall mobility of the DNA. Manning calculates the difference in mobility for an infinitely long polyelectrolyte in 100 mM LiCl compared to 100 mM KCl to be about 7%. Manning also discounts DNA mobility data in $(CH_3)_4N^+$ due to its atypical DNA binding behavior (38, 54). Organic cations (quaternary amines bearing a formal positive charge) are recognized (54) to interact act with aromatic groups (bases in the DNA). This *unconventional* ionic bonding (proposed to be more stable than those with anionic residues) is capable of producing electrophoretic behavior unaccounted for in simple theory.

Evaluation of the mobility data of $pd(A)_{20} \cdot pd(T)_{20}$ from the AEA (Figures 3, 4, 5 and Table 2) reveals that there is a cation dependence to μ. It appears to follow the strength of the affinity of the cation for DNA [it also follows the radius of the unhydrated cation and, with the exception of $(CH_3)_4N^+$, the mobility of the cation] similar to experiments performed on large DNA by Ross and Scruggs in 1964. They proposed that the closer a cation is able to approach the DNA (smaller radius), the higher its affinity for the DNA and the better it is able to shield the macroion from the E field thereby yielding lower mobilities.

The magnitude of the differences in μ between the different cations is larger than would be predicted from the difference in cation radius (DH) but in reasonable agreement with MCC. The AEA mobility data cannot substantiate either the significance of cation affinity for DNA or MCC as the correct description of the cation dependent mobility of $pd(A)_{20} \cdot pd(T)_{20}$. It does appears however, that the AEA measured mobilities exhibits both charge and

hydrodynamic influences.

The SSE data of $pd(A)_{20}$•$pd(T)_{20}$ presented in Figures 10, 11, 19, 20 and in Tables 4 and 5 do not demonstrate clear cation type dependence. The variability of individually determined Q_{app}'s limits interpretation. The combined fits provide more insight. Neglecting $(CH_3)_4N^+$, the slope of the best fit line to σ versus E yields range of Q_{app}'s of 5.0 ± 0.5 e. The sensitivity of the slope to individually determined σ's reduces the precision of this technique (this is more readily seen in the KCl concentration experiments). The Q_{app}'s from the global fits are ~ 5 e and have over lapping 95% confidence intervals. Global fit Q_{app}'s appear to a better way of presenting SSE data because it yields consistent values, combines *all* of the actual data and can use scans from a broader range of E field.

The similarity of the SSE determined charge of $pd(A)_{20}$ •$pd(T)_{20}$ under theses experimental conditions [with the exception of $(CH_3)_4N^+$] suggest that there is no significant cation dependence. This is in accordance with the MCC theory. The SSE procedure appears to produce conditions that isolate the actual charge of a macroion.

Comparing the charge properties determined from SSE and μ demonstrates the current state of development of the AEA. The Q_{app} determined from the two procedures yield different values (~ 5 e and ~ 6.5 e respectively). Additionally, μ data exhibits greater solvent dependence than SSE. Consolidation of the two procedures is currently in progress. The sensitivity of the μ determination to solution conditions might allow particular influences to be evaluated that augment the basic charge determined by SSE

Effects of Varying the Ionic Strength on the Electrophoretic Properties of $pd(A)_{20}$•$pd(T)_{20}$

The role of counterion shielding of macromolecular charge is an important concept in

understanding macromolecular interactions. Theoretical prediction for the reduction of macroion charge by counterions starts with coulombic attraction and thermodynamic distribution. The AEA measured electrophoretic flux of $pd(A)_{20} \cdot pd(T)_{20}$ is expected to increase with decreasing KCl concentration.

The DH theory predicts that the counterion shielding of a macroion will be proportional to the square root of the ionic strength. The high salt conditions used in these experiments ($\kappa a \not< 1$ as required in the derivation of Equations 12,13 and 15) limit the validity of predicted DH values for the DNA in the different salt conditions but can still be useful in describing the potential effects of ionic strength. Increasing the KCl concentration from 20 mM to 100 mM (20 mM Tris, pH 8.0) is predicted to reduce the charge of $pd(A)_{20} \cdot pd(T)_{20}$ if the basic principles of the Poisson-Boltzmann equation hold at these high salt concentrations.

Evaluation of Simple Theories in the Context of AEA Measurements

An essential aspect in the development of the AEA is to provide experimental data that can be used to evaluate macromolecular charge theory. Figure 38 combines the theoretical predictions and experimentally determined values for the apparent charge of $pd(A)_{20} \cdot pd(T)_{20}$ in 100 mM KCl. The large degree of variability in the predicted values is evident. Predictions based on the AEA determined mobility and both procedures for the interpretation of the SSE data yield Q_{app}'s that are lower than theoretical predictions. It appears that charge on macroion capable of experiencing the E field in the AEA exhibits a greater level of shielding than expected.

Of all the AEA techniques, SSE has the greatest potential for accurately determining the Q_{app}. The balancing of fluxes discussed in the derivation of the Q_{app} equation allows the

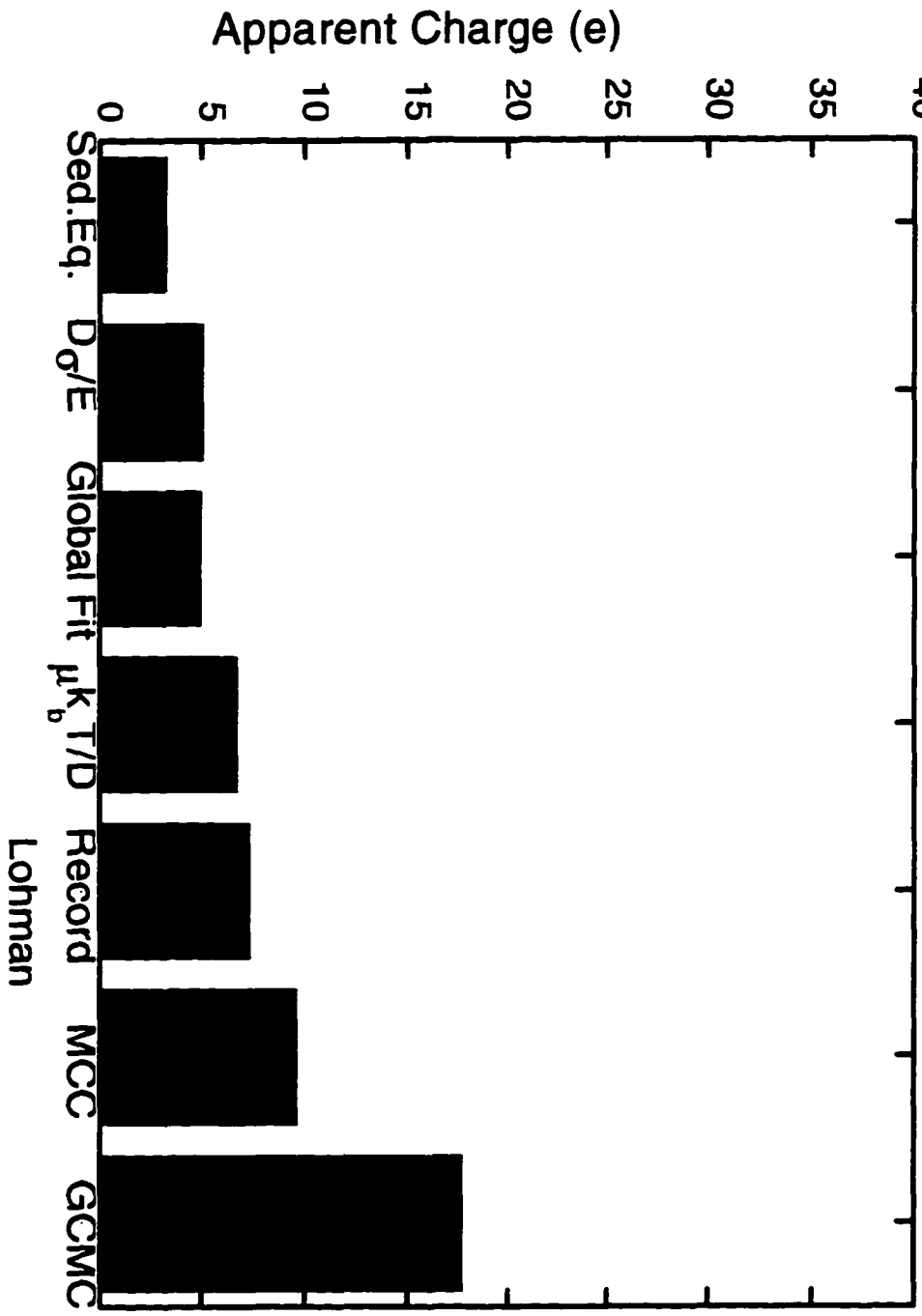

Comparison of experimental and theoretical estimates for the Q_{app} of $pd(A)_{20}pd(T)_{20}$ in 100 mM KCl, 20 mM Tris, pH 8.0, 20 °C

Procedure

hydrodynamic component of the electrophoretic migration to be eliminated or dramatically reduced. This is consistent with the constant value of ~ 5 e returned from global fit data over the range of solvent conditions. It also in line with the apparent solvent dependence with μ determination and not SSE.

Current polyelectrolyte theories involve a complex mixture of counterion condensation and counterion shielding. Electrophoretic mobility determination in the AEA can be used to investigate the dynamics of the counterion distribution around a macroion. The velocity of a moving boundary is distinctly affected by the *drag* of its counterion atmosphere and the degree of condensation. Mobility in the AEA can be used assess the characteristic interactions between macroion and counterion and to complement the basic charge values obtained from SSE.

Determining the diffusion and friction coefficients of particles migrating in an electric field is a critical feature in interpreting AEA results. The development of mathematical models describing the diffusion behavior of particles in the AEA has been an important advancement its development. However, additional study is still required to interpret the excess spreading of the moving boundary in μ determination. The hydrodynamic information obtained from D_e suggests an decreasing frictional coefficient with increasing E fields that is not consistent μ and SSE data. For this reason, the diffusion coefficient used for charge property calculations is one taken in the absence of an E field.

It appears that there are better techniques for obtaining a D_o than the AEA. The D_o determination in the AEA is potentially susceptible to extraneous forces or any type of convection. Sedimentation velocity gives cleaner and more reproducible numbers. Previous

experiments (12, 62) on 20 base pair DNA have yielded results similar to sedimentation. Further refinement of the D_o procedure is still required.

The current level of AEA data cannot offer conclusive evidence in support or opposition to the different theoretical predictions. The GCMC predictions appear distinctly large compared AEA determined μ and Q_{app} values but the results of the measurements can be interpreted within the parameters of DH and MCC. Mobility data as a function of ionic strength is consistent with the Debye length (Equation 12) of the DH theory. However, μ determination of $pd(A)_{20} \cdot pd(T)_{20}$ in the different chloride salts shows a cation dependence in excess of predictions.

The Manning counterion condensation theory uses solution dynamics (equivalent conductance, intrinsic frictional coefficient) to describe the observed differences in the mobilities of polyelectrolyte. The apparent consistency of the global fit SSE data (frictional factors cancel) and the solvent dependence in μ determination are in general agreement with his basic contentions but do not specifically validate them.

The Record and Lohman prediction of an apparent charge of ~7.6 appears to be the closest approximation to AEA values. The combination of counterion condensation and DH shielding is consistent with the large degree of charge reduction in SSE and μ determination.

CONCLUSION

The development of devices capable of analytical electrophoresis is essential in expanding the understanding of charge-related properties of macromolecules. The AEA has been shown to generate and monitor the electrophoretic migration of macroions. Theoretical descriptions of the electrostatic and hydrodynamic nature of a macros allows the apparent charge and electrophoretic mobility of the species to be determined.

Evaluation of the AEA measurements under a variety of E fields and solvent conditions shows that there are regions of measurements that yield consistent, reproducible values and regions of possible anomalous behavior. Influences of the concentration distribution on the macroion unaccounted for in simple theory have been sought and investigated in the context of using a model compound. Solvent conditions were chosen to evaluate aspects of polyelectrolyte theory. While charge determinations from different procedures have not been consolidated into a consistent theory, advancements in the scope and understanding of the AEA's potential have been made.

APPENDICES

Appendix 1

ELECTROPHORETIC MOBILITY (μ)

In a mobility experiment, the forces on the particles are balanced so that a constant-velocity boundary is observed. During electrophoresis there are four forces acting upon the macro-ions:

1) The electrophoretic force, $F1 = Q \cdot E$ where Q is the residual charge and E is the electric field

2) The hydrodynamic frictional force, $F2 = -f_t \cdot v$ with f_t is the Stokes frictional coefficient (this is justified as long as neither the macro-ion's size nor the solution viscosity are affected greatly by the field) and v is the particle's velocity

3) The electrophoretic or charged solvent effect , F3. This *drag* arises from the attraction of the counterions to the opposite electrode

4) The relaxation or field asymmetry effect, F4. The distortion of the counterion cloud around the particle (in the opposite direction of the poarticles migration) creates a dipole that opposes the E field.

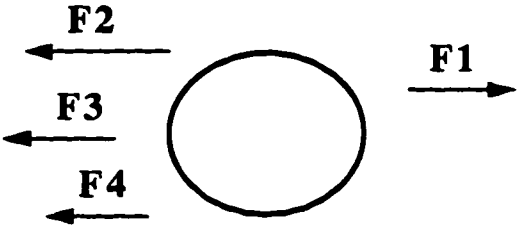

The total force on the macro-ion is zero:

$$F1 + F2 + F3 + F4 = 0 \qquad \text{or} \qquad -F2 = f_t v = F1 + F3 + F4$$

F3 and F4 are directly proportional to the applied field. However, there is uncertainty surrounding their contributions. They are therefore combined with f_t into a friction coefficient in the presence of an E field, f_e. The μ can than be describe as follows;

$$-f_e \cdot v = F1 + F3 + F4 = Q_{app} \cdot E$$

therefore

$$\mu = v/E = Q_{app}/f_e$$

APPENDIX 2

REFERENCES

1. Alexeev, D. G., Lipanov, A. A., and Skuratovskii, I. Y., (1987) "Poly(dA)-Poly(dT) is a B-type Double Helix With a Distinctively Narrow Minor Groove." *Nature*, **325**:821-823

2. Anderson, C., and Records, T., (1993) "The Salt-dependence of Oligoions-polyion Binding: A Thermodynamic Description Based on Preferential Interaction Coefficients." J. *Phys. Chem.*, **97**: 7116-7126

3. Arakawa, T., Timasheff, S. N., (1985) "Calculation of the Partial Specific Volume of Proteins in Concentrated Salt and Amino Acid Solutions" *Methods in Enzymology*, **117**:60-65

4. Behling, R. W, Kearns, D. R., (1986) "^{1}H Two-Dimensional Nuclear Overhauser Effect and Relaxation Studies of Poly(dA)-Poly(dT)." *Biochemistry*, **25**: 3335-3346

5. Bier, M., (1959) Electrophoresis: Theory, Methods, and Applications, (Contributions by Tiselius, A., Overbeek, J. Th. G., and Lijklema, J.,) Academic Press (London and New York) pp. xv-xix and 1-20

6. Burgess, J., (1988) "Solvation Numbers" in Ions in Solution, Ellis Horwood Limited, Chichester, pp.28-35

7. Cantor, C. R., and Schimmel, P. R., (1980) Biophysical Chemistry, Part II W. H. Freeman and Co., San Fransisco, pp. 614-616

8. Chapman, D. L., (1913) *Phil. Mag.*, **25**: 475

9. Conrad, J., Troll, M., and Zimm, B. H., (1988) "Ions Around DNA: Monte Carlo Estimates of Distribution with Improved Electrostatic Potentials." *Biopolymers*, **27**: 1711-1732

10. Debye, P., and Huckel, E., (1988) "On the Theory of Electrolytes. II. Limiting Law for Electric Conductivity." in The Collected Works of Peter J. E. Debye, Ox Bow Press, Woodbridge, CT. pp. 264-317

11. Durschlag, H., (1986) "Specific Volumes of Biological Macromolecules and Some Other Molecules of Biological Interest." in Thermodynamic Data for Biochemistry and Biotechnology, Springer-Verlag, New York

12. Eimer, W., and Pecora, R., (1990) "Rotational and Translational Diffusion of Short Rod-Like Molecules in Solution: Oligonucleotides." *J. Chem. Phys.*, **94**: 2324-2329

13. Eisenberg, D., Crothers, D., (1979) Physical Chemistry with Applications to the Life Sciences, The Benjamin/Cummings Publishing Company , Inc. Menlo Park Ca. 353-358 and 700-718

14. Feynman R. P., Leighton, R. B., Sands, M., (1964) The Feynman Lectures on Physics Vol. 1, Addison-Wesley Publishing Company, Reading Ma, Menlo Park Ca., 43-9

15. Fixman, M., (1979) "The Poisson-Boltzmann Equation and its Application to Polyelectrolytes.", *J. Chem. Phys.*, **70**: 4995-5005

16. Foster, K., Parker, G. A., (1970) "The Fluid Mechanics of Jet, Wall Attachment, and Vortices." in Fluidics, Wiley-Interscience, London, New York, Sydney, Toronto, pp. 99-101

17. Godfrey, J. E., (1989) "Steady-State Electrophoresis: A Technique for Measuring Physical Properties of Macro-ions.", *Proc. Nat. Acad. Sci.*, **86**: 4479-4483

18. Graetz, (1914) Handbuch der Elektrizität und des Magnetismus II (Contributions by von Smoluchowski, M.) Liepzig, pp. 366

19. Gouy, G., (1910) *J. Phys. Théor. Appl.*, **9**: 457

20. Gouy, G., (1917) *Ann. Phys.*, **7**: 129

21.Harding, S. E., Rowe, A. J., and Horton, J. C., (1992) "Computer-Aided Interpretation of Analytical Sedimentation Data for Proteins. By Laue et. al" in Analytical Ultracentrifugation in Biochemistry and Polymer Science, The Royal Society of Chemistry, Cambridge, pp. 109-111

22. Hardy, W. B., (1905) *J. Physiol.* (London), **33**: 251

23. Harned, H., French, D., (1945) *Ann. N. Y. Acad. Sci*, **46**: 267

24. Haschemeyer, R. H., and Bowers, W. F., (1970) "Exponential Analysis of Concentration and Concentration Difference Data for Discrete Molecular Weight Distribution In Sedimentation Equilibrium.", *Biochemistry*, **9**: 435-445

25. Hayes, D. B, (1993) Ph.D. Dissertation: Equilibrium Electrophoresis Results from the Second Prototype, University of New Hampshire

26. Helmholtz, H. (1979) *Wied. Ann.*, **7**: 337

27. Henry, D., (1948) "The Electrophoresis of Suspended Particles. IV. The Surface Conductivity Effect." *Trans. Faraday Soc.*, **44**: 1021-1026

28. Johnson, M. L., Correia, J. C., Yphantis, D. A., and Halvorson, H. R.,(1981) "Analysis of Data from the Analytical Ultracentrifuge by Nonlinear Least-Squares Technique." *Biophysical J.*, **36**: 578-588

29. Kochoyan, Z. M, Lancelot, G., Leroy, J. L., (1988) "Study of Structure, Base-pair Opening Kinetics and Proton Exchange Mechanism of the d-(AATTGCAATT) Self-complementary Oligodeoxynucleotide in Solution."*Nucleic Acids Res.*, **16**: 7685-7701

30. Kopka, M. L., Fratini, A. V., Drew, H. R., and Dickerson, R. E., (1983) "Ordered Water Structure around a *B*-DNA Dodecamer; A Quantitative Study" *J. Mol. Biol.*, **163**: 129-146

31. Kortüm, G., (1965) "Results and Applications of Conductance Measurements" in Treatise on Electrochemistry, Elsevier Publishing Co., Amsterdam, London-New York, pp. 247-251

32. Kruyt, H. R., (1952) Colloid Science Vol. I. (Chapter by Overbeek, J. Th. G.) Elsevier Publishing Co. Amsterdam, Houston , New York, and London, pp.194-204

33. Laue, T. M., Hazared,. A., Ridgeway, T., and Yphantis, D., (1989) "Direct Determination of Macromolecular Charge by Equilibrium Electrophoresis.", Analytical Biochemistry, **182**: 337-342

34. Leroy, J. L., Kochoyan, Z. M., Huynh-Dinh, T., and Guéron, M., (1988) "Characterization of Base-pair Opening in Deoxynucleotide Duplexes using Catalyzed Exchange of the Imino Proton." *J. Mol. Biol.*, **200**: 223-238

35. Manning, G., (1969 a) "Limiting Laws and Counterion Condensation in Polyelectrolyte Solutions. I. Colligative Properties." *J. Chem. Phys.*, **51**: 924-933

36. Manning, G., (1969 b) "Limiting Laws and Counterion Condensation in Polyelectrolyte Solutions. III. An Analysis Based on the Myer Ionic Solution Theory." *J. Chem. Phys.*, **51**: 3249-3252

37. Manning, G. S., (1978) "The Molecular Theory of Polyelectrolyte Solutions With Applications to the Electrostatic Properties of Polynucleotides." *Quarterly Review of Biophysics II*, **2**: 1796-246

38.Manning, G.S., (1989) "Counterion Binding in Polyelectrolyte Theory.", *Accts. Of Chemical Research*, **12**: 443

39. Marcus, Y., (1985) "Ion Hydration" in Ion Solvation, John Wiley & Son Limited, Chichester, pp.87-113

40. Marky, L.A., Patel, D.,and Breslauer, K. J.(1981) "Effect of Teteramethylammonium Ion on the Helix-to-coil Transition of poly (deoxyadenylythymidine): a Nuclear Magnetic Resonance and Calorimetric Investigation", *Biochemistry*, **20**: 1427-1431

41. McCloy, D., and Martin, H. R., (1980), "Fluid Controlling Elements" in Control of fluid Power: Analysis and Design; 2nd (Revised) Edition, Ellis Horwood Limited, Chichester, pp. 92-94

42. McRorie, D. K., and Voelker, P. J., (1993) Self-Associating Systems in the Analytical Ultracentrifuge, Beckman Instruments, Inc., Fullerton Ca., pp.16-22

43. Michaelis, L., (1909), *Biochem. Z.*, **16**: 81

44. Olmsted, M. C., Anderson, C. F., and Records, M. T., (1989) "Monte Carlo Description of Oligoelectrolyte Properties of DNA Oligomers: Range of the End Effects and the Approach of Molecular and Thermodynamic Properties to the Polyelectrolyte Limits.", *Proc. Natl. Acad. Sci.*, **86**: 7766-7770

45. Olmsted, M. C., Anderson, C. F., and Records, M. T., (1991) "Importance of Oligoelectrolyte End Effects for the Thermodynamics of Conformational Transition of Nucleic Acid Oligomers: A Grand Canonical Monte Carlo Analysis." *Biopolymers*, **31**: 1599-1604

46. Onsager, L., Fuoss, R. M., (1932) "Irreversible Processes in Electrolytes. Diffusion, Conductance, and Viscous Flow in Arbitrary Mixtures of Strong Electrolytes." *J Phys. Chem.*, **36**: 2689

47. Polson, A., (1953) "Multi-Membrane Electrocantation and its Application to Isolation and Purification of Proteins and Viruses." *Biochimica et Biophysica Acta*, **11**: 315-325

48. Quignard, E., Téoule, R., Guy, A., and Fazakerley, G. V., (1985) "An NMR Study of A-T Base Pair Opening Rates in Oligonucleotides. Influence of Sequence and of Adenine Methylation." *Nucleic Acids Res.*, **13**: 7829-7836

49. Record, M. T., and Lohman, T. M., (1978) "A Semiempirical Extension of Polyelectrolyte Theory to the Treatment of Oligoelectrolytes: Application to Oligonucleotide Helix-Coil Transitions." *Biopolymers*, **17**: 159-166

50. Record, M. T., Anderson, C.F., and Lohman, T. M., (1978) "Thermodynamic Analysis of Ion Effects on the Binding and Conformational Equilibria of Proteins and Nucleic Acids:

the Role of Ion Association or Release, Screening, and Ion Effects on Water Association." *Quart. Rev. Biophys.*, **11**: 103-178

51. Ridgeway, T. M., Hayes, D. B., Anderson, A. L., Levasseur, J. H., Demaine, P. D., Kenty, B. E., and Laue, T. M., (1994) "Possible Clinical Application for the Direct Molecular Charge Determination by Equilibrium Electrophoresis." In *Biochemical Diagnostic Instrumentation*, SPIE Proceedings. Vol 2136, Bonner. R. F. Cohn, G. E., Laue, T. M., and Priezzhev, A.V., (eds) SPIE, Bellingham, Wa, pp.236-274

52. Ross, P. D., Scruggs, R. L., (1964) "Electrophoresis of DNA. II. Specific Interactions of Univalent and Divalent Cations with DNA." *Biopolymers*, **2**: 79-89

53. Ross, P. D., Scruggs, R. L., (1961) "Electrophoresis of DNA. III. The Effect of Several Univalent Electrolytes on the Mobility of DNA." *Biopolymers*, **2**: 231-236

54. Scrutton, N. S., Raine, A. R. C., (1996) "Cation-π Bonding and Amino-Aromatic Interactions in the Biomolecular Recognition of Substitiuted Ammonium Ligands."

55. Shaw, D. J., (1969) Electrophoresis Academic Press (London and New York) pp. 1-10

56. Shepard. H. K, Wilson, T. J., Moody, T. P., Wooll, J. O., Laue, T. M., (Paper in progress) "Determination of Macroion Diffusion Coefficient Using an Analytical Electrophoresis Apparatus." *European Biophysics Journal*

57. Stafford, W. F., (1992) "Boundary Analysis in Sedimentation Transport Experiments: A Procedure for Obtaining Sedimentation Coefficients Using Time Derivatives of the Concentration Profiles." *Analytical Biochemistry*, **203**: 259-301

58. Stigter, D., (1995) "Evaluation of the Counterion Condensation Theory of Polyelectrolytes." *Biophysics J.*, **69**: 380

59. Stigter, D., (1978) "Electrophoresis of Highly Charged Colloidal Cylinders in Univalent Salt Solutions. 2. Random Orientation in External Field and Application to Polyelectrolyte" *J of Phys. Chem.*, **12**: 1424-1429

60. Tanford, C., (1961) Macroions in Thermodynamics. in: Physical Chemistry of Macromolecules, John Wiley & Son, Inc., New York, pp. 221-237

61. Timasheff, S. N., (1992) "Water as a Ligand: Preferential Binding and Exclusion of Denaturants in Protein Unfolding" *Biochemistry*, **31**: 9857-9864

62. Tirado, M. M., Martinez, C. L, de la Torres, J. G., (1984) "Comparison of Theories for the Translational and Rotational Diffusion Coefficients of Rod-Like Macromolecules.

Application to Short DNA Fragments." *J. Chem. Phys.*, **81**: 2047-2053

63. Wilson, W. D., Zuo, E. T., Jones, R. L., Zon, G. L. and Baumstark, B. R., (1987) "Sequence Dependent Electrophoretic Mobilities and Melting Temperatures for A-T Containing Oligodeoxyribonucleotides." *Nucleic Acids Res.*, **15**: 105-118

64. Van Holde, K. E., (1985) "Transport Processes, Sedimentation" in Physical Biochemistry, Prentice Hall, New Jersey, pp 93-117

65. Yphantis, D., (1964) "Equilibrium Ultracentrifugation of Dilute Solutions." *Biochemistry*: **3** 297-317